ÇUKUROVA UNIVERSITY
INSTITUTE OF NATURAL AND APPLIED SCIENCES

PhD THESIS

Mehmet OĞLAKÇI

SYNTHESES AND THERMOLUMINESCENCE STUDIES OF UNDOPED AND RARE EARTH DOPED $NaBaBO_3$ MATERIALS

DEPARTMENT OF PHYSICS

ADANA-2021

DEDICATION

This PhD thesis is dedicated to my beloved family…

ABSTRACT

PhD THESIS

SYNTHESES AND THERMOLUMINESCENCE STUDIES OF UNDOPED AND RARE EARTH DOPED $NaBaBO_3$ MATERIALS

Mehmet OĞLAKÇI

ÇUKUROVA UNIVERSITY
INSTITUTE OF NATURAL AND APPLIED SCIENCES
DEPRATMENT OF PHYSICS

Supervisor : Prof.Dr. Mustafa TOPAKSU
II Supervisor : Prof.Dr. Nurdoğan CAN

Year: 2021, Pages: 135

Jury : Prof.Dr. Mustafa TOPAKSU
: Prof.Dr. Cebrail GÜMÜŞ
: Prof.Dr. Ayşe POLATÖZ
: Prof.Dr. Ahmet Necmeddin YAZICI
: Assoc.Prof. Vural Emir KAFADAR

In this study undoped $NaBaBO_3$ phosphor was synthesized by combustion synthesis method. Same methodology was also applied to the Cerium (Ce^{3+})-doped, Gadolinium (Gd^{3+})-doped, and Terbium (Tb^{3+})-doped $NaBaBO_3$ syntheses of phosphors, respectively. Dopant concentrations were 0.5, 1, 2, 3, 4, 5 weight% for Gd-doped and Tb-doped phosphor samples; but for the optimal concentration study 0.25, 6, 7, 8% concentrations were extra synthesized for Ce^{3+}-doped $NaBaBO_3$ study. Each phosphor was exposed to beta particle irradiation source $^{90}Sr/^{90}Y$ for thermoluminescence (TL) study. In the TL study, main TL dosimetry properties were investigated and determined in terms of optimal TL bandpass filter, optimal dopant concentration, linear dose range, behavior under various heating rates (VHR), and electron trap parameters, reusability quality to see how much detection sensitivity deviates. Additionally, electron trap parameters such as activation energy, vibration frequency, kinetic order were determined experimentally by conducting T_{max}-T_{stop} experiment; they were also determined theoretically by using computerized glow curve deconvolution (CGCD) method for each material.

Keywords: Thermoluminescence Dosimeter, LexygSmart, Sodium Barium Borate, Cerium, Gadolinium, Terbium

ÖZ

DOKTORA TEZİ

SAF VE NADİR TOPRAK ELEMENTİ KATKILI $NaBaBO_3$ MALZEMELERİNİN TERMOLÜMİNESANS ÇALIŞMALARI VE SENTEZİ

Mehmet OĞLAKÇI

ÇUKUROVA UNIVERSITY
INSTITUTE OF NATURAL AND APPLIED SCIENCES
DEPRATMENT OF PHYSICS

Danışman : Prof.Dr. Mustafa TOPAKSU
II Danışman : Prof.Dr. Nurdoğan CAN
Yıl: 2021, Sayfa: 135
Jüri : Prof.Dr. Mustafa TOPAKSU
: Prof.Dr. Cebrail GÜMÜŞ
: Prof.Dr. Ayşe POLATÖZ
: Prof.Dr. Ahmet Necmeddin YAZICI
: Doç.Dr. Vural Emir KAFADAR

Bu tez çalışmasında $NaBaBO_3$ fosforu yanma yöntemi ile sentezlenmiştir. Aynı metodoloji ile Seryum (Ce^{+3})-katkılı, Gadolinyum (Gd^{+3})-katkılı, Terbiyum (Tb^{+3})-katkılı $NaBaBO_3$ fosforlarının sentezlerinde de kullanılmıştır. Uygun katkı oranı çalışmasında, katkı derişimi, Gd^{+3}-katkılanmış ve Tb^{+3}-katkılanmış $NaBaBO_3$ fosforları için ağırlıkça %0,5, 1, 2, 3, 4, 5'tir; ama Ce^{+3} katkılı $NaBaBO_3$ için %0,25, 6, 7, 8 konsantrasyonları fazladan sentezlenmiştir. Her bir fosfor, termolüminesans (TL) çalışması için beta radyasyonu kaynağına ($^{90}Sr/^{90}Y$) maruz bırakılmıştır. TL çalışmasında ana TL dozimetri özellikleri araştırılmış ve optimal TL bant geçiren filtre, optimal katkı konsantrasyonu, doğrusal doz aralığı, çeşitli ısıtma hızları (VHR) altında davranış, tekrar kullanılabilirlik kalitesi ve elektron tuzak parametreleri belirlenmiştir. Aktivasyon enerjisi, kaçış frekansı, kinetik mertebe gibi elektron tuzak parametreleri, her malzeme için deneysel olarak T_{max}-T_{stop} deneyi ile; bilgisayarlı ışıma eğrisi ayrıştırma (CGCD) yönteminden faydalanılarak de teorik olarak belirlenmiştir.

Anahtar Kelimeler: Termolüminesans Dozimetresi, LexygSmart, Sodyum Baryum Borat, Seryum, Gadolinyum, Terbiyum

EXTENDED SUMMARY

Radiation is the reality of nature; and since it is utilized in many human activities, monitoring it is necessary for protection from the harms of it. Hence, the importance of the monitoring by means of the measurement has key role in such activities.

Dosimeters are utilized with the purpose of radiation dose measurement and they can also be categorized as solid-state dosimeters, gas filled detectors, and scintillators. Most commonly solid-state dosimeters are used in the field of radiation dosimetry. Sensitive dose range mainly determining the field that such a dosimeter be used.

For the solid-state dosimetry, a material must be a phosphorescent material. Band structure of such a solid-state material needs to be either insulator or semiconductor that in the forbidden band gap of that material there can exist electron trap or traps. When such material interacts with the radiation, some amount of the incident energy may be absorbed. When heated, this absorbed energy is emitted back as photons while trapped electrons get free and go to their ground energy level. This physical phenomenon is known as thermoluminescence; and such materials are called as thermoluminescence phosphor.

In the literature there are many studies on thermoluminescence dosimeters including the crystal containing the boron element; borates in other words. In this thesis study $NaBaBO_3$ host material is synthesized via combustion synthesis routine. In order to optimize the synthesis, different temperature values were applied and x-ray diffraction spectra of resulting crystal structures were compared with the reference $NaBaBO_3$ pattern data (98-008-0110). After determining the optimal synthesis temperature, this time thermal treatment duration varied and one more time XRD spectra of synthesized materials compared to reference pattern data. With this synthesis optimization, correct crystal structure obtained successfully.

After host crystal was synthesized, this time its main thermoluminescence dosimetric properties were investigated. With this purpose, powder formed sample ground and pelletized for analysis. LexygSmart TL/OSL reader system was utilized for all the TL analysis of this thesis work. This system has internal β particle source ($^{90}Sr/^{90}Y$) for irradiation purpose with a dose rate of ~0.11 Gy. System uses nitrogen gas for cooling and for some its pneumatic subsystem.

TL analysis of undoped phosphor was started with determining the optimal TL band pass filter combination for detection of the emitted photons more sensitively. Four different TL filter combinations were used for this experiment. Their names are: BSL, TL

365nm; IRSL, TL 410nm; IRSL, TL 565nm; IRSL, TL wideband blue. Experimentally it was determined that filter combination "IRSL, TL 565nm" is the optimal for TL analysis of undoped $NaBaBO_3$ phosphor. Dose sensitivity and linear dose range was determined via dose response experiment. Sample was irradiated with of β dose from ~0.11 up to 50 Gy by using above mentioned optimal TL filter combination. Thermal stimulation was done with a heating rate of 2°C/s from room temperature up to 450°C then immediately cooled back to 25°C. Additionally, a preheat value of 130°C was applied from dose response experiment. Each main TL signal and its background signal were recorded with this optimal filter combination. Linear dose interval was determined from the linearity of log-log scaled distribution graph of total TL curve area per irradiation dose, and it was determined that up to ~14 Gy of β dose this material dosimetry linearity is perfectly linear. A heating-rates-experiment of undoped $NaBaBO_3$ was conducted to investigate the characteristics of the material under different heating rates to observe if it is normal or anormal, and if there is any effect of thermal quenching. Other than that, methods using peak temperatures for each heating rate were used to estimate the activation energy or trap depth within the host material's conduction and valence bands. Material's reusability quality was investigated by irradiating and reading its TL signal under the same conditions 10 times. It was observed that these 10 readouts gave barely 1% standard deviation of the sensitivity, which is less than 5% limit of dosimetry. Trap parameters of undoped sample was estimated through computerized glow curve deconvolution (CGCD) which is theoretical approach; but with the reference values which are obtained from T_m-T_{stop} experiment and repeated initial rise analysis method. From those analysis four electron traps were determined corresponding to peak temperatures 75, 123, 166, 190°C; with depths as 0.76, 1.34, 1.05, 0.98 eV; with escape frequencies of electrons as 1.26×10^{10}, 2.02×10^{16}, 1.18×10^{11}, 5.19×10^{9} s^{-1}; and kinetic orders as 2, 2, 2, 1.6 respectively for each trap.

For the TL study of Ce^{3+} doped $NaBaBO_3$ phosphor, different dopant concentrations as 0.25, 0.5, 1, 2, 3, 4, 5, 6, 7, 8 weight% samples were synthesized via aforementioned optimized synthesis routine. Crystal structure of obtained samples were confirmed via XRD analysis. Optimal TL filter was determined as IRSL-TL 565nm and optimal dopant concentration was determined as 0.5% Ce^{3+}. A preheat test experiment was conducted to determine optimal preheat temperature and duration; and it was determined that a preheat with an increase in temperature by 2°C/s up to 160°C and holding for 20 seconds was the optimal preheat condition for $NaBaBO_3$:Ce^{3+}(0.5%) phosphor. Dose response characteristics of this phosphor exhibited a linearity from 0.5 to 5 Gy of β dose. A

heating rates experiment was conducted and it was observed that there is no anormal behavior. Dominant trap parameters were also estimated from peak temperatures from different heating rates by using multiple VHR methods. It was determined from ten times irradiating and reading under same conditions that $NaBaBO_3:Ce^{3+}$ (0.5%) phosphor's dose measurement sensitivity exhibited 1.7% standard deviation, which is also less than the 5% dosimetry limit. Trap parameters of $NaBaBO_3:Ce^{3+}$(0.5%) phosphor was estimated through theoretical approach of CGCD analysis. It was estimated that glow curve has six peaks with peak temperatures as 67, 83, 120, 137, 183, 326 °C; trap depths as 1.02, 0.99, 0.78, 1.13, 0.72, 1.31 eV; escape frequencies of electrons as 2.3×10^{14}, 1.47×10^{13}, 1.07×10^{9}, 1.16×10^{13}, 6.1×10^{6}, 8.88×10^{9} s^{-1}; and kinetic orders as 1.4, 1.9, 1.01, 1.8, 1.3, 2 respectively for each peak.

Synthesis of Gd^{3+} doped $NaBaBO_3$ phosphor was completed for Gd^{3+} concentrations as 0.5, 1, 2, 3, 4, 5% in weight. Optimal synthesis routine for the undoped crystal was used and at the synthesis step dopant element was added to the reaction. Crystal structures of synthesized samples were confirmed via XRD analysis. For the thermoluminescence study, optimal TL filter combination was determined as IRSL-TL 410 nm for Gd^{3+} doped samples. TL intensity quality was the highest at the 1% Gd^{3+} dopant concentration and it was determined as the optimal rate of Gd^{3+} ion addition to the $NaBaBO_3$ host lattice. For the TL dosimetry study, an optimal TL preheat condition study was conducted with a heating rate of 2 °C/s; and it was determined that, heating up 215 °C and holding at this temperature for 12 seconds is the optimal TL preheat condition. For the dose response experiment, pelletized sample was irradiated with β particles from 0.1 up to 20 Gy. Up to 20 Gy dose measurement was nearly linear (b parameter is 1.09); but for the dose range 0.5-7 Gy it is perfectly linear (≈1). A heating-rates-experiment was conducted and it was observed that there is no anormal behavior. Dominant trap parameters were also estimated from peak temperatures which were determined from different heating rates by using multiple VHR method. Dose measurement deviation was tested with ten times irradiation-reading cycles. From the experimental results it was determined that dose measurement of $NaBaBO_3:Gd^{3+}$(1%) exhibits the standard deviation for measurement sensitivity as 0.9% which is far less than 5% dosimetry measurement deviation limit. Trap parameters of $NaBaBO_3:Gd^{3+}$(1%) was estimated with computerized glow curve deconvolution analysis theoretically; but staying in the experimentally estimated most probable activation energy and peak temperature value intervals. Trap parameters of six peaks were estimated for peak temperature as 89, 120, 163, 200, 310, 359 °C; for trap depth

as 0.92, 1.13, 1.05, 1.22, 1.35, 1.18 eV; for vibration frequency of electrons as 9.42×10^{11}, 4.7×10^{13}, 1.62×10^{11}, 1.21×10^{12}, 4.02×10^{10}, 1.6×10^{8} s^{-1}; and for kinetic order as 2, 1.74, 2, 1.82, 1.35, 1.62 respectively for each peak.

Synthesis of the Tb^{3+} doped $NaBaBO_3$ phosphor was completed by using the determined optimal synthesis routine of undoped $NaBaBO_3$ phosphor, for different Tb^{3+} concentrations as 0.5, 1, 2, 3, 4, 5% in weight. Optimal TL filter combination was determined as IRSL-TL wideband blue. The highest TL emission intensity was observed from the $NaBaBO_3:Tb^{3+}$(2%) phosphor sample. Optimal preheat condition was determined as heating up to 145 °C with a heating rate of 2 °C/s and keeping at this temperature for 17 seconds then cooling back to room temperature. Dose response behavior of this sample was investigated for a dose range of 0.1-40 Gy and it was determined as super-linear with b=1.36 value. A heating-rates-experiment was conducted and it was observed that there is no anormal behavior. Dominant trap parameters were also estimated from peak temperatures from different heating rates by using multiple method of VHR. Standard deviation of dose measurement sensitivity was tested by irradiating and immediately reading TL signal ten times. It was determined that sensitivity of dose measurement exhibits 1.6% standard deviation which is less than 5% acceptance limit for TL dosimetry in the literature. Trap parameters were estimated through CGCD analysis. Fit parameters of most probable peak temperature and activation energy values required for CGCD analysis were obtained from T_m-T_{stop} experiment and repeated initial rise analysis. Glow curve estimated to have at least seven peaks. Parameters were estimated for those peaks respectively as follows: peak temperature as 86, 118, 145, 184, 230, 291, 341 °C; for trap depth as 1.2, 1.2, 1.2, 1.3, 1.4, 1.6, 1.3 eV; for frequency factor as 1.38×10^{16}, 4.79×10^{14}, 4.36×10^{13}, 3.02×10^{13}, 1.27×10^{13}, 2.17×10^{13}, 3.59×10^{9} s^{-1}; for kinetic order as 1.5, 1.5, 1.5, 1.5, 1.5, 1.5, 1.17.

It can be concluded that undoped $NaBaBO_3$, $NaBaBO_3:Ce^{3+}$(0.5%), $NaBaBO_3:Gd^{3+}$(1%), and $NaBaBO_3:Tb^{3+}$(2%) phosphors are promising candidates for TL dosimetry. All four TL phosphor materials are new contributions to TL dosimetry studies in literature.

GENİŞLETİLMİŞ ÖZET

Radyasyon doğanın gerçeğidir ve birçok insan faaliyetinde kullanılması ile izleme ve gerektiğinde zararlardan korunma şarttır. Bu nedenle, bu tür faaliyetlerde ölçüm yoluyla izlemenin önemi anahtar role sahiptir.

Radyasyon doz ölçümü amacıyla kullanılan doz ölçerler, katı hal dozimetreleri, gaz dolu dedektörler ve sintilatörler olarak da sınıflandırılabilir. Radyasyon dozimetrisi alanında en yaygın olarak katı hal dozimetreleri kullanılır. Hassas doz aralığı esas olarak böyle bir doz ölçerin kullanılacağı alanı belirler.

Katı hal dozimetrisi için kullanılacak malzeme fosforlu bir malzeme olmalıdır. Böyle bir katı hal malzemesinin bant yapısının ya yalıtkan ya da yarı iletken olması gerekir ki, o malzemenin yasak bant aralığında elektron tuzak veya tuzakları olabilsin. Malzeme radyasyonla etkileşime girdiğinde, gelen enerjinin bir kısmı soğururken, ısıtıldığında, bu emilen enerji fotonlar olarak geri yayılır. Tuzaklanan elektronlar serbest kalır ve yer enerji seviyelerine giderler. Bu fiziksel olay termolüminesans olarak bilinir ve bu tür malzemelere termolüminesans fosfor denir.

Literatürde bor tabanlı kristal (boratlar) içeren termolüminesans dozimetreler ile ilgili birçok çalışma bulunmaktadır. Bu tez çalışmasında, $NaBaBO_3$ ana (ev sahibi) materyali, yanma sentezi ile sentezlenmiştir. Sentezi optimize etmek için, farklı sıcaklık değerleri uygulanmış ve elde edilen kristal yapıların x-ışını kırınım spektrumları, referans $NaBaBO_3$ model verileriyle (98-008-0110) karşılaştırılmıştır. Optimal sentez sıcaklığı belirlendikten sonra, bu sefer ısıl işlem süreleri ile bir kez daha sentezlenen malzemelerin XRD spektrumları referans model verileriyle karşılaştırılmıştır. Bu sentez optimizasyonu ile doğru kristal yapı başarıyla elde edilmiştir.

Ev sahibi kristal sentezlendikten sonra malzemenin temel termolüminesans doz ölçer özellikleri araştırıldı. Bu amaçla numune öğütülerek toz haline getirilmiş ve analiz için peletlenmiştir. Bu tez çalışmasının tüm TL analizlerinde LexygSmart TL/OSL okuyucu sistemi kullanılmıştır. Bu sistem, ~0,11 Gy doz hızında ışınlama amaçlı dahili β partikül kaynağına ($^{90}Sr/^{90}Y$) sahiptir. Sistem, soğutma ve bazı pnömatik alt sistemleri için nitrojen gazı kullanır.

Yayılan fotonların daha hassas bir şekilde saptanması için optimal TL bant geçiren filtre kombinasyonunun belirlenmesi ile katkısız fosforun TL analizleri yapılmıştır. Bu deney için dört farklı TL filtre kombinasyonu kullanıldı. İsimleri: BSL, TL 365nm; IRSL, TL 410nm; IRSL, TL 565nm; IRSL, TL geniş bant mavi. Deneysel olarak, “IRSL, TL

565nm" filtre kombinasyonunun, katkısız $NaBaBO_3$ fosforunun TL analizi için optimal olduğu belirlendi. Doz duyarlılığı ve doğrusal doz aralığı, doz yanıt deneyi ile belirlendi. İncelenen örnek, yukarıda belirtilen optimal TL filtre kombinasyonu kullanılarak ~0,11'den 50 Gy'e kadar β dozu ile ışınlandı. Termal uyarım, oda sıcaklığından 450°C'ye kadar 2°C/s'lik bir ısıtma hızıyla yapıldı ve ardından hemen tekrar 25°C'ye soğutuldu. Ek olarak, doz yanıt deneyinden 130°C'lik bir ön ısıtma değeri uygulanmıştır. Her ana TL sinyali ve arka plan sinyali bu optimal filtre kombinasyonu ile kaydedildi. Işınlama dozu başına toplam TL eğri alanının log-log ölçekli dağılım grafiğinin doğrusallığından doğrusal doz aralığı belirlendi ve ~14 Gy β dozuna kadar bu malzeme dozimetri doğrusallığının mükemmel doğrusal olduğu belirlendi. Normal veya anormal olup olmadığını ve termal söndürmenin herhangi bir etkisinin olup olmadığını gözlemlemek için farklı ısıtma hızları altında malzemenin özelliklerini araştırmak için katkılanmamış $NaBaBO_3$'ün bir ısıtma hızları deneyi gerçekleştirilmiştir. Bunun dışında, ana malzemenin iletim ve değerlik bantları içindeki aktivasyon enerjisini veya tuzak derinliğini tahmin etmek için her ısıtma hızı için tepe sıcaklıkları kullanan yöntemler kullanıldı. Malzemenin yeniden kullanılabilirlik kalitesi, aynı koşullar altında 10 kez ışınlanarak ve TL sinyali okunarak araştırıldı. Bu 10 okumanın standart sapmasının, %5 dozimetri sınırının içerisinde kalarak %1 standart sapma verdiği gözlemlenmiştir. Katkısız numunenin tuzak parametreleri teorik yaklaşım olan bilgisayarlı ışıma eğrisi ayrıştırma (CGCD) ile tahmin edilmiştir ve bu tahminde T_m-T_{stop} deneyi ve tekrarlanan ilk yükselme analizi yönteminden elde edilen referans değerlerler kullanılmıştır. Bu analizlerden 75, 123, 166, 190°C tepe sıcaklıklarına karşılık gelen dört elektron tuzağı belirlendi; 0,76, 1,34, 1,05, 0,98 eV derinliğinde; elektronların kaçış frekansı $1,26\times10^{10}$, $2,02\times10^{16}$, $1,18\times10^{11}$, $5,19\times10^{9}$ s^{-1}; ve kinetik sıra her bir tuzak için sırasıyla 2, 2, 2 ve 1,6 olduğu belirlenmiştir.

Ce^{+3} katkılı $NaBaBO_3$ fosforunun TL çalışması için, ağırlıkça %0,25-0,5-1- 2-3-4-5-6-7-8 gibi farklı katkı konsantrasyonları yukarıda bahsedilen optimize edilmiş sentez rutini ile sentezlendi. Elde edilen numunelerin kristal yapısı XRD analizi ile doğrulanmıştır. Optimal TL filtre IRSL-TL 565nm ve optimal katkı konsantrasyonu %0,5 Ce^{+3} olarak belirlendi. Optimum ön ısıtma sıcaklığını ve süresini belirlemek için bir ön ısıtma testi deneyi yapıldı; $NaBaBO_3$:Ce^{+3}(%0,5) fosfor için en uygun ön ısıtma koşulunun, 160°C'ye kadar 2°C/s sıcaklık artışı ve 20 saniye bekletme ile ön ısıtma olduğu belirlendi. Bu fosforun doz tepkisi özellikleri, 0,5 ila 5 Gy β dozu arasında bir doğrusallık sergiledi. Isıtma oranları deneyi yapılmış ve anormal bir davranışın olmadığı gözlemlenmiştir. Baskın tuzak parametreleri, birden fazla VHR yöntemi kullanılarak farklı ısıtma hızlarından elde

edilmiş olan pik sıcaklıkları kullanılarak da tahmin edildi. Aynı koşullar altında on kez ışınlama ve okumadan $NaBaBO_3:Ce^{+3}$(%0,5) fosforunun doz ölçüm duyarlılığının %1,7 standart sapma gösterdiği ve bu da %5 dozimetri kabul sınırının altında olduğu belirlendi. $NaBaBO_3:Ce^{+3}$(%0,5) fosforun tuzak parametreleri, CGCD analizinin teorik yaklaşımıyla tahmin edildi. Kızdırma eğrisinin 67, 83, 120, 137, 183, 326 °C pik sıcaklığına sahip altı tepe noktası olduğu tahmin edilmiştir; tuzak derinliği 1,02-0,99-0,78-1,13-0,72-1,31 eV olarak; elektronların titreşim frekansı $2,3\times10^{14}$, $1,47\times10^{13}$, $1,07\times10^{9}$, $1,16\times10^{13}$, $6,1\times10^{6}$, $8,88\times10^{9}$ s^{-1}; ve kinetik sıra her bir pik için sırasıyla 1,4-1,9-1,01-1,8-1,3-2 şeklindedir.

Ağırlıkça %0,5-1-2-3-4-5 Gd^{+3} konsantrasyonları için Gd^{+3} katkılı $NaBaBO_3$ fosfor sentezi tamamlanmıştır. Katkısız kristal için optimal sentez rutini kullanıldı ve sentez aşamasında reaksiyona katkı maddesi eklendi. Sentezlenen örneklerin kristal yapıları XRD analizi ile doğrulandı. Termolüminesans çalışması için Gd^{+3} katkılı numuneler için optimal TL filtre kombinasyonu IRSL-TL 410nm olarak belirlendi. TL yoğunluk kalitesi %1 Gd^{+3} katkı konsantrasyonunda en yüksekti ve Gd^{+3} iyonunun $NaBaBO_3$ konak kafesine optimal oranı olarak belirlendi. TL dozimetri çalışması için, 2°C/s'lik bir ısıtma hızıyla optimal bir TL ön ısıtma durumu çalışması yapılmıştır; 215 °C'ye kadar ısıtmanın ve bu sıcaklıkta 12 saniye tutmanın optimal TL ön ısıtma koşulu olduğu belirlendi. Doz tepkisi deneyi için, pelet haline getirilmiş numune 0,1 ila 20 Gy arasında β partikülleri ile ışınlandı. 20Gy'ye kadar doz ölçümü neredeyse doğrusaldı (b parametresi 1,09'dur); ancak 0,5-7Gy doz aralığı için tamamen doğrusaldır (≈1). Isıtma oranları deneyi yapılmış ve anormal bir davranışın olmadığı gözlemlenmiştir. Baskın tuzak parametreleri, birden fazla VHR yöntemi kullanılarak farklı ısıtma hızlarından elde edilmiş olan pik sıcaklıkları kullanılarak da tahmin edildi. Doz ölçüm sapması, on kez ışınlama okuma döngüsü ile test edildi. Deneysel sonuçlardan $NaBaBO_3:Gd^{+3}$(%1)'nin doz ölçümünün, ölçüm duyarlılığı için standart sapmayı %0,9 olarak gösterdiği ve bu da %5 dozimetri ölçüm sapma sınırının çok altında olduğu belirlendi. $NaBaBO_3:Gd^{+3}$(%1)'nin tuzak parametreleri CGCD analizi ile teorik olarak tahmin edildi; ancak deneysel olarak tahmin edilen en olası aktivasyon enerjisi ve tepe sıcaklık değeri aralıklarında kalmak. Altı tepe noktasının tuzak parametreleri, tepe sıcaklığı için 89, 120, 163, 200, 310, 359 °C olarak tahmin edildi; 0,92-1,13-1,05-1,22-1,35-1,18 eV tuzak derinliği için; elektronların kaçış frekansı için $9,42\times10^{11}$, $4,7\times10^{13}$, $1,62\times10^{11}$, $1,21\times10^{12}$, $4,02\times10^{10}$, $1,6\times10^{8}$ s^{-1}; ve kinetik sıra için her bir pik için sırasıyla 2-1,74-2-1,82-1,35-1,62.

Tb^{3+} katkılı $NaBaBO_3$ fosforunun sentezi, katkısız $NaBaBO_3$ fosforun belirlenen optimal sentez rutini kullanılarak, ağırlıkça 0,5-1-2-3-4-5 farklı Tb^{+3} konsantrasyonları için

tamamlanmıştır. Optimal TL filtre kombinasyonu IRSL-TL geniş bant mavi olarak belirlendi. En yüksek TL emisyon yoğunluğu $NaBaBO_3:Tb^{+3}$(%2) fosfor numunesinden gözlemlendi. Optimum ön ısıtma koşulu, 2 °C/sn ısıtma hızı ile 145 °C'ye kadar ısıtmak ve bu sıcaklıkta 17 saniye tutulduktan sonra tekrar oda sıcaklığına soğutmak olarak belirlendi. Bu örneğin doz tepki davranışı 0,1-40Gy doz aralığında araştırılmış ve b=1,36 değeri ile süper lineer olarak belirlenmiştir. Isıtma oranları deneyi yapılmış ve anormal bir davranışın olmadığı gözlemlenmiştir. Baskın tuzak parametreleri, birden fazla VHR yöntemi kullanılarak farklı ısıtma hızlarından elde dilmiş olan pik sıcaklıkları kullanılarak da hesaplandı. Doz ölçüm hassasiyetinin standart sapması, malzemeyi on kez ışınlayarak ve TL sinyalini hemen okuyarak test edildi. Doz ölçüm duyarlılığının literatürde TL dozimetri için %5 kabul sınırının altında olan %1,6 standart sapma gösterdiği belirlenmiştir. Tuzak parametreleri CGCD analizi ile tahmin edildi. CGCD analizi için gerekli olan sıcaklık ve aktivasyon enerjisi değerlerinin başlangıç değerleri için, T_m-T_{stop} deneyinden ve tekrarlanan ilk yükselme analizinden elde edilmiş olan en olası değerler aralığı kullanıldı. TL ışıma eğrisinin en az yedi enerji basamağından (pikten) oluştuğu öngörülmüştür. Bu pikler için parametreler sırasıyla şu şekilde tahmin edilmiştir: 86, 118, 145, 184, 230, 291, 341 °C pik sıcaklığı olarak; 1,2-1,2-1,2-1,3-1,4-1,6-1,3 eV tuzak derinliği olarak; frekans faktörü için $1{,}38\times10^{16}$, $4{,}79\times10^{14}$, $4{,}36\times10^{13}$, $3{,}02\times10^{13}$, $1{,}27\times10^{13}$, $2{,}17\times10^{13}$, $3{,}59\times10^{9}$ s^{-1} olarak; kinetik mertebe için 1,5-1,5-1,5-1,5-1,5-1,5-1,17 olarak.

Katkısız $NaBaBO_3$, $NaBaBO_3:Ce^{+3}$(%0,5), $NaBaBO_3:Gd^{+3}$(%1) ve $NaBaBO_3:Tb^{+3}$(%2) fosforlarının TL dozimetri için umut verici adaylar olduğu sonucuna varılabilir. Dört TL fosfor malzemesinin herbiri, literatürdeki TL dozimetri çalışmalarına yeni katkılardır.

ACKNOWLEDGEMENTS

I would like to thank my Ph.D. supervisors, Prof. Dr. Mustafa TOPAKSU and Prof. Dr. Nurdoğan CAN, for supporting me with their knowledge and experience during my thesis study.

I am thankful to my friends from working group Assoc. Prof. Dr. Mehmet YÜKSEL, Dr. Sibel AKÇA-ÖZALP, Dr. Ziyafer Gizem PORTAKAL-UÇAR, Dr. Kenan BULCAR, Sümeyra BALCI-YEĞEN, M.Sc. Hasan YAZAN, and master students Savaş SARIKÇI, Semi ATASÖZ, Muammer SONSUZ for their helps.

I am also thankful to the Çukurova University Scientific Research Projects Unit for supporting my thesis with Project No: FDK-2017-9622. I would like to thank Dr. Sibel AKÇA-ÖZALP, Dr. Ziyafer Gizem PORTAKAL-UÇAR, Dr. Kenan BULCAR exclusively for their extra supports to me while working remotely.

I am grateful to my family, especially to my wife Seda, for supporting me and giving me strength to overcome the difficulties which I faced during my thesis study.

CONTENTS **PAGE**

LIST OF TABLES **PAGE**

LIST OF FIGURES **PAGE**

ABBREVIATIONS

b	: Kinetic order
CGCD	: Computerized Glow Curve Deconvolution
E	: Activation energy
E_a	: Activation energy level
E_c	: Conduction band energy level
E_f	: Fermi energy level
E_T	: Trap energy level
E_v	: Valence energy level
eV	: Electron volt
Gy	: Grey
h	: Concentration of trapped holes
I_m	: Maximum intensity value or peak intensity
k	: Boltzmann constant
N	: Concentration of electron traps
$NaBaBO_3$	: Sodium barium borate
$NaBaBO_3:Ce^{3+}$	: Cerium doped sodium barium borate
$NaBaBO_3:Gd^{3+}$	: Gadolinium doped sodium barium borate
$NaBaBO_3:Tb^{3+}$	: Terbium doped sodium barium borate
n	: Concentration of trapped electrons
n_c	: Concentration of free electrons in conduction band
n_0	: concentration of trapped electrons at $t = 0$
OTOR	: One trap one recombination center
OSL	: Optically stimulated luminescence
p	: Escape probability of an electron from trap
t	: Time in seconds
s	: Vibration frequency of electrons or frequency factor
sec	: Seconds

T	: Absolute temperature in Kelvin
T_0	: Temperature at $t = 0$
T_m	: Peak temperature
T_r	: Re-trapping probability
TL	: Thermoluminescence
TLD	: Thermoluminescence dosimeter
XRD	: X-ray diffraction
VHR	: Various heating rates

1. INTRODUCTION

Radiation is physical reality of nature. In physics, it can be described as transfer of the energy as waves or particles. There are many scientific studies which are already using types of radiation in order to study and learn more about the natural mechanisms and then create new technologies if possible. It is used in many human activities; medical activities, generating electricity, academic studies, industrial activities, space exploration, agriculture, archeology, law enforcement, geological activities, scientific research centers which are using particle accelerators (linear and/or circular types) and etc. But working with the radiation requires monitoring and protection. For monitoring, dosimeters (as solid-state detectors) are also used besides the gas-filled detectors, and scintillators.

1.1. Thermoluminescence

An insulator or semiconductor material absorbs some energy when irradiated and then if they are heated this deposited energy is released as photon emission; this physical phenomenon is known as thermoluminescence. Here “thermo” word is meaning thermal energy and should not be understood as the primary source for electron induction. There is another physical phenomenon, incandescence in which a material starts to glow when heated beyond ~200°C. This is because heated material releases the vibration energy as photons, and this phenomenon is also known as “thermal radiation” or “blackbody radiation”. Incandescence and the thermoluminescence are two different physical phenomena and thermoluminescence should not be confused with it. In other words, for thermoluminescence material firstly needs to be exposed to a radiation source then heated. If such material assumed to be heated up to ~450°C linearly then cooled to room temperature, all the electrons which were excited via radiation will be in their stable states again. If heated one more time after this process, only emission will be due to thermal radiation and/or internal structural defects of the crystal structure. In

order to get the previous thermoluminescence emission, such material should once more be irradiated then heated.

In thermoluminescence, primary source for the induction of electrons of insulator or semiconductor materials is the radiation. Induced electrons can pass the forbidden energy gap of material no matter the material is semiconductor or insulator. With the effect of absorbed energy, electrons can go free from valence energy state to conduction band; but this is not a stable state for them and such electrons tend to go back to stable energy state. But some of them are trapped between the valence and conduction bands. Such traps are either due to internal defects or impurities of crystal structure. Energy state for this electron trap is also metastable and depending on the energy of trap which electrons can stay in such metastable energy states from minutes up to 4.9×10^9 years (McKeever, 1985).

When such materials are heated, those trapped electrons once more will go to conduction band and when they recombine with the holes, energy difference will be released as photon. As mentioned above, this type of phosphorescence which uses thermal energy - to release the deposited energy of irradiation via trapped electrons-called as “thermoluminescence” (McKeever, 1985). But some of the researchers preferred naming this phenomenon as “Radiation Induced Thermally Stimulated Luminescence (RITSL)”. Some others shorten this as “radio thermo luminescence (RTL)” with emphasizing the role of radiation in induction of the electrons. And some of the researchers prefer naming as “Thermally Stimulated Luminescence (TSL)” (McKeever et al.,1995). But in contemporary studies in the literature, thermoluminescence (TL) is used (McKeever et al., 1995; Sunta, 2015).

Dosimeters are solid state detectors which can absorb some of the incident radiation’s energy during the exposure to radiation. Active dosimeters show this dose rate immediately and cumulative dose amount as well, passive dosimeters show the recorded total dose at reading and require reading periodically. Dosimeter types can be classified mainly with respect to their sensitivity range and/or particle

type which they are sensitive to. Hence, they can be concluded as personnel, environmental, clinical, and high dose dosimeters.

In the readout phase of energy deposition, which is stored within the dosimeter, a stimulation process is applied. In this thesis, temperature is used for the stimulation process. Since temperature is stimulator here, process is mainly named as “thermally stimulated luminescence” or very commonly used form in contemporary literature “thermoluminescence”. Dosimeters which are sensitive for such a process is named “thermoluminescence dosimeters” (TLDs). Photon emission during the thermal stimulation is recorded as TL intensity versus temperature and resulting pattern is one or more peaks in a total spectrum of emitted photons. Number of emitted photons is proportional to the absorbed dose.

Other than the standard thermoluminescence dosimeters (TLDs) there are many studies for solid state dosimetry on many types of material including boron-based ones. Turkey owns more than half of globally known borate mineral deposit reserves on planet Earth. Thus, studies using this richness has another important point beside the importance of their subject.

1.2. Thesis Statement

In this thesis study, synthesis process and TL analyses of undoped sodium-barium-borate ($NaBaBO_3$), Cerium (Ce) activated sodium-barium-borate ($NaBaBO_3:Ce^{3+}$), Gadolinium (Gd) activated sodium-barium-borate ($NaBaBO_3:Gd^{3+}$), Terbium (Tb) activated sodium-barium-borate ($NaBaBO_3:Tb^{3+}$), ytterbium (Yb) activated sodium-barium-borate ($NaBaBO_3:Yb^{3+}$), and Europium (Eu) activated sodium-barium-borate ($NaBaBO_3:Eu^{3+}$) materials had been synthesized and studied in detail to determine their thermoluminescence characteristics.

This Ph.D. thesis consists of five chapters. In the “introduction” chapter general and brief information about the radiation, dosimeters thermoluminescence are given.

In the “literature review” chapter, international standard TLDs, their chemical structures are given. Other than that; examples of dosimetry material studies and a classification about the materials are told.

“Material and method” chapter has more information about the required chemical materials to synthesize the $NaBaBO_3$, $NaBaBO_3:Ce^{3+}$, $NaBaBO_3:Gd^{3+}$, $NaBaBO_3:Tb^{3+}$, $NaBaBO_3:Yb^{3+}$, and $NaBaBO_3:Eu^{3+}$. Besides that, laboratory equipment is also introduced under methods subtitle. Chemical equations and detail about the synthesis, general information about the x-ray diffraction (XRD) analysis and its purpose, TL, TL kinetic models, methodology of TL analysis steps for TL characterization are given under “methods” subtitle.

In the “results and discussion” chapter, all the experimental procedures of abovementioned undoped and doped versions of $NaBaBO_3$ phosphors are given starting from the chemical synthesis, XRD analysis results of each material set. Then, each step of thermoluminescence characterization analyses is given with detail.

In the “conclusions” chapter, all the obtained results from the calculations through analyses, and observations from the experiments are concluded. And then recommendations are given for the researchers if they use this thesis work as a source for them.

2. LITERATURE REVIEW

Thermoluminescence phenomenon has been known for a long time. It was scientifically and experimentally proven by Du Fay in 1738 (Du Fay, 1738) as "delayed phosphorescence" when working on natural quartz mineral which is now known as natural TL material. But utilization of thermoluminescence phenomenon in dosimetry happened in 1953 by Farrington Daniels, Charles A. Boyd, Donald F. Saunders with the title of "Thermoluminescence as a Research Tool" (Daniels et al., 1953).

Many insulators or semiconductors have been subject to TL dosimetry studies in literature with the purpose of developing new TLD materials. Some of them are internationally accepted as standard TL dosimeters (e.g., TLD-100 which is Magnesium (Mg) and Titanium (Ti) doped LiF; TLD-200 which is Dysprosium (Dy) doped CaF_2; TLD-300 which is Thulium (Tm) doped CaF_2; TLD-400 which is Manganese (Mn) doped CaF_2). Other than the standard TLDs, there are also studies on many insulators or semiconductor phosphors for TL dosimetry (Milijanic et al., 2002; Fasasi et al., 2007; Sanyal et al., 2010; Rozalia et al., 2016; Begum et al., 2018).

Boron based structures are also utilized in such studies. Those structures are known for their chemically and thermally stability. Besides, they are capable of forming different structures.

$NaBaBO_3$ crystal structure was reported in 1995 (Tu and Keszler, 1995) with solid state synthesis routine. But in this thesis study it was synthesized with combustion synthesis routine and studied with beta particle radiation for its TL properties first time in the literature.

In this chapter only the TL studies related literature review will be given for TL studies of some of the borate materials, although they can be found in some other studies for other properties other than TL dosimetry. Since this thesis study contains the TL results of undoped, Tb^{3+}, Ce^{3+}, and Gd^{3+} doped $NaBaBO_3$ results,

some of the Tb^{3+}, Ce^{3+}, and Gd^{3+} activated borate structures utilized in TL dosimetry studies are concluded from the literature below:

Nagpure and Omanwar reported TL and photoluminescence (PL) properties of Tb^{3+} doped $NaSrBO_3$ with different concentrations (as 0.1, 0.5, 1, 2%). For their study, crystal structure was synthesized by combustion synthesis method. As reported in their study, TL glow curve of 1% Tb^{3+} doped sample's which was recorded after gamma irradiation has single peak at around 434 K (or at 161 °C). Other than that, they also reported the TL sensitivity of their samples to be greater than LiF:Mg, Cu, P in terms of the TL intensity. They also reported the trap depth as 0.897 eV and vibration frequency of the trapped electrons as 8.75×10^{9} s^{-1}, and second order kinetics from the geometrical factor of the peak shape (Nagpure and Omanwar, 2012).

Hemam et al. reported the TL properties of Tb^{3+} doped CaB_4O_7. They reported that synthesis routine was solution combustion and thermal annealing treatment. 1% Tb^{3+} doped sample was also reported to be optimal value for the TL quality of the material after irradiated with beta particles. After deconvolution of the peaks, they also reported the structure have five electron traps located at respectively 145, 276, 312, 352, 399 °C with the depths respectively as 0.67, 1.19, 1.39, 1.47, 1.71 eV; and escape frequencies of those trap levels respectively as 2.23×10^{7}, 1.81×10^{10}, 2.01×10^{11}, 1.41×10^{11}, 1.36×10^{12} s^{-1}; and with the kinetic orders respectively as 2, 1.4, 2, 2, 2. In their study they also reported the OSL properties of this material (Hemam et al., 2018).

In another TL study, Jiang et al. reported the TL properties of Thulium activated $LiSrBO_3$. For the synthesis they used high temperature solid state reaction. For the TL study they irradiated the samples with gamma rays. For the optimal concentration of Tm^{3+}, in terms of TL sensitivity, found to be 1%. After the CGCD analysis, they also reported the peaks to be located at 118.92, and 193.58 °C; and trap depths of the peaks to be 0.63, and 0.96 eV respectively;

escape frequencies of trapped electrons respectively as 2.62×10^{7}, and 5.85×10^{9} s^{-1}; and kinetic orders as 1.26, and 2 respectively (Jiang et al., 2010).

Yazici et al. reported the TL dosimetry properties of Ce^{3+} activated, and undoped BaB_4O_7 samples. In their study they used melting method to synthesize the samples. They also irradiated the samples with beta particles for TL experiments. After CGCD analysis they have reported the TL glow curve to have four peaks for undoped BaB_4O_7 and five peaks for Ce^{3+} doped BaB_4O_7 sample. Peak locations of those four peaks for undoped sample were reported to be at 117±4, 195±2, 255±4, 365±4 °C respectively; trap depths were reported as 0.41±0.04, 0.79±0.08, 0.32±0.04, 0.91±0.09 eV respectively; natural logarithm of vibration frequency was reported as 11.13±1.2, 18.61±2, 5.12±1, 5.24 respectively; kinetic order for each peak was reported as 1, 1.18±0.1, 1, 1. Peak temperature for aforementioned five peaks of Ce^{3+} doped BaB_4O_7 sample were reported to be at 90±3, 135±2, 195±2, 250±2, 331±2 °C respectively; trap depth for each peak was reported as 0.6±05, 0.5±0.05, 0.97±0.1, 1.01±0.1 eV respectively; natural logarithm values of vibration frequency of trapped electron were reported to be 18.65±1.8, 13.3±1.3, 23.5±2, 22±2.2, 18.3±1.7 respectively; and kinetic order was reported to be 1, 1, 1.41±0.15, 1.31±0.1, 1.12±0.1 respectively for each peak (Yazici et al., 2006).

In 2007, Jiang at al., published an article about the TL properties of Ce^{3+} activated $LiSr_4(BO_3)_3$. Samples were synthesized by high temperature solid state reaction for 0.5, 1, 2, 4, 6, 8% Ce^{3+} molar concentrations. They have irradiated their samples with gamma ray. Regarding the TL glow curve intensity, they have reported optimal Cerium concentration as 1 mol%. Resulting TL glow curve also reported to exhibit single peak around at 200 °C. Trap depth of this peak, vibration frequency of the trapped electrons, and kinetic order were also reported to be, respectively, 1.095 eV and 2.949×10^{10} s^{-1}, and 2 (Jiang et al., 2007).

In 2017, Dogan et al. published an article about the TL results of Ce^{3+} doped ZnB_2O_4 phosphor. They have synthesized their samples with nitric acid

method to produce ZnB_2O_4 phosphors with different Ce^{3+} concentrations. They have calculated the kinetic parameters using VHR method on the glow curves of the samples which were recorded after beta irradiation. In their analysis they have used 1, 4, 10% Ce^{3+} doped ZnB_2O_4 samples. They have concluded that TL behavior can be different for different amount of dopant concentrations, regarding the VHR behavior of the samples which they studied on. They have also reported that glow curves exhibited two peaks that one of them is located around 75 °C and the other one is around 150 °C. For 1% Ce^{3+} doped sample: activation energy, respectively for the first and second peak, 0.49±0.02, 0.61±0.02 eV; frequency factor as 1.23×10^6, 1.82×10^6 s^{-1} respectively. For 4% Ce^{3+} doped sample: activation energy, respectively for the first and second peak, 0.47±0.02, 0.62±0.02 eV; frequency factor as 9.12×10^5, 2.27×10^6 s^{-1} respectively. For 10% Ce^{3+} doped sample: activation energy, respectively for the first and second peak, 0.53±0.02, 0.65±0.03 eV; frequency factor as 8.94×10^6, 6.76×10^6 s^{-1} respectively (Dogan et al., 2017).

Annalakshmi et al. synthesized undoped, Gd^{3+} doped, Gd^{3+} and Li^{1+} co-doped MgB_4O_7 samples via solid state sintering method. For the Gd^{3+} activated sample was reported to be synthesized for 0.05, 0.1, 0.2, 0.3, 0.4, 0.5 mole%; and for the TL quality, 0.2% Gd^{3+} concentration was observed as the optimal one. In their study, they have irradiated their samples with gamma rays. They have also reported that Gd^{3+} doped sample exhibited single peak around at 250 °C. In this study they also co-doped the Gd^{3+} doped sample with Li^{1+} ions and they observed that this co-doped sample has as much as five times higher intensity than the Harshaw brand TLD-100 (Annalakshmi et al., 2013).

Leonardo V.S. França and Oswaldo Baffa published an article about the TL/OSL results of undoped, Gd^{3+} doped, Ag^{1+} doped, Gd^{3+} and Ag^{+1} co-doped CaB_6O_{10} phosphors via solid state reaction and irradiated their samples with x-rays. Optimal concentrations were found to be as 2% for Gd^{3+} doped; 0.1% for Ag^{1+} doped CaB_6O_{10} samples from the OSL studies and same used for TL. For the co-

doped sample study 2% Gd^{3+} co-doped with 0.1% Ag^{1+}, and 2% Gd^{3+} co-doped with 0.5% Ag^{1+} concentrations were also prepared as they reported. In terms of the TL intensity, Gd^{3+} co-doped with Ag^{1+} samples showed higher intensity when compared to the Gd^{3+} doped, undoped, Ag^{1+} doped samples. In this study they did not give any detail about the TL kinetic parameters of the samples (Leonardo V.S. França and Oswaldo Baffa, 2020).

3. MATERIAL AND METHOD

3.1. Materials

3.1.1. Required Chemical Materials

3.1.1.1. Synthesis Materials of $NaBaBO_3$

In this Ph.D. thesis study; for the synthesis of main crystal structure of $NaBaBO_3$ following materials were used: Sodium nitrate-$NaNO_3$ as sodium source, barium nitrate-$Ba(NO_3)_2$ as barium source, boric acid-H_3BO_3 as boron source, urea-$CO(NH)_2$ as fuel, and ammonium nitrate-NH_4NO_3 as oxidizer. Details about those materials are given in Table 3.1 below.

Table 3.1. Required chemical materials for the synthesis of $NaBaBO_3$

Material	CAS Number	Brand and Purity	Purpose
$NaNO_3$	7631-99-4	Sigma-Aldrich (99.9%)	Na source
$Ba(NO_3)_2$	10022-31-8	Sigma-Aldrich (99.9%)	Ba source
H_3BO_3	10043-35-3	Alfa Aesar (99.9%)	B source
CH_4N_2O	57-13-6	Sigma-Aldrich (99.9%)	fuel
NH_4NO_3	6484-52-2	Sigma-Aldrich (99.9%)	oxidizer

3.1.1.2. Synthesis Materials of Cerium (Ce^{3+}) Doped $NaBaBO_3$

Synthesis of Ce^{3+} doped $NaBaBO_3$, with different rate of cerium concentrations required the following materials: Sodium nitrate-$NaNO_3$ as sodium source, barium nitrate-$Ba(NO_3)_2$ as barium source, boric acid-H_3BO_3 as boron source, urea-$CO(NH)_2$ as fuel, ammonium nitrate-NH_4NO_3 as oxidizer, and for dopant material, here cerium, cerium nitrate is used. In Table 3.2 some necessary details of above-mentioned materials' which are required for the synthesis of cerium doped $NaBaBO_3$ are tabulated. That information is chemical formula, chemical abstracts service (CAS) number, brand, purity, purpose of usage for the synthesis process of cerium doped $NaBaBO_3$ phosphor.

Table 3.2. Required chemical materials for the synthesis of $NaBaBO_3:Ce^{3+}$

Material	CAS Number	Brand	Purpose
$NaNO_3$	7631-99-4	Sigma-Aldrich (99.9%)	Na source
$Ba(NO_3)_2$	10022-31-8	Sigma-Aldrich (99.9%)	Ba source
H_3BO_3	10043-35-3	Alfa Aesar (99.9%)	B source
CH_4N_2O	57-13-6	Sigma-Aldrich (99.9%)	fuel
NH_4NO_3	6484-52-2	Sigma-Aldrich (99.9%)	oxidizer
$Ce(NO_3)_3 \cdot 6H_2O$	10294-41-4	Sigma-Aldrich (99.9%)	Ce source

3.1.1.3. Synthesis Materials of Gadolinium (Gd^{3+}) Doped $NaBaBO_3$

For the synthesis of Gd^{3+} doped $NaBaBO_3$ sodium nitrate-$NaNO_3$ is used as sodium source; barium nitrate-$Ba(NO_3)_2$ is used as barium source; boric acid-H_3BO_3 is used as boron source; urea-$CO(NH)_2$ is used as fuel; ammonium nitrate-NH_4NO_3 is used as oxidizer; for dopant material, -gadolinium- gadolinium nitrate is used. Table 3.3 gives the details of those employed materials.

Table 3.3. Required chemical materials for the synthesis of $NaBaBO_3:Gd^{3+}$

Material	CAS Number	Brand and Purity	Purpose
$NaNO_3$	7631-99-4	Sigma-Aldrich (99.9%)	Na source
$Ba(NO_3)_2$	10022-31-8	Sigma-Aldrich (99.9%)	Ba source
H_3BO_3	10043-35-3	Alfa Aesar (99.9%)	B source
CH_4N_2O	57-13-6	Sigma-Aldrich (99.9%)	fuel
NH_4NO_3	6484-52-2	Sigma-Aldrich (99.9%)	oxidizer
$Gd(NO_3)_3 \cdot 6H_2O$	19598-90-4	Sigma-Aldrich (99.9%)	Gd source

3.1.1.4. Synthesis Materials of Terbium (Tb^{3+}) Doped $NaBaBO_3$

As the starting materials for the synthesis of Tb^{3+} doped $NaBaBO_3$; sodium nitrate-$NaNO_3$ is used as sodium source; barium nitrate-$Ba(NO_3)_2$ is used as barium source; boric acid-H_3BO_3 is used as boron source; urea-$CO(NH)_2$ is used as fuel; ammonium nitrate-NH_4NO_3 is used as oxidizer; for dopant material, terbium nitrate is used as terbium source. Table 3.4 gives the details of the chemical materials employed in the synthesis of terbium doped $NaBaBO_3$.

Table 3.4. Required chemical materials for the synthesis of $NaBaBO_3:Tb^{3+}$

Material	CAS Number	Brand and Purity	Purpose
$NaNO_3$	7631-99-4	Sigma-Aldrich (99.9%)	Na source
$Ba(NO_3)_2$	10022-31-8	Sigma-Aldrich (99.9%)	Ba source
H_3BO_3	10043-35-3	Alfa Aesar (99.9%)	B source
CH_4N_2O	57-13-6	Sigma-Aldrich (99.9%)	fuel
NH_4NO_3	6484-52-2	Sigma-Aldrich (99.9%)	oxidizer
$Tb(NO_3)_3 \cdot 5H_2O$	57584-27-7	Sigma-Aldrich (99.9%)	Tb source

3.1.1.5. Synthesis Materials of Ytterbium (Yb^{3+}) Doped $NaBaBO_3$

For the synthesis of Yb^{3+} doped $NaBaBO_3$; sodium nitrate-$NaNO_3$ is used as sodium source; barium nitrate-$Ba(NO_3)_2$ is used as barium source; boric acid-H_3BO_3 is used as boron source; urea-$CO(NH)_2$ is used as fuel; ammonium nitrate-NH_4NO_3 is used as oxidizer; for dopant material, ytterbium nitrate is used as Yb^{3+} source. Tabulated information in Table 3.5 is about the materials required for this synthesis.

Table 3.5. Required chemical materials for the synthesis of $NaBaBO_3:Yb^{3+}$

Material	CAS Number	Brand and Purity	Purpose
$NaNO_3$	7631-99-4	Sigma-Aldrich (99.9%)	Na source
$Ba(NO_3)_2$	10022-31-8	Sigma-Aldrich (99.9%)	Ba source
H_3BO_3	10043-35-3	Alfa Aesar (99.9%)	B source
CH_4N_2O	57-13-6	Sigma-Aldrich (99.9%)	fuel
NH_4NO_3	6484-52-2	Sigma-Aldrich (99.9%)	oxidizer
$Yb(NO_3)_3 \cdot 5H_2O$	35725-34-9	Sigma-Aldrich (99.9%)	Yb source

3.1.1.6. Synthesis Materials of Europium (Eu^{3+}) Doped $NaBaBO_3$

For the synthesis of Eu^{3+} doped $NaBaBO_3$; sodium nitrate-$NaNO_3$ is used as sodium source; barium nitrate-$Ba(NO_3)_2$ is used as barium source; boric acid-H_3BO_3 is used as boron source; urea-$CO(NH)_2$ is used as fuel; ammonium nitrate-NH_4NO_3 is used as oxidizer; for dopant material, europium nitrate is used as Eu^{3+} source. Tabulated information in Table 3.6 is about the materials required for synthesis of europium doped $NaBaBO_3$.

Table 3.6. Required chemical materials for the synthesis of $NaBaBO_3:Eu^{3+}$

Material	CAS Number	Brand and Purity	Purpose
$NaNO_3$	7631-99-4	Sigma-Aldrich (99.9%)	Na source
$Ba(NO_3)_2$	10022-31-8	Sigma-Aldrich (99.9%)	Ba source
H_3BO_3	10043-35-3	Alfa Aesar (99.9%)	B source
CH_4N_2O	57-13-6	Sigma-Aldrich (99.9%)	fuel
NH_4NO_3	6484-52-2	Sigma-Aldrich (99.9%)	oxidizer
$Eu(NO_3)_3 \cdot 5H_2O$	63026-01-7	Sigma-Aldrich (99.9%)	Eu source

3.1.1.7. Absolute Ethanol and Acetone

Laboratory equipment are carefully cleaned before and after using each production process. One of the absolute ethanol (C_2H_5OH) and acetone (C_3H_6O) was used for the purpose of such cleaning of unwanted residuals from the surface of the physical equipment used.

3.1.2. Laboratory Equipment

3.1.2.1. Analytical Balance

All the chemical input materials which were used to synthesize all subject materials within the scope of this Ph.D. thesis work, weighed out with Precisa brand digital analytical balance (Figure 3.1). This balance has; 0.1mg weighing out sensitivity, from 0.1mg up to 220g weighing out range, 0.2mg tolerance, four adjustable legs to level horizontally, water gage to check the adjusted level, calibration.

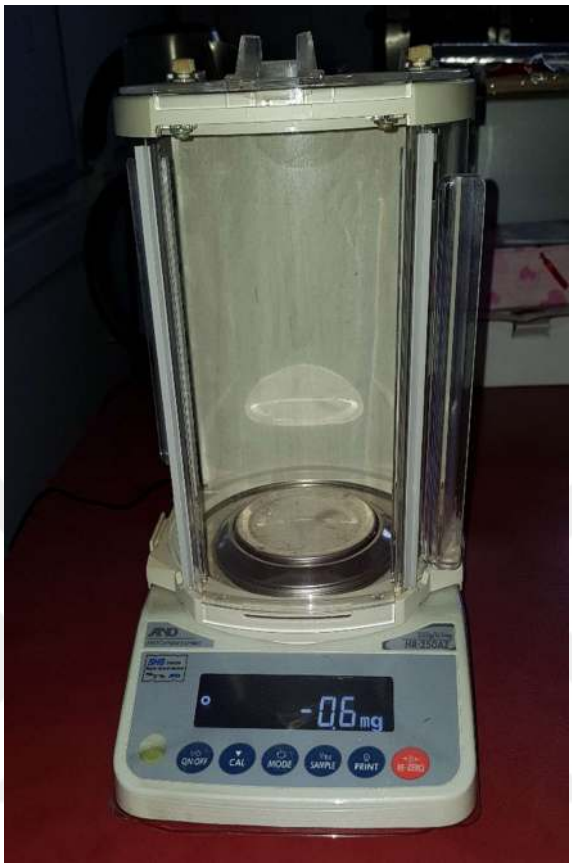

Figure 3.1. Precisa brand digital analytical balance

3.1.2.2. Agate Mortar

In this study, all of the chemical materials of all syntheses' inputs' mixtures were pestled by using an agate mortar (Figure 3.2.). Purpose of this process is to make powder formed materials be more homogenous in terms of particle size, and to avoid the effect of triboluminescence. Besides this also makes the mixture mix well. This process is also applied to resulting materials of all syntheses. Agate mortar is very strong and resistant against scratches, and hard to get broken; hence pestling process is guaranteed that no contamination might appear from its surface to the material which is pestled within it.

Figure 3.2. Agate mortar which was used to pestle all chemical inputs and output materials

3.1.2.3. Alumina Crucible

For the synthesis of each studied material of this thesis work, an individual alumina crucible belonging to each synthesis was used. The purpose of selecting such crucibles made of alumina is both to be resistant to the high melting effect of boric acid and sodium nitrate when they become liquid at the temperature levels reached for the reactions of this thesis study and to be affordable compared to platinum crucibles. One of the crucibles which was used during one of the production processes of object materials of present thesis can be seen in Figure 3.3. For the production purposes undoped (1) and Ce-doped (6), Gd-doped (6) , Yb-

doped (6), Eu-doped (6), Tb-doped (6) $NaBaBO_3$ phosphor samples, 31 in total of such crucibles were used for each dopant concentration's production. Each of them was used first time while synthesizing corresponding material synthesis process.

Figure 3.3. One of the alumina crucibles which were used for the syntheses.

3.1.2.4. Ash Furnace

All of the synthesis processes are completed by using a "Protherm" brand ash furnace which is programmable and makes it possible to apply any required heating process plan. As an example, it is possible to program this device via its front panel to work at different temperatures for desired temperatures and durations either linearly or non-linearly. Top heating capacity of this furnace is 1350°C but it is advised in its manual to use it 1300°C for maximum temperature. This model does not contain any extra inert gas atmosphere possibility, which means all the

reactions were occurred under normal atmospheric conditions. In Figure 3.4 Protherm brand ash furnace is shown.

Figure 3.4. Protherm brand ash furnace.

3.1.2.5. Hydraulic Press

All the subject materials of this thesis study, ground after reaction via agate mortar and then converted into pellet formed samples before the measurement. For this purpose, "Carver" brand hydraulic press used. All of the powder samples stressed under 2 ton/cm^2(196.1 MPa) pressure.

Figure 3.5. Carver brand hydraulic press and its parts.

In the Figure 3.5 carver brand, hydraulic press can be seen. All the samples which are studied in this thesis work were turned into pellet by using this press machine. Each time of pressing process, each part of the machine which contacts with the material were cleaned with absolute methanol carefully to protect each sample from the contamination probability of any unwanted material. Surface of the parts contacting with sample are made of stainless steel.

3.1.2.6. Lexyg Smart TL/OSL Reader System

In this thesis study, thermoluminescence experiments were conducted via using Lexyg Smart thermoluminescence/optically stimulated luminescence (TL/OSL) reader system which can be seen in Fig.3.6.

Figure 3.6. Freiberg Instruments Lexyg Smart TL/OSL reader system.

This automated reader TL/OSL system has β source internally, namely this source is $^{90}Sr/^{90}Y$, and as of recent updated calibration shows that its irradiation rate is 0.11 Gy/s. System holds samples via planchets positioned on sample wheel (carousel) which is on the tray (Fig.3.7). This way it is possible to hold the samples separate from the measurement chamber for elimination of cross irradiation and effects of bleaching during OSL, between the samples on the queue and the one being measured (Richter et al., 2012; 2013).

Figure 3.7. Sample cups(planchets) on the sample wheel(carousel).

Samples to be measured are placed on the sample wheel (carousel) within cup/disc (planchet) to be separated from measurement chamber due to aforementioned reasons. The cups have radius ~10mm, thickness of 0.5mm, and a maximum height of 2.5mm (sample included). Sample wheel is removable and thus it is possible to replace it with another sample wheel for an efficient work in terms of time management. Other than that, there is also possibility to remove, add, and/or change of planchets while a measurement is ongoing but only when there is no transportation in between the sample wheel and measurement chamber (Richter et.al, 2015).

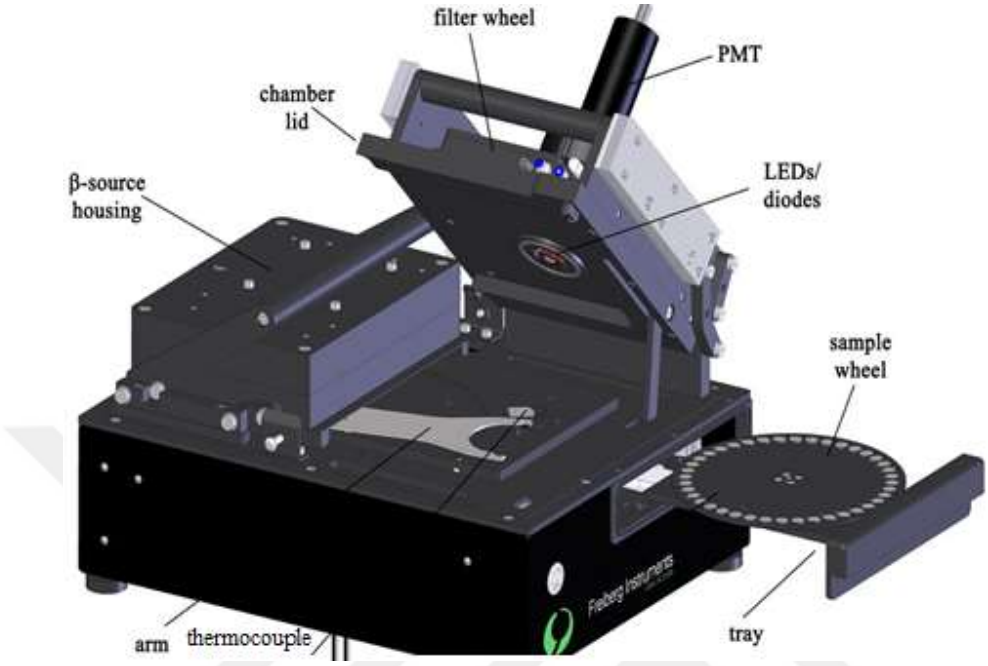

Figure 3.8. Freiberg Instruments Lexyg Smart TL/OSL reader system's schematic view (Richter et al., 2015).

When a sample is targeted for measurement, its position on the sample wheel is turned to match the sample elevator's position. Then, it is lifted from its position through a slit via a piston (sample elevator) into the measurement chamber. After that point on sample's position controlled via a sample arm, in between the positions top of slit, heater, and irradiation source's chamber. Measurement chamber gets sealed before any stimulation process starts. This protects below awaiting samples on the sample wheel from unnecessary stimulations and also decreasing the nitrogen (N_2) gas consumption.

Heating element is also sealed with another material made of quartz (Sico SQ1), this part can be evacuated and filled with inert gas (Richter et. al, 2015). Filter wheel, chamber lid and source shutter are pneumatically controlled; but rest of the mechanical actions are controlled via electrical step motors (Richter et. al, 2015).

Heater unit has the ability of heating rate from 0.1 up to 20 Ks^{-1}. This part is metal plated ceramic and can heat the sample homogenously again and again with the same sensitivity and accuracy (Lomax et. al, 2014). The Lexyg Smart system has the capability of OSL as well as TL, but this is beyond the scope of the current doctoral thesis study. Therefore, details on the OSL capabilities of the TL/OSL system are given here very briefly. For the OSL, system offers continuous wave OSL (Cw-OSL) and linear-modulated OSL (LM-OSL) modes at room and elevated temperatures, and user defined measurement time and light emitting diode (LED) power which is in unit of $mW \cdot cm^{-2} \cdot s^{-1}$ and has a deviation smaller than 0.2% (Lomax et. al, 2014).

Freiberg Instruments Lexyg Smart TL/OSL reader system has one photomultiplier tube (PMT) and optical bandpass filters located between measured sample and the PMT for luminescence detection. Luminescence emission from sample might have different wavelengths; and those wavelengths may correspond different physical properties. For that reason, a need of restriction -which can be achieved by filters-in the detection arises (Rendell et al., 1993; Townsend, 1994; Krbetschek et al.; Huntley et al.) In the system there is a filter module for combinations of filters. Sizes for such band pass filters are 1 inch (25.4 mm) for diameter and up to 7.5mm for height. There is also a filter changer part which helps to change filter combination. Thus, bands of the detection wavelength which will be used while working on a sample is also changed. Its mechanism is pneumatic as aforementioned. Gas pressure is supplied with the nitrogen gas tube which is also used for cooling of the sample. It has 6 positions for filters, height is limited up to 7.5mm. In the Table 3.7 possible detector filter combinations of present filter module, and the names of filters in the combinations.

Table 3.7. Filter combinations which are installed on the present system

Name of Combination	Filter (height)
BSL, TL- 365nm	• Hoya-U340-Glass (2.5mm) • Delta-BP 365/50 EX-Interference (5mm)
BSL, TL- 365nm (0.25)	• Hoya-U340-Glass (2.5mm) • Delta-BP 365/50 EX-Interference (5mm) • Schott-NG 4-Glass(1.2mm)
IRSL, TL- 410nm	• Schott-BG 39-Glass (3mm) • AHF-Brightline HC 414/46 interference (3.5mm)
IRSL, TL- 410nm (0.25)	• Schott-BG 39-Glass (3mm) • AHF-Brightline HC 414/46 interference (3.5mm) • Schott-NG 4-Glass(1.2mm)
IRSL, TL- 565nm	• Schott-BG 39-Glass (3mm) • AHF-Brightline HC 575/25 interference (5mm)
IRSL, TL wideband blue	• Schott-KG 3-Glass(2mm) • Schott-BG 25-Glass(3mm) • Schott-BG 39-Glass(3mm)

From the Table 3.7 names of the filter combinations and individual name of each filter can be seen. Each filter has its own band pass wavelength. Here “BSL-TL 410 nm” and “IRSL, TL- 410nm” filter combinations have their secondary version with “(0.25)” which is meaning that PMT’s counter will decrease the photon count to ~1/4 of the original photon count per counting interval (photon channel time). This is done with the help of Schott-NG-Glass which has 1.2mm height. Wavelength transmission range of the combination is still the same; however, percentage of the light transmittance in terms of the number of photons is decreased in such process. Optimization of the filter combinations is done with consideration of the detection of target wavelength range while blocking

the stimulation light of OSL, and/or thermal noise of blackbody radiation/thermoluminescence (Richter et. al, 2015).

For the PMT, system is installed with a Hamamatsu bi-alkaline PMT which has 30% quantum efficiency for the wavelength range of 160-630nm (Richter et. al, 2015).

Lexyg Smart TL/OSL system is controlled with LexStudio software for every possible operation it can do. Graphical user interface of the system makes it possible for user to write a new or edit the existing measurement sequences. Visualization of the acquired data while the measurement is on-going is also possible. Collected measurement data is stored within an xsyg file which is lexyg format. In addition, all detailed information of the measurement settings supplied with the sequence file is also saved in this xsyg (Richter et. al, 2015). System also gives output with different formats. They are comma separated values (csv) files per sequence step, bin/binx, ASCII format.

Details of sequences for experiments of this thesis and analysis methodology will be given in “results and discussion” chapter.

3.2. Methods

3.2.1. Physical Mechanism and Kinetics of Thermoluminescence

The TL mechanism can be described by using band model of electron energy of solids. An ideal crystal structure of an insulator or a semiconductor possesses most of its outermost shell electrons at an energy level which is named valence band. Next energy level is conduction band, and those two energy levels are separated by a forbidden energy gap. But not all of the crystal structures are perfect, and they may have defects in their lattice structures and/or impurities that may give rise localized energy levels in between conduction band and valence band energy levels.

When a semiconductor or an insulator crystal structure is irradiated, pairs of electron-hole created. As electrons get free up to conduction band energy level,

in the valence band their corresponding pairs “holes” follow them on the valence band. When electrons move back to their energy-at-rest level they may move to the abovementioned localized energy levels (or electron traps in other words) which are between Fermi energy (E_F) level and conduction band energy (E_c) level as hole pairs of those electrons move to hole trap levels which are located between valence band energy (E_v) and E_F. The closer the electron trap energy level (E_T) to E_v, shallower it is; and corresponding hole trap level is so close to E_F.

In other words, the irradiation transfers some energy, and the electrons get to excited energy state with this energy. Those electrons tend to go back to stable energy level and this extra energy -which caused excitation- will be released as photons. Not all of the excited electrons fall back to valence band energy level; but may go to the localized energy levels of electron traps and stay at such energy levels unless an external source (like optical photons, temperature) stimulates and un-traps them. Those trapped electrons will get excited by thermal stimulation, and get free from the electron trap, and will go to E_c and then fall back and pair with the holes at the recombination centers thus energy differences are released as photons. Characteristics of each of the localized energy level is defined with:

- trap depth or activation energy (E_a) in eV
- frequency factor (s) in sec^{-1}
- kinetic order (b) which is unitless

The trapped electrons mentioned above are released even at room temperature (RT) depending on the depth of the energy level; but when excited by a linear heating rate, the photon emission progressively continue from shallow traps to deep traps (Chen and Kirsh, 1981). Additionally, such localized energy levels may be at similar levels. This causes the recorded photon emission versus either time or temperature to be combination of more than one distribution as

interwoven; thus, analyzing such structure is more different than single energy level. And after all the trapped electrons released only blackbody radiation will be observed; following this step, material cooled to RT, this time material thermally stimulated with the same linear heating rate as applied after irradiation step - background emission in other words-. Thus, only photon release from internal vibration energy and blackbody radiation will be observed. Difference of those two photon emissions with respect to the reference temperature values, will give the emission due to deposited energy only. In Figure 3.9, a characteristic TL spectrum of $NaBaBO_3$ is given as (a) emission of deposited energy + background emission, (b) background emission, and (c) emission of deposited energy are given. "IRSL,TL 565nm" filter combination was used to record with the optimal emission sensitivity. Applied irradiation dose is 5Gy of β and heating rate is 2 °C/s.

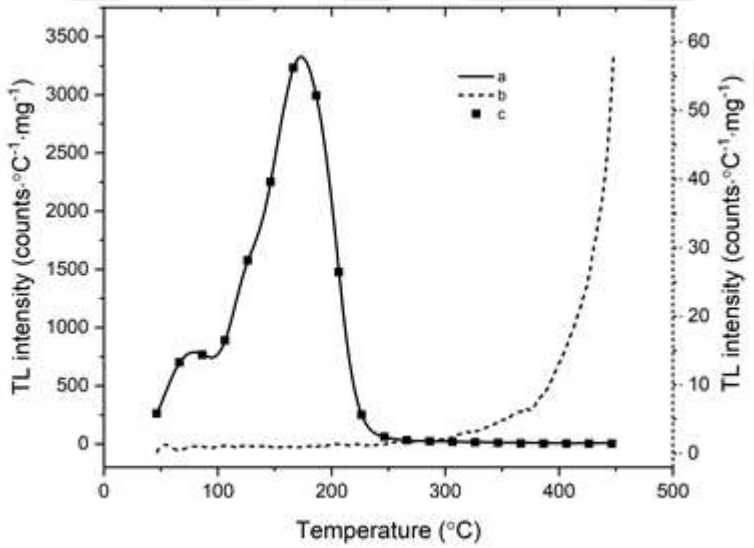

Figure 3.9. Curve "a" is the emission due to the deposited energy of irradiation+ background emission; "b" is background emission only; "c" is the background subtracted TL signal

The TL kinetics are used to describe the excitation, stimulation, and emission of the charge carriers, or electrons and holes namely; and uses

mathematical expressions to describe the model of the kinetics. Very general model is the starting point of such studies: “One Trap One Recombination” -or OTOR in abbreviation- model using energy band model given in Figure 3.10.

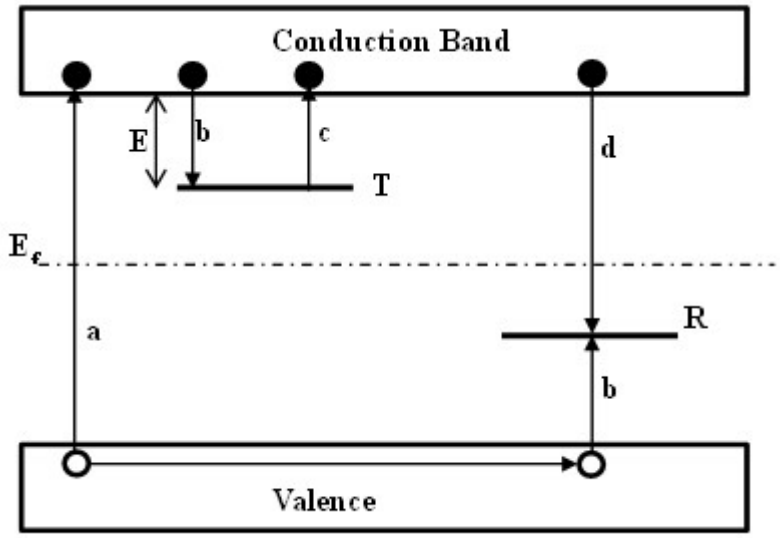

Figure 3.10. OTOR model (a) creation of electron-hole pair; (b) electron-hole gets trapped; (c) electron gets free with thermal stimulation; (d) recombination of electron and hole at recombination center. Here black and white circles are representing electron and hole respectively. Energy levels represented here with T and R are electron trap and recombination center, and Fermi energy level is given with E_f (McKeever et al., 1995)

In this model, escape probability per unit time for a trapped electron from a local electron trap energy level, during thermal stimulation can be expressed as;

$$p = s\,exp\left(-\frac{E}{kT}\right) \tag{3.1}$$

Where; p is the escape probability of trapped electron from the electron trap per unit time; E is the required energy for the electron to be released from the

trap ("activation energy" or "trap depth"); s is the vibration frequency or frequency factor; k is the Boltzmann constant; T is the absolute temperature in Kelvin (Chen and McKeever, 1997).

Probability of the recombination of electrons at the recombination center during thermal stimulation is;

$$R = I(t) = -\frac{dn}{dt} = -\frac{dh}{dt} = n_c A_h h \tag{3.2}$$

where n, n_c, and h are the concentration of trapped electron, concentration of free electrons in the conduction band, and concentration of trapped hole respectively at any time t. A_h is the constant of recombination probability for electron hole pair. Obtainable luminescence intensity is proportional to the recombination of free electrons in the conduction band with holes.

Re-trapping probability of electrons in the conduction band during thermal stimulation process can be given as;

$$T_r = n_c A_n (N - n) \tag{3.3}$$

where, n_c is concentration of free electrons in the conduction band, A_n is the constant of re-trapping of free electrons in the conduction band, N is the concentration of electron traps. This model assumes that each recombination of electron-hole produces a photon and each of those photons are detected. Luminescence efficiency (radiative transition efficiency) -during the thermal stimulation, and regarding both of the re-trapping and recombination probabilities of electrons- can be written as (Sunta, 2015);

$$F = \left(\frac{R}{R + T_r}\right) \tag{3.4}$$

Luminescence intensity can be written as a function of time with the given information about the escape, radiative transition, and re-trapping probabilities;

$$I(t) = -\frac{dn}{dt} = \frac{hA_h ns\, exp\left(-\frac{E}{kT}\right)}{(N-n)A_n + hA_h} \tag{3.5}$$

3.2.1.1. First Order Kinetics (Randall-Wilkins Approach)

Randall and Wilkins proposed that each of the trapped electrons, when thermally excited, would combine with a hole in the recombination center to emit a photon, or in other words, they assumed that probability of re-trapping these electrons is negligible (Randall and Wilkins, 1945).

$$I(t) = -\frac{dn}{dt} = ns\, exp\left(-\frac{E}{kT}\right) \tag{3.6}$$

The Eqn.3.6. is the differential equation for any TL emission -glow peak- that obeys the first-order kinetics. In the analysis of TL, temperature is usually increased linearly; temperature as a function of time is:

$$T(t) = T_0 + \beta t \tag{3.7}$$

here; β is the constant heating rate which means the increase in temperature per unit time. T_0 is the temperature at $\mathrm{t} = 0$. When Eqn.3.6 is updated and solved, it will give the results as given with Eqn.3.8:

$$I(t) = -\frac{dn}{dt} = n_0 s\, exp\left(-\frac{E}{kT}\right) exp\left(-s\int_0^t exp\left(-\frac{E}{kT(t')}\right)dt'\right) \tag{3.8}$$

where; n_0 is the number of trapped electrons at $t = 0$. And with Eqn.3.7, Eqn.3.8 transforms into TL intensity as a function of temperature;

$$I(T) = -\frac{1}{\beta}\frac{dn}{dt} = n_0 \frac{s}{\beta} exp\left(-\frac{E}{kT}\right) exp\left(-\frac{s}{\beta}\int_{T_0}^{T} exp\left(-\frac{E}{kT'}\right) dT'\right) \quad (3.9)$$

solution to the integral part of the equation 3.9 is;

$$\int_{T_0}^{T} exp\left(-\frac{E}{kT'}\right) dT' = \frac{kT^2}{E}\left(1 - \frac{2kT}{E}\right) exp\left(-\frac{E}{kT}\right) \quad (3.10)$$

Equation 3.9 is known as Randall-Wilkins equation for any single first order TL glow peak. Result of this equation will give a bell shaped but asymmetric distribution. Lower temperature half of the distribution of such a peak will be wider when compared to the higher temperature half with respect to the peak maximum temperature (T_m) where intensity of distribution gets the maximum value. In Figure 3.11 typical trends of temperature, TL intensity, and hole concentration are shown as a function of time during thermal stimulation with a linear heating rate for a first order single peak.

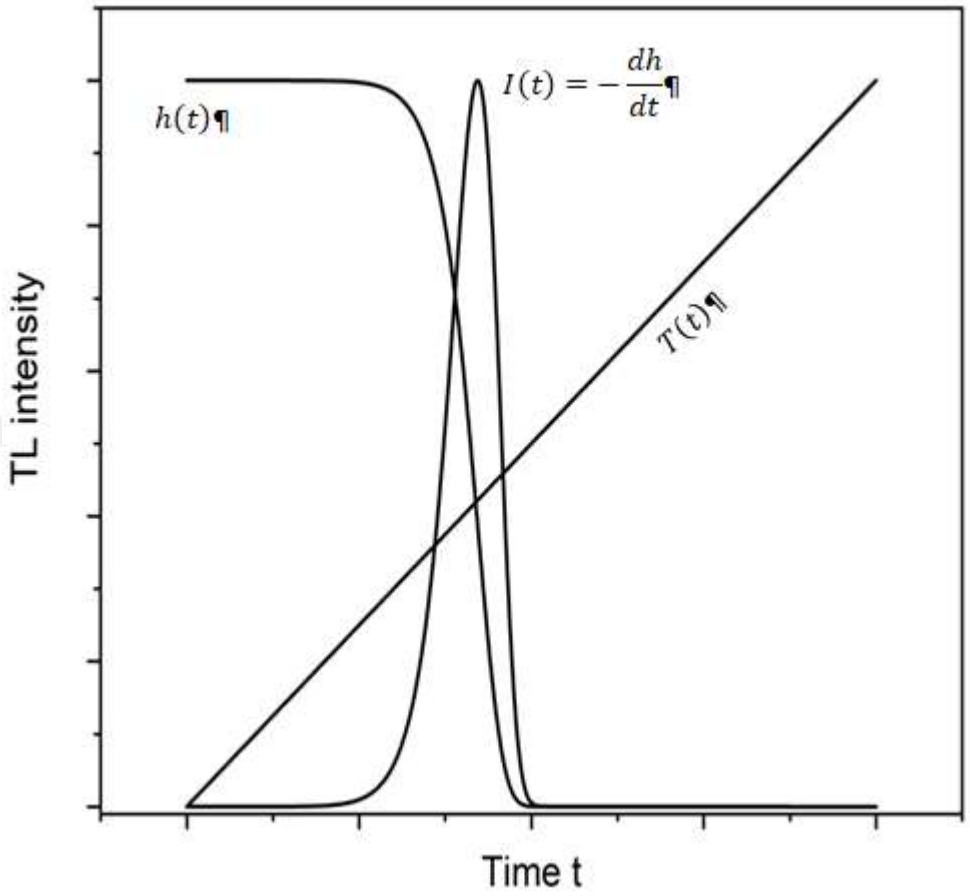

Figure 3.11. Temperature as a function of time, thermoluminescence intensity as a function of time, and concentration of holes as a function of time. This is a typical behavior for any first order peak emission, under a linear heating rate (Pagonis et al., 2006).

If $n_0 = 1$, $E = 1$ eV, $s = 10^{12}$ s^{-1}, and $\beta = 1$ K/s are applied to the Randall-Wilkins equation as initial parameters; and variate n_0, E, s, β respectively while keeping rest three parameters constant. This change is shown in Fig.3.12 below.

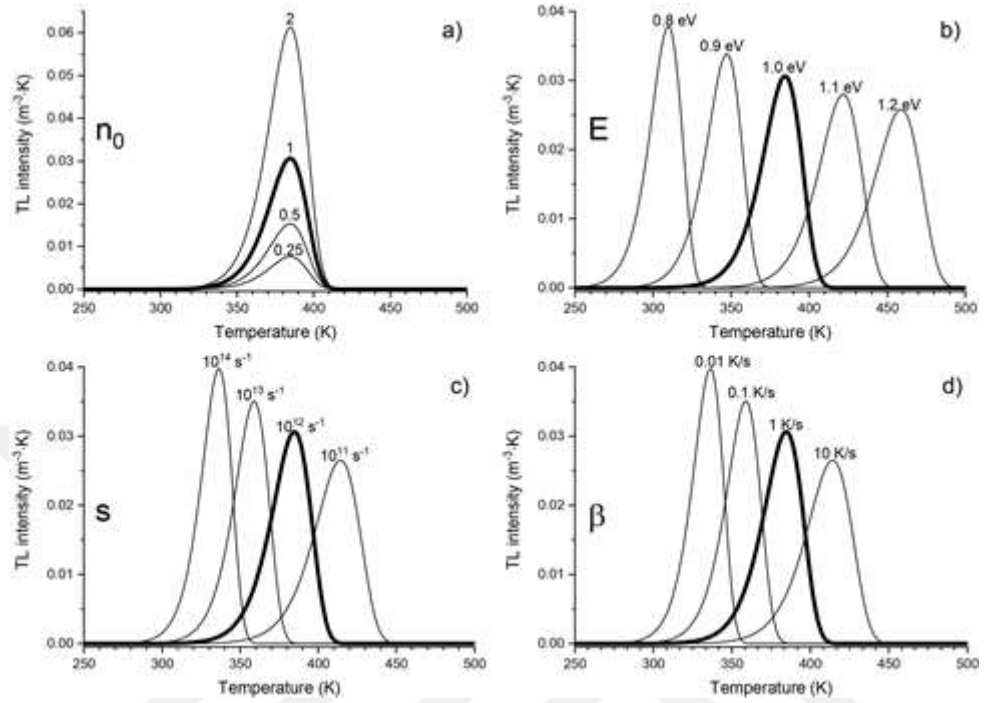

Figure 3.12. Variation of parameters for a single first order peak: a) variation in n_0; b) variation in activation energy E c) variation in frequency factor s; d) variation of heating rate-β. Initial parameters are $n_0 = 1$, $E = 1\,\text{eV}$, $s = 10^{12}\,\text{s}^{-1}$, and $\beta = 1\,\text{K/s}$ for this single first order peak (Chen and McKeever, 1997)

From the Fig.3.12.-a) it is easily seen that variation with the initial trapped charge carrier concentration does not affect the peak maximum location, or in other words; single peaks that obey the first order kinetics will have the same T_m value independent of the irradiation dose while they have higher I_m values. This is the most important feature of the first order peaks (Chen and McKeever, 1997).

3.2.1.2. Second Order Kinetics (Garlick-Gibson Approach)

According to second order kinetics, electrons trapped at the trap energy levels will either go directly pair with hole at the recombination center or will be trapped once more while being thermally stimulated. Garlick and Gibson, in their

phosphorescence study, assumed that the probability of re-trapping will be greater than probability of recombination during the thermal stimulation (Garlick and Gibson, 1948).

Mathematical expression of Garlick-Gibson approach can be written by assuming that $(N-n)A_n \gg hA_h$ within the Eqn.3.5 for emission intensity as a function of time given in OTOR model. Additionally, they also assumed that trap concentration is far greater than the trapped electron concentration ($N \ll n$); and concentrations of electron, and hole are identical ($n = h$). With those assumptions Eqn.3.5 becomes to Eqn.3.11;

$$I(t) = -\frac{dn}{dt} = s\frac{A_h}{NA_n}n^2\, exp\left(-\frac{E}{kT}\right) \tag{3.11}$$

if assumed ($A_n = A_h$) then $I(T)$ becomes:

$$I(T) = n_0^2\frac{s}{N}exp\left(-\frac{E}{kT}\right)\left[1+\frac{n_0 s}{N\beta}\int_{T_0}^{T} exp\left(-\frac{E}{kT'}\right)dT'\right]^{-2} \tag{3.12}$$

Eqn.3.12 is the Garlick-Gibson equation for the isolated TL glow peaks that have second order kinetics in their emission kinetics w.r.t. OTOR model. Solution to the integral part of this equation is in Eqn.3.10. Resulting TL emission peak of second order kinetics has nearly symmetric sides on right and left. Peak shape of first and second order kinetics are different in the first place. Being nearly symmetric is the result of the electrons re-trapped before recombination; and thus, TL emission is retarded and has wider range of temperature compared to peak shape of first order kinetics. For the peaks that obey second order kinetics, TL emission intensity related with squared the number of trapped electrons at the thermal stimulation (n_0^2). This affects the position of peak maximum too while

maximum intensity also changes. This means that with the higher irradiation dose level, peak maximum will shift to the lower temperature part. This shift in T_m can be approximated as (Bos et al., 1991);

$$T_{m_i} - T_{m_j} \approx \frac{T_{m_i} T_{m_j} k}{E} lnf$$

T_{m_i} is the temperature at peak maximum of a second order TL peak, and T_{m_j} is the temperature at peak maximum of the same peak; but emitted after a higher irradiation dose level relative to the first peak. f is the ratio of higher dose to the lower dose; k is Boltzmann constant; E is the activation energy. From Fig.3.12.a it can be seen that T_m shifts to the lower temperature side as the irradiation dose level increases. Relation between shift in temperature of any second order TL glow peak and the activation energy is inverse proportional; this means that lower the activation energy is higher the shift of temperature of peak or vice versa (Bos et al., 1991).

In Fig.3.13 behavior of a single second order TL glow peak which is produced using Garlick-Gibson equation with initial parameters of $n_0 = 1$, $E = 1$ eV, $s/N = 10^{12}\ s^{-1}$, and $\beta = 1$ K/s (Chen and McKeever, 1997). In each of them bold one is the peak produced with the reference initial value corresponding to the parameter.

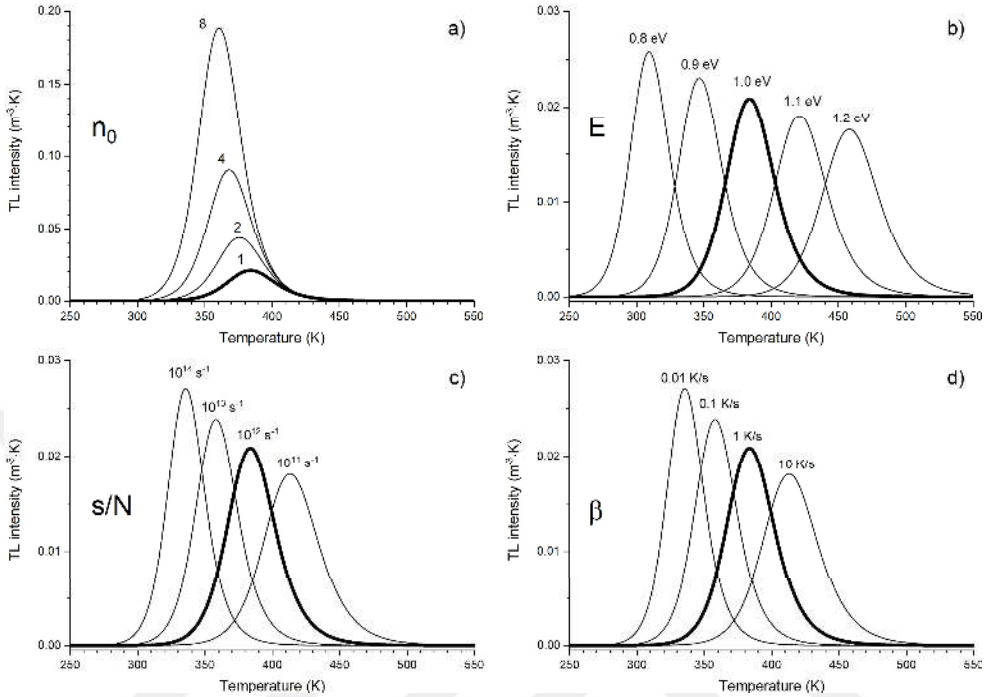

Figure 3.13. Variation of parameters for a single second order peak produced by using Garlick-Gibson equation for second order kinetics with initial parameters as $n_0 = 1$, $E = 1$ eV, $s/N = 10^{12}$ s^{-1}, and $\beta = 1$ K/s; a) variation in n_0; b) variation in activation energy E c) variation in s/N; d) variation of heating rate-β. While three of those parameters were kept constant only one of them was varying (Chen and McKeever, 1997).

3.2.1.3. General Order Kinetics (May-Partridge Approach)

Some of the experimental results for TL glow curves, analysis with first or second order equations may not be sufficient. Those type of intermediate kinetics are called general order kinetics (May and Partridge, 1964). May and Partridge again used single electron and single trap level for their assumption;

$$I(t) = -\frac{dn}{dT} = n^b s' \, exp\left(-\frac{E}{kT}\right) \tag{3.13}$$

here; b is kinetic order which is $1 < b \leq 2$; s' is the effective preexponential factor for general order kinetics equation and in units of $m^{3(b-1)}$ per second. When this equation transformed into intensity as a function of temperature for $b \neq 1$;

$$I(T) = s'' n_0 \, exp\left(-\frac{E}{kT'}\right)\left[1 + \frac{s(b-1)}{b}\int_{T_0}^{T} exp\left(-\frac{E}{kT'}\right) dT'\right]^{\frac{-b}{b-1}} \qquad (3.14)$$

where $s'' = s' n_0^{(b-1)}$ which is effective frequency factor in units of s^{-1}. General order kinetics equation can be approximated to first and second order kinetics when $b \to 1$ and $b \to 2$ respectively.

In figure 3.14. general shape comparison of peaks produced by using first, second and general order kinetics equations with the numeric parameters for the activation energy as $E = 1$ eV; for frequency factor and effective frequency factor as $s'' = s = 10^{12}$ s^{-1}, total trap concentrations and initial trapped electron concentrations as $n_0 = N = 1$ m^{-3}; and heating rates as $\beta = 1\, K/s$. Kinetic orders for the peaks produced with general order have b=1.3 and $b = 1.6$.

Updates for general order kinetics equation has been modified by other researchers (Kitis et al., 1998; Gomez-Roz and Kitis, 2002). Additionally, semi-analytical expression for OTOR has also been of interest for many researchers by using Lambert W function (Kitis and Vlachos, 2013; Sadek et al., 2015; Kitis et al., 2016); and by using Wright Omega function (Singh and Gartia, 2013; 2014; 2015)

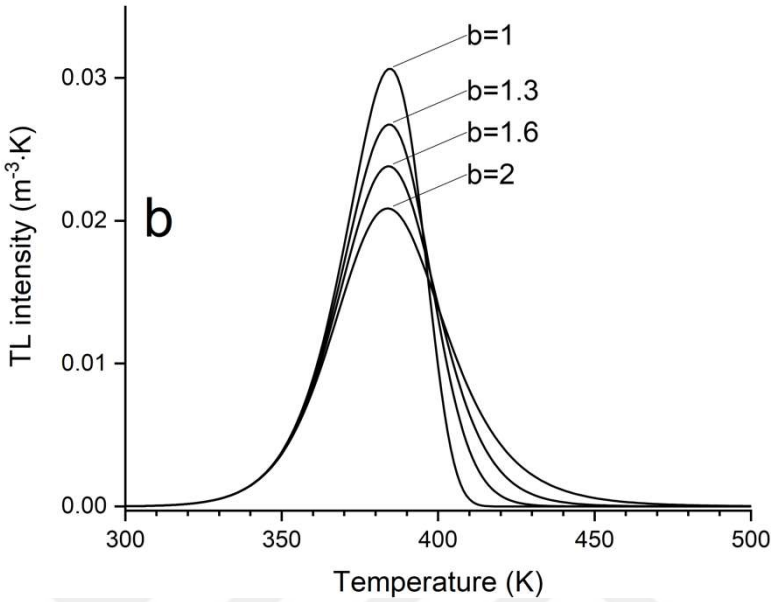

Figure 3.14. Peak shapes comparison for single peak produced by using equations of first- order, second-order, and general-order kinetics. $n_0 = 1\ \mathrm{m}^{-3}$, $N = 1\ \mathrm{m}^{-3}$, $E = 1$ eV, $s/N = 10^{12}\ \mathrm{s}^{-1}$, and $\beta = 1\ \mathrm{K/s}$; for general-order one $b = 1.3$ and $b = 1.6$ (Chen and Horowitz, 1984).

3.3. Thermoluminescence Analysis Methods

In the study of thermoluminescence, methods of analysis are mainly focused on understanding the trap structure of any subject material. Those methods are employed for determining characteristics of trap levels within the subject material of corresponding analysis, mainly in terms of activation energy and frequency factor, then the kinetic order included. In experimental observations, trap level may vary with different energy levels, thus observed spectra are generally superposition of sub-isolated peaks.

3.3.1. Initial Rise Method

This method is presented firstly by Garlick and Gibson (1948) to determine the activation energy of any isolated peak order independently. In the lower temperature part of the TL glow peak, trapped charge carrier concentration as a

function of temperature ($n(T)$) is nearly constant and its dependence on temperature is neglected. First exponential part of first order and second order kinetics equations increases with the increase of temperature but the rest of the part remains nearly constant (Garlick and Gibson, 1948);

$$I(T) = Cexp(-\frac{E}{kT}) \tag{3.15}$$

where; E is activation energy in eV, k is the Boltzmann's constant in eV/K, T is the temperature in units of K, and C is the constant representing the rest of the equation that are assumed to be nearly constant. This assumption is applied up a limit of 15% of maximum intensity (Pagonis et al., 2006). In Figure 3.15. this up-to-15%-part is shown in bold line for a synthetic peak which is produced by using first-order kinetic equation with the parameters as; $E = 1$ eV, $n_0 = N = 10^{10}$, $s = 10^{11}$ s^{-1}, $\beta = 1$ K/s.

When $\ln(I)$ versus $1/kT$ is plotted and fitted with a line, activation energy E will be equal the absolute value of this line's slope. In Fig.3.16 y-axis is natural logarithm of thermoluminescence intensity of above given first order peak, and the x-axis is $1/kT$ is shown and fitted with a line. r^2 for this fit is 0.999 and slope of the line -0.999 which can be accepted as -1 and absolute value is equal to the given activation energy.

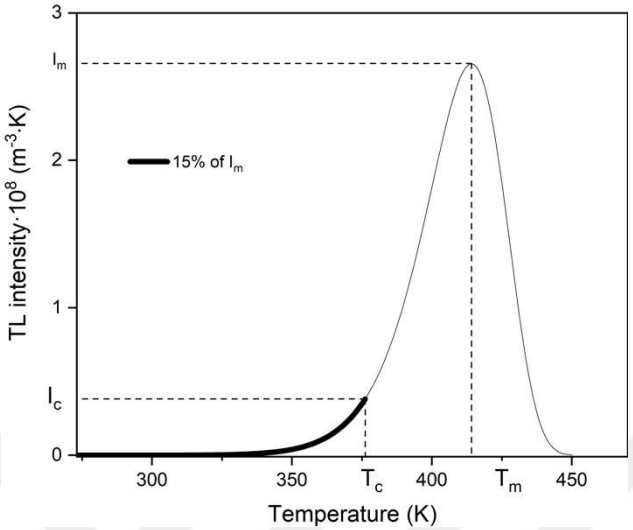

Figure 3.15. 15% of I_m for a TL glow curve. Here I_c and T_c are cutoff values for intensity (15% of I_m) and temperature corresponding to I_c respectively (Pagonis et al., 2006).

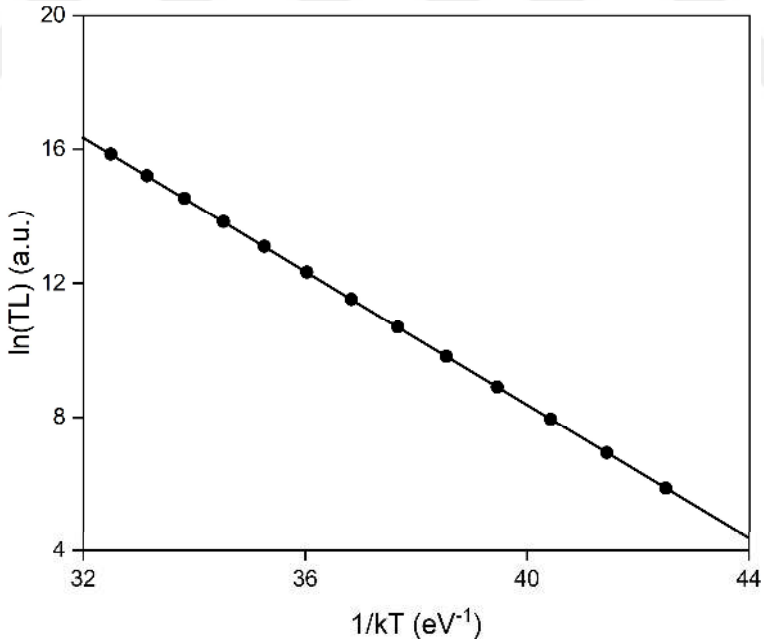

Figure 3.16. Initial rise plot of glow curve given in Fig.3.14. (Pagonis et al., 2006).

For any isolated TL glow curve, it is feasible to apply initial rise method to determine the activation energy; but when glow curve has more than one peak and if they are so close to each other's, there are different approaches for such a situation (Pagonis et al., 2006). Such a situation is represented in Fig. 3.17. One of the techniques is called "thermal cleaning" which involves heating the sample up to a temperature level above the first peak's T_{m_1} of I_{m_1}, then cooling back to ambient temperature; and re-heated afterwards beyond the second peak's T_{m_2} of I_{m_2} and cooled again. This procedure is applied all the local maxima on any TL glow curve spectrum in order to get a clean initial rise curve (Nicholas and Woods, 1964).

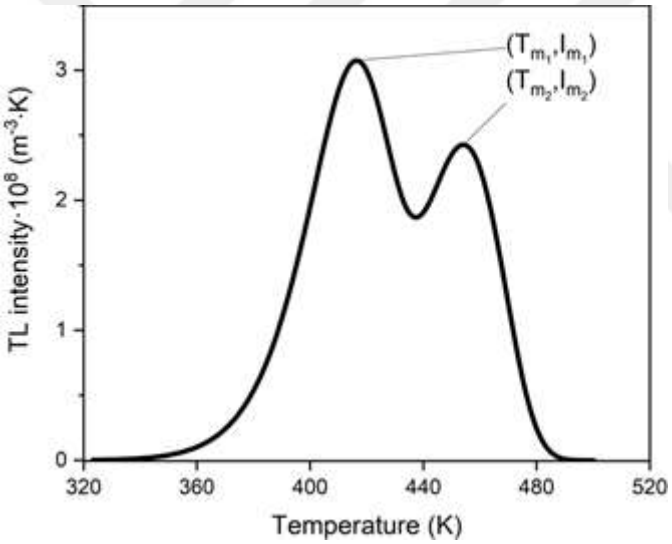

Figure 3.17. Representation of a composite curve consisting of overlapping peaks (Pagonis et al., 2006).

Using thermal cleaning and initial rise method repeatedly is another method in which from the lower temperature side of spectrum is cleaned by heating up from the ambient temperature to first preheat temperature (or T_{stop}) then cooled rapidly to ambient temperature; this is repeated to cover the glow curve and, in each cycle, preheat value is increased (assuming 5 °C). Activation energy for each

cycle is determined from initial rise plot; and then activation energy versus T_{stop} plot which will have generally expected to be a staircase-like pattern be created. There is another method in which doing the same above-mentioned procedure for repeated irradiating-preheating-reading cycles for initial rise and creating also T_{m} vs T_{stop} graph which tells the number of trap energy levels. For the first and/or second order kinetics pattern of this graph will have staircase-like plateaus unless there closely overlapping peaks co-exist. In such a case structure will have line or lines with a slope value of nearly 1 for both first-order and second-order kinetics. Such regions also called as "quasi-continuous distribution" (McKeever, 1980).

3.3.2. Various Heating Rates Method

Linear heating rate directly affects the peak position or T_m in other words. Using the maximum condition equation for first order TL glow peak given below;

$$\frac{\beta E}{kT_m^2} = s\, exp(-\frac{E}{kT_m}) \tag{3.16}$$

and using two different heating rates β_1, β_2, and corresponding T_{m_1}, T_{m_2} to the heating rates here, and re-arrangement of this the equation will be;

$$E = k\frac{T_{m_1}T_{m_2}}{T_{m_1} - T_{m_2}} ln\left[\frac{\beta_1}{\beta_2}\left(\frac{T_{m_2}}{T_{m_1}}\right)^2\right] \tag{3.17}$$

This is the calculation of activation energy of a first order TL glow peak from two different heating rates (Bohun, 1954; Porfianovitch, 1954; Booth, 1954). Activation energy calculated with Eqn.3.17 will be accurate up to 5% if the accuracy of temperature maxima is up to 1 ºC (Pagonis et al., 2006). Effect of heating rate on a TL glow peak can be seen from Fig.3.18.

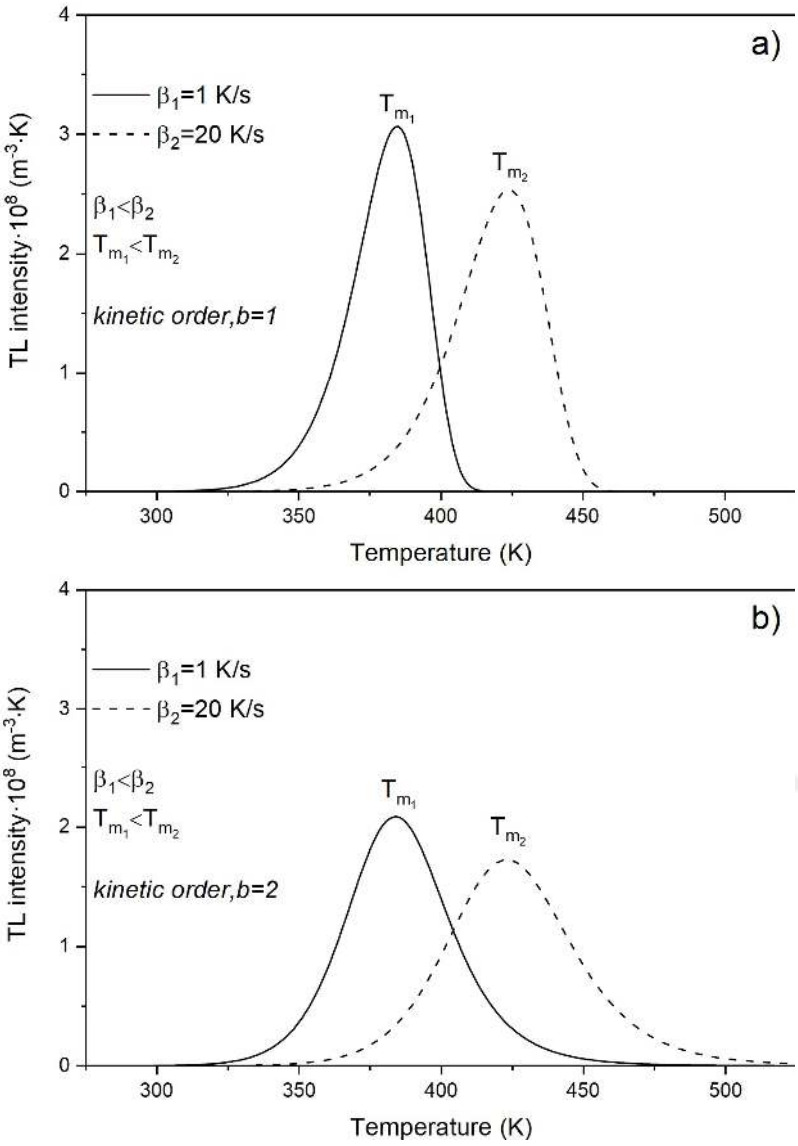

Figure 3.18. Representation of the heating rate effect on I_m and T_m for first-order and second-order TL glow peaks (Pagonis et al., 2006).

Starting from the first kinetic order equation, there is another proposed method to calculate the activation energy using several different heating rates and the corresponding T_{m} values for these heating rates. In other words;

$$ln\left(\frac{T_m^2}{\beta}\right) = \frac{E}{kT_m} ln\left(\frac{E}{sk}\right) \quad (3.18)$$

from Eqn.3.18, a plot with x-axis is as $1/kT_{\mathrm{m}}$ and y-axis is $\ln(T_{\mathrm{m}}^2/\beta)$ will result a distribution of line whose slope is equal to activation energy-E and intercept of y-axis is $\ln(E/sk)$ (Hoogenstraaten, 1958).

Another method that is like the method given with Eqn.3.19. But in this method not only the β and T_{m} values; but also, the I_{m} values are used to calculate the activation energy;

$$E = k\frac{T_{m_1}T_{m_2}}{T_{m_1} - T_{m_2}} ln\left(\frac{I_{m_1}}{I_{m_2}}\right) \quad (3.19)$$

for any order of kinetics between 1.1 and 2.5 with an error of up to 1% (Gartia et al., 1991). Here one should be careful that TL intensity should be counts per unit time.

In the measurement of TL glow peak or curve, thermocouple temperature is recorded not the temperature of the sample. With the increasing heating rate, difference between actual temperature of the sample and the measured temperature of the thermocouple will be greater. This effect is known as temperature lag. Kitis and Tuyn (1999) have developed a methodology to correct the effect of temperature lag for the correct calculation of activation energy and frequency factor by using below given equation;

$$T_{m_j} = T_{m_i} - c\ ln\left(\frac{\beta_i}{\beta_j}\right) \quad (3.20)$$

where; $T_{\mathrm{m_j}}$ is corrected temperature value of the TL glow peak, $T_{\mathrm{m_i}}$ is the value that is already corrected or at the beginning this value is of the peak recorded with

the lowest heating rate. Correction is done consecutively for the T_m values. c is the temperature lag correction constant which is calculated with the two lowest heating rates; since, for the lowest heating rate the effect of the temperature lag is assumed to be negligible. First two of the heating rates are the lowest two, then c can be calculated as:

$$c = \frac{T_{m_2} - T_{m_1}}{ln\left(\frac{\beta_2}{\beta_1}\right)} \tag{3.21}$$

Effect of the heating rate on a typical TL glow peak results decrease in peak maximum intensity-I_{m}, increase in intensity maximum's temperature- T_{m}, peak will get broader or increase in full width half maxima of peak; but peak integral should stay the same. Peak integral should be calculated like below;

$$Int_{peak} = \frac{1}{\beta}\sum_i I_{TL}(t)\Delta T_i \tag{3.22}$$

where, sum of TL intensity is multiplied by sampling interval of temperature and divided by heating rate.

As the heating rate increases, the efficiency of the TL emission efficiency may decrease (Curie, 1963). This effect is known as thermal quenching. Effect of thermal quenching can be understood from the peak area versus heating rate graph. If trend is decreasing, then thermal quenching is in effect. In such a case, quenching parameter W and C can be calculated by the equation given below (Akselrod et al., 1998; Pagonis et al., 2006);

$$\frac{A}{I_{QUE}} - 1 = C\ exp\left(-\frac{W}{kT_m}\right) \tag{3.23}$$

where; A is the peak integral of the curve with the lowest heating rate, I_{QUE} is the peak integral of quenched TL glow peaks or rest of the peak integrals except the one with the lowest heating rate. C is unitless and W is in units of eV, T_{m} is temperature of the peak, k is Boltzmann constant. A graph of $\ln[(A/I_{\mathrm{QUE}}) - 1]$ versus $1/kT_m$ will give linear-like a distribution. Slope of linear fit of this line is $-W$ and intercept of fit is $\ln(C)$.

For the experimentally observed glow curves of present thesis study's materials, there are many overlapping peaks; but assuming the local maxima values on the glow curve as dominant constituents, activation energies for such maximum locations were evaluated with Boot-Bohun-Porfianovitch's method using Eqn.3.17, and Hoogenstraaten's method by using Eqn.3.18. both before and after doing temperature lag corrections. Quenching parameters were determined for local maxima of the observed glow curves.

3.3.3. Peak Shape Method

Activation energy can also be estimated from the peak's shape quantities which are given in Figure 3.19. In literature there are many studies about peak shape analysis (Grossweiner,1953; Chen, 1969-a, 1969-b; Luschick,1956; Halperin and Braner, 1960; Balarin, 1979)

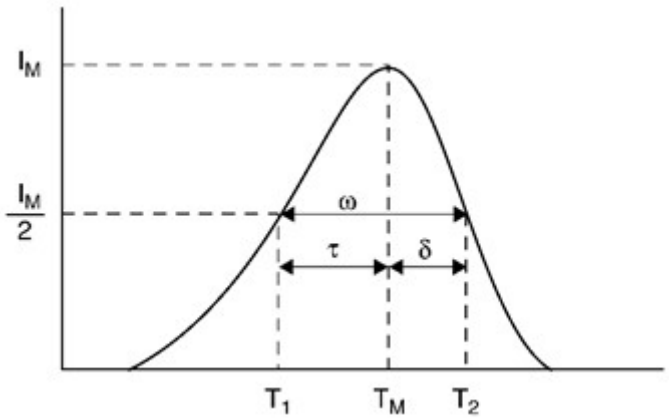

Figure 3.19. Peak shape quantities (Pagonis et al., 2006).

A very general expression to estimate activation energy from peak's shape for $0.1\,eV \leq E \leq 2.0\,eV$; $10^5 s^{-1} \leq s \leq 10^{23} s^{-1}$ and kinetic order independent (Chen, 1969-b)

$$E_\alpha = c_\alpha \left(\frac{kT_m^2}{\alpha}\right) - b_\alpha (2kT_m) \tag{3.24}$$

where here $\mu = \delta/\omega$ is geometrical factor, $\alpha = \tau, \delta, \omega$ and c_α and b_α are:

$$c_\tau = 1.510 + 3(\mu - 0.42) \qquad b_\tau = 1.58 + 4.2(\mu - 0.42)$$
$$c_\delta = 0.976 + 7.3(\mu - 0.42) \qquad b_\delta = 0$$
$$c_\omega = 2.52 + 10.2(\mu - 0.42) \qquad b_\omega = 1$$

In Fig.3.20, a graph of $\mu = \delta/\omega$ versus kinetic order (Chen, 1969-b) and $\gamma = \delta/\tau$ versus kinetic order (Balarin, 1979) can be seen.

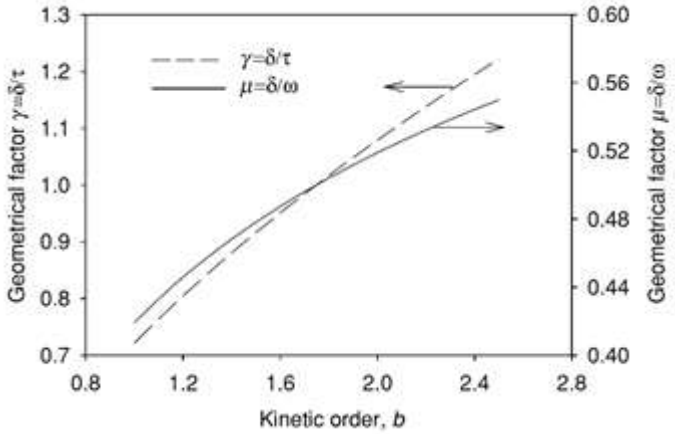

Figure 3.20. Relation of geometrical factors and kinetic order (Pagonis et al., 2006).

After activation energies are determined, frequency factor can be evaluated with below formulas for first order (Eqn. 3.25), seconds order (Eqn.3.26) and general order (Eqn.3.27) respectively.

$$s = \frac{\beta E}{kT_m^2}\, exp(\frac{E}{kT_m}) \tag{3.25}$$

$$s = \frac{\beta E}{kT_m^2}\, exp(\frac{E}{kT_m}) \left[1 + (\frac{2kT_m}{E})\right]^{-1} \tag{3.26}$$

$$s = \frac{\beta E}{kT_m^2}\, exp(\frac{E}{kT_m}) \left[1 + (b-1)(\frac{2kT_m}{E})\right]^{-1} \tag{3.27}$$

3.3.4. Computerized Glow Curve Deconvolution (CGCD)

For any given spectrum it is possible to separate it into constituent subparts. In thermoluminescence study also, glow curve spectrum may be superposition of multiple energy levels. If it is assumed to be a compact structure, constituents of it can be estimated. This estimation involves trial and error loop. Using TL kinetics equations, and their variables in terms of activation energies, frequency factors, kinetic orders, TL intensities and etc. Idea is simply guessing the initial parameters and then trying each parameter in their own limits until getting the sum of estimated peaks are very similar of the reference (let's say experimentally observed) spectrum. This estimated distribution is also named as "fit", and in general the quality of fit is shown with its "R^2" value; but other than that, figure of merit (FOM) is the main parameter the check the quality of fitting in terms of mathematical computational estimation. FOM is not alone the overall quality of deconvolution process and its formula is:

$$FOM = 100 \times \left| \sum_{i}^{n} \frac{N_i^{observed} - N_i^{fit}}{N_i^{fit}} \right| \quad (3.28)$$

where, $N_i^{observed}$ is i^{th} indexed data point of observed TL glow curve, N_i^{fit} is the data point of sum of estimated distributions corresponding to the same index. Regarding the FOM value, fit is valued as good, fair, and bad for the respective values of 0-2.5%, 2.5-3%, and >3.5% (Balian and Eddy, 1977; Misra and Eddy 1979).

Physical quality of deconvolution process is directly related with the experimentally observed possible energy level, peak position, kinetic order, and any parameter that can be determined through experimental observation. Then, glow curve deconvolution will be the theoretical explanation of the experimental observation. It is possible to write a new program to do the TL glow curve deconvolution process or using already written and tested programs available. In this thesis study TL glow curve deconvolution processes were done by using "tgcd" named R package which is free and open-source program (Peng et al., 2016). Program has many kinetic models including those models' updated versions. This program is also updated with respect to the literature. As kinetic model, general order kinetic is chosen and equation is given below (Gomez-Ros and Kitis, 2002);

$$I(T) = I_m exp\left(\frac{E}{kT_m^2}(T - T_m)\right)\left[\frac{1}{b} + \frac{b-1}{b} exp\left(\frac{E}{kT_m^2}(T - T_m)\right)\right]^{-\frac{b}{b-1}} \quad (3.29)$$

4. RESULTS AND DISCUSSION

4.1. Syntheses, XRD, TL Filter Test, and Preheat Test Results of Samples

4.1.1. Synthesis, XRD, TL Filter Test, and Preheat Test Results of Undoped $NaBaBO_3$ Samples

Aforementioned materials given in "Materials and Methods" chapter and their details in Table 3.1 are used in this synthesis step. Here, the chemical formulation of the synthesis is given in two parts as induction and reduction since the main reaction is redox type;

Reduction:

$$20\{3e^- + 3H^+ + H_3BO_3 + NaNO_3 + Ba(NO_3)_2 \rightarrow 3NO_2 + NaBaBO_3 + H_2O\}$$

Induction:

$$3\{6H_2O + NH_4NO_3 + CO(NH_2)_2 \rightarrow 4NO_2 + CO_2 + 20H^+ + 20e^-\} \quad (4.1)$$

Net Reaction:

$$20H_3BO_3 + 20NaNO_3 + 20Ba(NO_3)_2 + 3NH_4NO_3 + 3CO(NH_2)_2 \rightarrow 72O_2 + 20NaBaBO_3 + 42H_2O + 3CO_2$$

Eqn.4.1 shows the induction, reduction, and net reaction which is total of induction and reduction steps. After obtaining the net reaction, for the synthesis; firstly, different sintering temperatures for combustion were applied in a range of 600-1000°C with an interval of 100°C for a duration of 2 hours. Then, each of the synthesized $NaBaBO_3$ sample's X-ray diffractogram was compared with the reference X-ray diffraction (XRD) pattern data file of $NaBaBO_3$ to determine the optimal temperature value for synthesis process. In Fig.4.1 comparison of reference XRD pattern (98-008-0110) and XRD results of $NaBaBO_3$ samples produced with

Eqn.4.1 for different sintering temperatures as 600°C, 700°C, 800°C, 900°C, 1000°C is given.

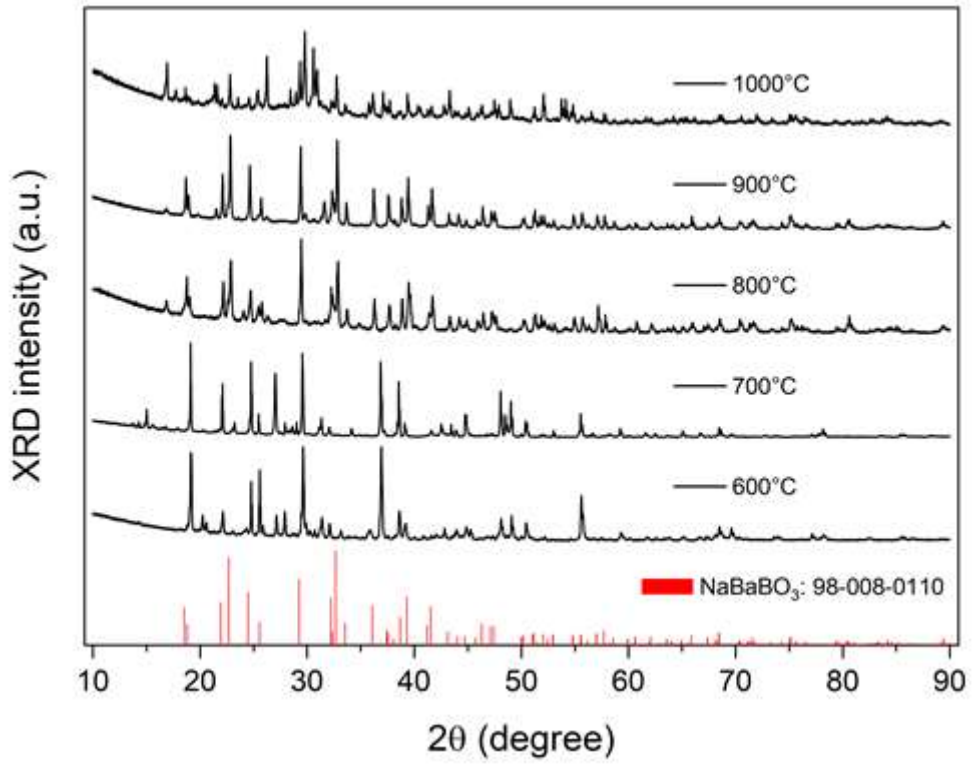

Figure 4.1. Reference XRD pattern data file of $NaBaBO_3$ compared with the synthesized $NaBaBO_3$ samples at different sintering temperatures for constant sintering duration of 2 hours

From the XRD results comparison given in Fig.4.1, it was determined that; 900°C is the optimal value and XRD results of the sample produced with that sintering temperature, though there were some impurities. Sintering duration is increased from 2 hours to 4 hours in order to overcome those impurities; but this time impurity (peak-like noise) in the XRD spectrum increased instead of decrease. Then, a calcination step at 400°C for 1 hour of duration was included to the

synthesis procedure before sintering at 900°C. Thus, synthesis was tested with the samples from following thermal procedures:

- 2 hours of sintering at 900°C
- 4 hours of sintering at 900°C
- 1 hour of calcination at 400°C +2 hours of sintering at 900°C
- 1 hour of calcination at 400°C +4 hours of sintering at 900°C
- 1 hour of calcination at 400°C +5 hours of sintering at 900°C

After synthesizing each of the undoped $NaBaBO_3$ samples with above given thermal treatment list for the synthesis procedure, XRD patterns were compared with the reference $NaBaBO_3$ XRD-pdf.

Fig.4.2 shows the XRD diffractogram comparison of new procedure of synthesis with the calcination. This time sintering duration varied while keeping the sintering temperature at 900°C, and both of the calcination temperature and duration (at 400°C for 1 hour). It can be observed that inclusion of the calcination process positively affected the XRD results of the samples; so that, results of samples from “1 hour of calcination at 400°C +2 hours of sintering at 900°C”, “1 hour of calcination at 400°C +4 hours of sintering at 900°C”, and “1 hour of calcination at 400°C +2 hours of sintering at 900°C” had nearly similar pattern when compared with the reference XRD pattern data. Therefore, optimal thermal procedure for the synthesis was determined after the TL quality comparison.

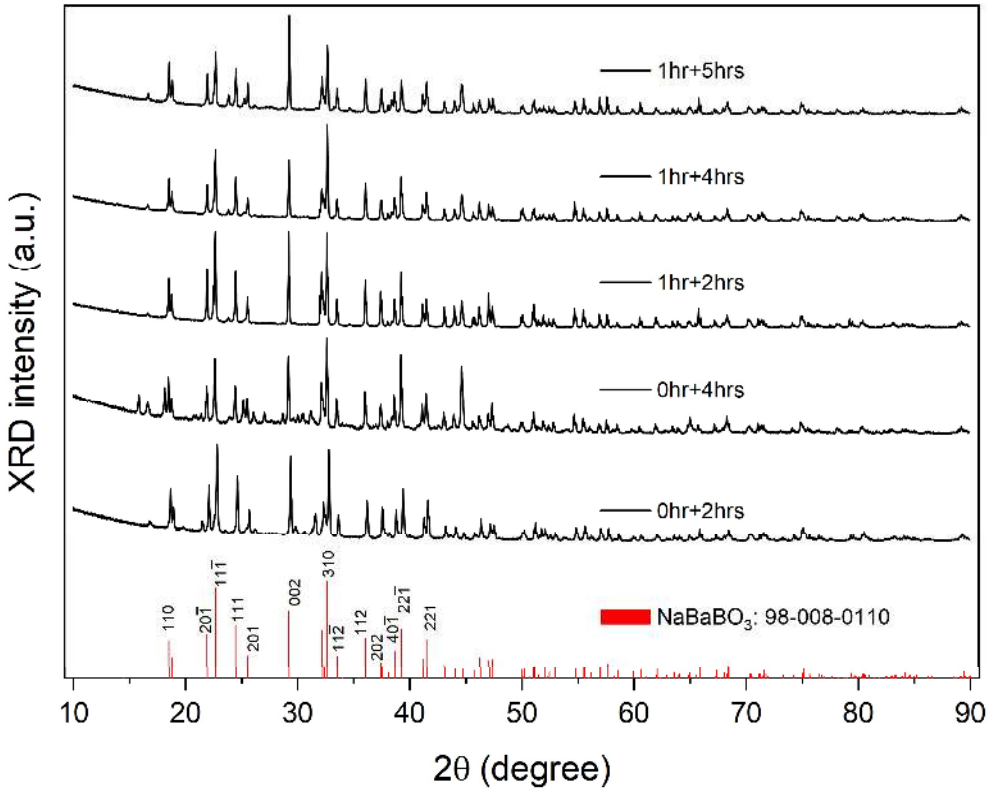

Figure 4.2. Reference XRD pattern data file of $NaBaBO_3$ compared with the synthesized $NaBaBO_3$ samples. First duration is calcination, second one is for sintering.

After XRD pattern comparison to prove the crystal structure of $NaBaBO_3$, TL filter test conducted for the samples presented in Fig. 4.2. For this step, a linear heating rate of 2°C/s from room temperature up to 450C°, a 5Gy of beta irradiation dose, 1 second of PMT channel time were applied to the sequence settings in this experiment. Each of the powder sample were pressed with a pressure of 2 ton/cm^2 for a duration 10 minutes to form a pellet which is ~25mg and 4mm in radius and ~1mm in height. Before irradiating the samples 2 times reading were applied: First one to empty trapped electrons which may be stimulated due to pressure or ambient light; second one is to read the background signal to record the thermal radiation of the crystal. Then, irradiation step applied. After that, thermoluminescence signal

recorded. Lastly the background signal is one more time recorded. This irradiation-TL reading-background reading process was completed for four filter combinations given in Table 3.7:

- IRSL, TL wideband blue
- BSL, TL 365nm
- IRSL, TL 410nm
- IRSL, 565nm

Details of TL filter test sequence are given in Fig.4.3 as a screenshot taken from LexStudio graphical user interface (gui).

Nr.	Block	Detection Window	Sample Status	Heating	Irradiation/Stimulation	Detection
1	Load sample					
2	TL	IRSL, TL wideband blue	Natural	with 2°C/s to 450°C, cool to 25°C	not used	H7360-02 (UV/VIS) for 212s, channel time 1s
3	TL	IRSL, TL wideband blue	Background	with 2°C/s to 450°C, cool to 25°C	not used	H7360-02 (UV/VIS) for 212s, channel time 1s
4	Beta Irradiation			not used	48s	not used
5	TL	BSL, TL - 365 nm	Dose	with 2°C/s to 450°C, cool to 25°C	not used	H7360-02 (UV/VIS) for 212s, channel time 1s
6	TL	BSL, TL - 365 nm	Background	with 2°C/s to 450°C, cool to 25°C	not used	H7360-02 (UV/VIS) for 212s, channel time 1s
7	Beta Irradiation			not used	48s	not used
8	TL	IRSL, TL - 410 nm	Dose	with 2°C/s to 450°C, cool to 25°C	not used	H7360-02 (UV/VIS) for 212s, channel time 1s
9	TL	IRSL, TL - 410 nm	Background	with 2°C/s to 450°C, cool to 25°C	not used	H7360-02 (UV/VIS) for 212s, channel time 1s
10	Beta Irradiation			not used	48s	not used
11	TL	IRSL, TL - 565 nm	Dose	with 2°C/s to 450°C, cool to 25°C	not used	H7360-02 (UV/VIS) for 212s, channel time 1s
12	TL	IRSL, TL - 565 nm	Background	with 2°C/s to 450°C, cool to 25°C	not used	H7360-02 (UV/VIS) for 212s, channel time 1s
13	Beta Irradiation			not used	48s	not used
14	TL	IRSL, TL wideband blue	Dose	with 2°C/s to 450°C, cool to 25°C	not used	H7360-02 (UV/VIS) for 212s, channel time 1s
15	TL	IRSL, TL wideband blue	Background	with 2°C/s to 450°C, cool to 25°C	not used	H7360-02 (UV/VIS) for 212s, channel time 1s
16	Unload sample					

Figure 4.3. TL measurement sequence details of TL filter test experiment conducted to determine the optimal filter combination.

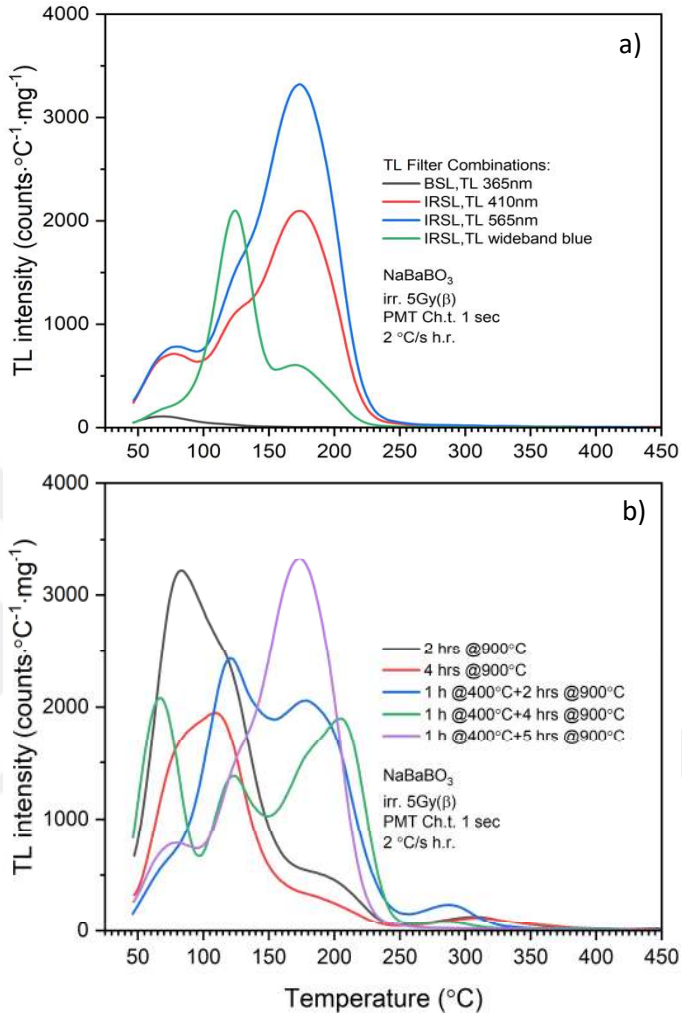

Figure 4.4. TL filter combination results: a) Results of sample calcinated for1h at 400°C then sintered at 900°C for 5 hours b) TL glow curves of five samples produced with different thermal conditions. Each individual curve is recorded by using the optimal filter combination, namely IRSL, TL 565nm.

In figure 4.4. TL filter combination results are given. In Fig.4.4-a, optimal photon counts are collected with IRSL, TL 565nm combination for undoped samples. Although, Fig.4.4-a shows the results of single sample (which was thermally treated at 400°C for 1 hour and then at 900°C 5 hours), similar TL signal

quality was observed for the rest four samples in terms of sensitivity to the TL emission under same condition by using the same filter combination. TL emission spectra of five undoped samples -which are thermally treated as aforementioned- are given In Fig.4.4.-b. Optimal condition for undoped is determined to use thermal treatment "at 400°C 1 hour and then at 900°C 5 hours" is optimal for TL quality while having the same crystal structure; and it is also determined that IRSL, TL 565nm filter combination is the most sensitive filter to collect photons from TL emission. Thus, rest of the TL experiments for undoped $NaBaBO_3$ were completed by using the same filter combination. In this study, for the thermal conditions, thermal treatment at 400°C 1 hour and then at 900°C 5 hours were also applied in the synthesis of doped versions of $NaBaBO_3$ the samples. Other than that, a preheat value of 130°C with 0 second preheat duration was applied for the rest of the experimental steps of undoped $NaBaBO_3$ in order to clean the trapped electrons trapped-in in very shallow traps which has very short lifetime.

4.1.2. Synthesis, XRD, TL Filter Test, and Preheat Test Results of Ce^{3+} Doped $NaBaBO_3$ Samples

A series of $NaBaBO_3$ samples doped with different concentrations of Cerium (Ce^{3+}) were synthesized by Eqn.4.1 and chemical materials given in Table 3.2 with thermal treatment at 400°C 1 hour and then at 900°C 5 hours. Cerium concentrations were calculated with respect to total weight of doped cerium weight+$NaBaBO_3$ weigh; and added during the mixing the input materials of synthesis given in Eqn.4.1. Each of the cerium doped $NaBaBO_3$ samples were synthesized with different cerium concentration which are 0.25%, 0.5%, 1%, 2%, 3%, 4%, 5%, 6%, 7%, 8% in total weight of Cerium+$NaBaBO_3$. Crystal structure for each Ce doped version of $NaBaBO_3$ is proved with XRD analyses. In Fig.4.5 XRD analyses results for those samples and undoped $NaBaBO_3$ are given with the reference pattern. It is clearly seen that each of the produced sample is matching the undoped structure, hence the reference $NaBaBO_3$ pattern data. Additionally,

Cerium dopant concentrations were physically mixed withing the host crystal's structure without creating any chemical bounds.

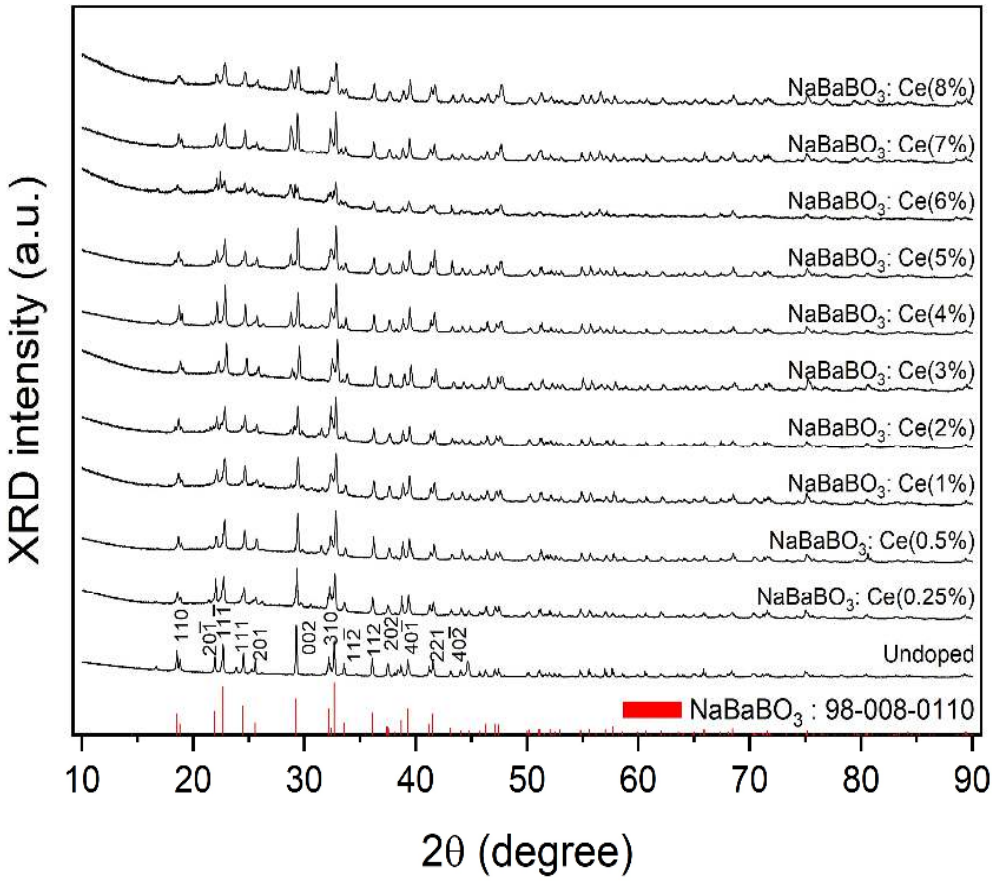

Figure 4.5. XRD pattern data of $NaBaBO_3$ as reference, and all the produced samples undoped, different Cerium concentrations doped $NaBaBO_3$.

After XRD analysis, a TL filter test conducted to determine the optimal TL filter combination for Cerium doped samples. In Figure.4.6 and it was observed that optimal TL filter combination is IRSL, TL 565nm. For this TL filter test sequence given in Fig. 4.3 was used but with a β irradiation dose of 1Gy, again heating rate is 2 °C/s, channel time of photo multiplying tube as 1 second.

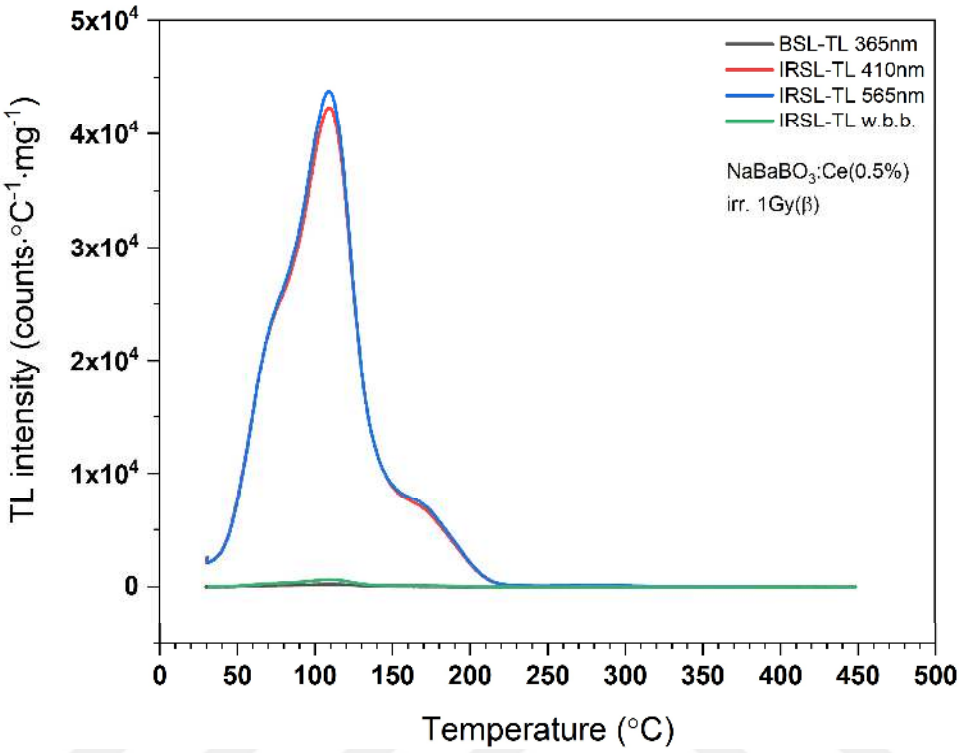

Figure 4.6. TL emession spectra of $NaBaBO_3$:Ce(0.5%,wt) recorded with four different standard TL filter combinations after 1Gy of β irradiation, with a heating rate of 2°C/s and PMT channel time of 1second.

Following the TL filter test, a preheat value at temperature as 130°C and a 0 second of preheat duration, since it was applied to undoped version of $NaBaBO_3$. Then with this preheat conditions, all of the cerium doped samples' TL emission spectra were recorded with only the optimal filter combination. In figure 4.7 thermoluminescence emission spectra of $NaBaBO_3:Ce^{3+}$ samples with concentrations of 0.25%, 0.5%, 1%, 2%, 3%, 4%, 5%, 6%, 7%, 8% with respect to the total weight of the Ce+$NaBaBO_3$ crystal. Applied β dose is 1Gy, heating rate is 2°C/s, PMT channel time is 1second. Inset graph show the maxima at higher temperature (~290°C) but relatively with less intensity with respect to the maxima around 160°C.

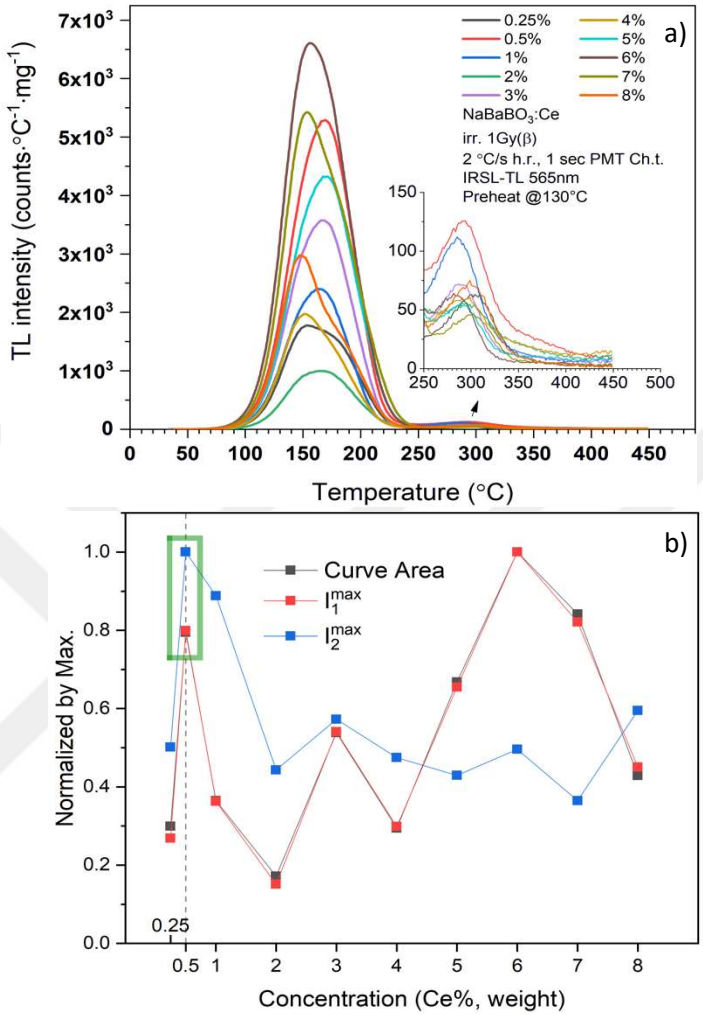

Figure 4.7 TL glow curves of $NaBaBO_3:Ce^{3+}$(x%, weight; x= 0.25, 0.5, 1, 2, 3, 4, 5, 6, 7, 8) recorded after β dose of 1Gy, heating rate of 2°C/s from room temperature up to 450°C, and with IRSL-TL wideband blue filter combination. b) TL glow curve area per dopant concentration. All values normalized by maximum one.

From Fig. 4.7. It was determined that 0.5% Ce^{3+} concentration to be optimal for TL quality regarding the TL intensities, total curve area, maxima positions in terms of temperature (curve area and maxima are marked in green).

After dopant concentration was determined, a preheat test was conducted for a series of temperatures firstly and then a preheat duration test.

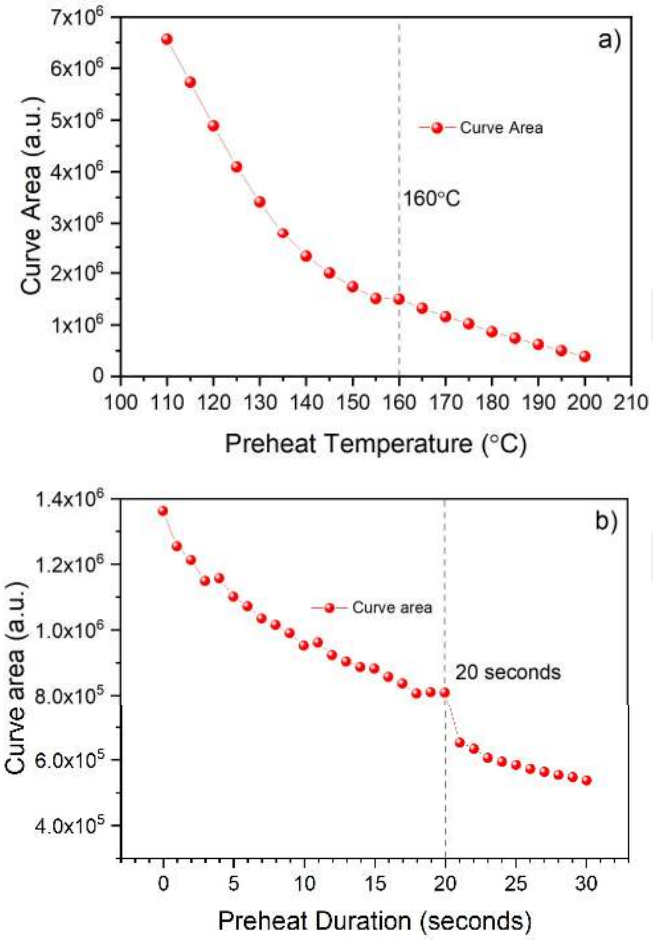

Figure 4.8. Preheat test of $NaBaBO_3:Ce^{3+}$(0.5%, wt) with constant heating rate, irradiation dose, PMT channel time a) Preheat temperature trend b) Preheat duration trend at 160 °C.

In Fig.4.8-a Preheat temperature applied to the $NaBaBO_3:Ce^{3+}$ (0.5%,wt) sample in a range of 50-200 °C but here it is shown from 110 °C to 200 °C. For the preheat values of 155 °C and 160 °C curve area is nearly constant. For a better

selection a platue with at least 3 pointswould be better but in the experimental observation there was only one plateu with 2 points. Platue means an energy step and preheat temperature was chosen from this range's higher end as 160 °C. After that, with the same condition 160 °C prehat temperature included, preheat duration was varied between 0 to 20 seconds. Preheat duration trend had a plateu containing 18, 19, and 20 seconds. 160 °C preheat temperature with a duration of 20 seconds of preheat duration was determined to be optimal preheat thermal conditions with a heating rate of 2 °C/s for $NaBaBO_3:Ce^{3+}$ (0.5%,wt). Rest of the TL experiments for this sample completed with this TL preheat conditions to clean up traps with short life time.

4.1.3. Synthesis, XRD, TL Filter Test, and Preheat Test Results of Gd^{3+} Doped $NaBaBO_3$ Samples

A series of Gadolinium (Gd^{3+}) doped $NaBaBO_3$ samples were synthesized with combustion synthesis using Eqn.4.1 and chemical reagents given in Table 3.3 with the optimal thermal conditions determined for undoped $NaBaBO_3$ synthesis. Dopant concentrations used in this series are 0.5%, 1%, 2%, 3%, 4%, 5% Gd in weight of Gd^{3+}+$NaBaBO_3$ crystal. As done with Cerium, Gadolinium also mixed before the thermal treatment with host material-$NaBaBO_3$'s chemical reagents. Again, doped element is physically mixed while host crystal structure synthesized. This is observed with XRD analysis results.

In Fig.4.9 x-ray diffraction analysis spectrum for each Gd doped $NaBaBO_3$ sample with abovementioned concentrations, and undoped $NaBaBO_3$ compared with the reference diffraction data pattern. It was observed from the XRD analysis results that, crystal structures of synthesized $NaBaBO_3$: x%Gd^{3+} (x=0.25, 0.5, 1, 2, 3, 4, 5 in weight) have diffraction patterns that each of it matching the reference undoped $NaBaBO_3$ (98-008-0110)'s diffraction pattern data.

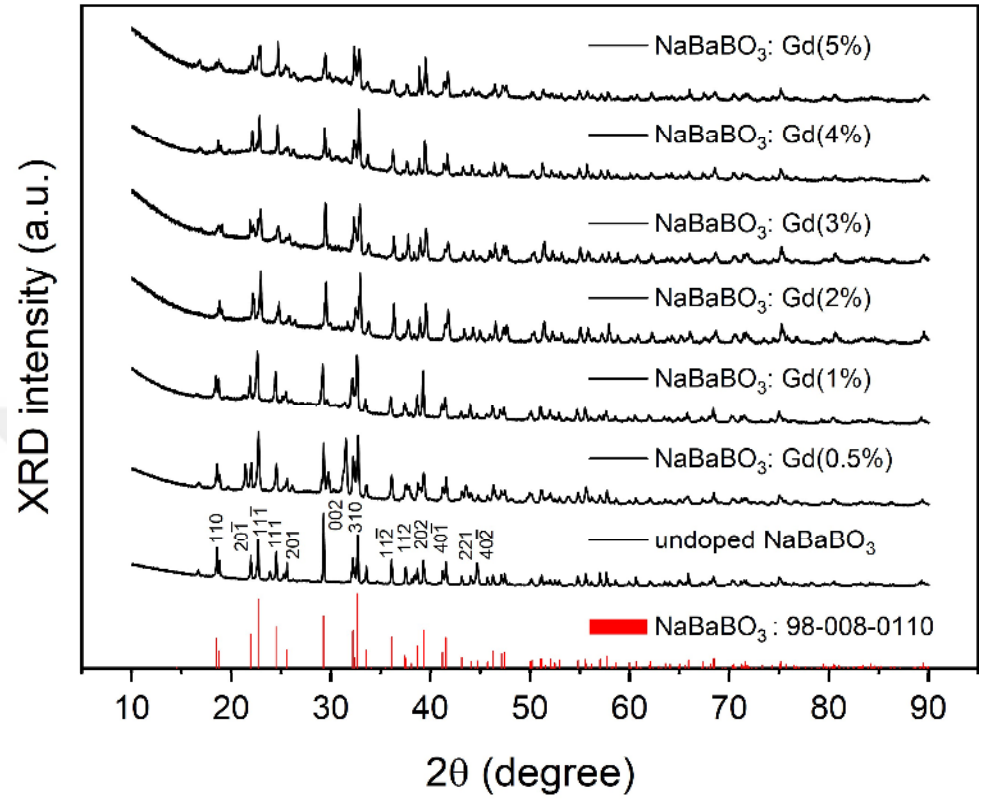

Figure 4.9. XRD pattern data of $NaBaBO_3$ as reference (98-008-0110), and all the produced samples as undoped, Gadolinium doped $NaBaBO_3$ with different concentrations as 0.5%, 1%, 2%, 3%, 4%, 5% in total weight of Gd^{3+}+$NaBaBO_3$.

After XRD analysis of synthesized gadolinium doped $NaBaBO_3$ samples, a TL filter experiment was completed for each of them by using 4 different TL filter combinations after a β irradiation dose of 1Gy, with a constant heating rate of 2 °C/s, and a PMT channel time of 1 second, from room temperature up to 450°C by a sequence file similar to the one given in Fig.4.3. In Figure 4.10 TL emission spectra of $NaBaBO_3$:Gd^{3+}(1%, weight) after abovementioned sequence and recorded with four TL filter combinations can be seen.

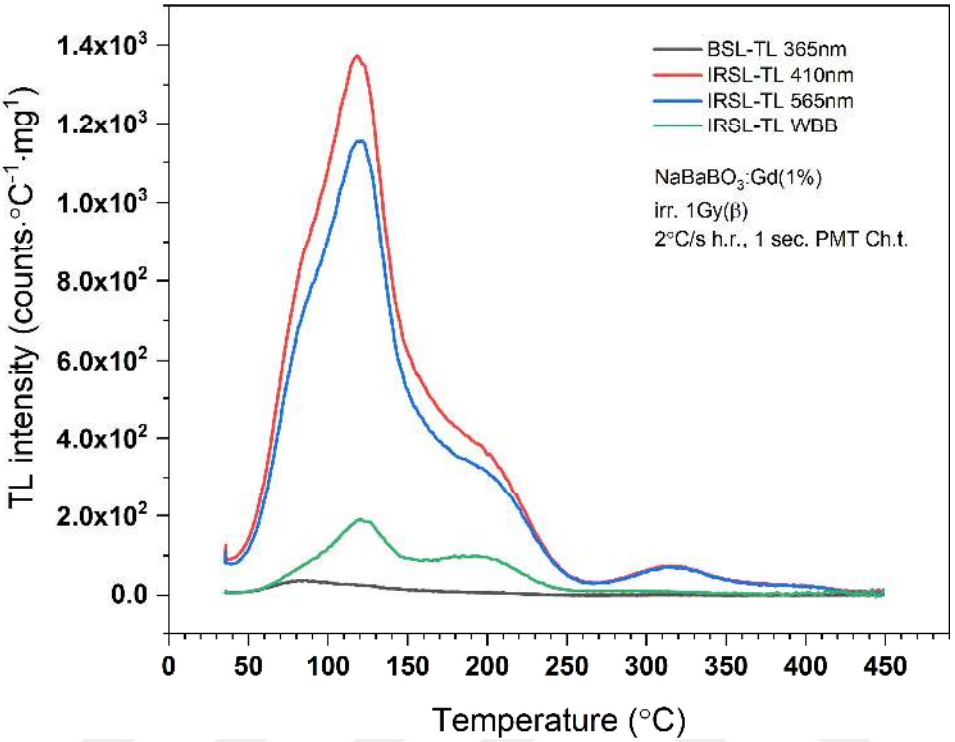

Figure 4.10. TL glow curves of $NaBaBO_3:Gd^{3+}$(1%, weight) recorded after β dose of 1Gy, heating rate of 2°C/s from room temperature up to 450°C, and with four different filter combination.

IRSL, TL 410 nm filter combination found to be the optimal one among the other three combination options in terms of the photon counting performance per unit temperature. All the samples have the result but here only one of them is shown to save space. But all the TL glow curves recorded by using same filter for each of the synthesized $NaBaBO_3:Gd^{3+}$(x%, weight, x=0.5, 1, 2, 3, 4, 5) are shown in Figure 4.11 to choose the optimal filter. TL glow curves of all Gd doped samples and curve area per gadolinium concentration trend are given in Fig.4.11-a and b, respectively. As this trends shows, optimal gadolinium concentration for TL study is observed at 1% Gd in weight of the sample.

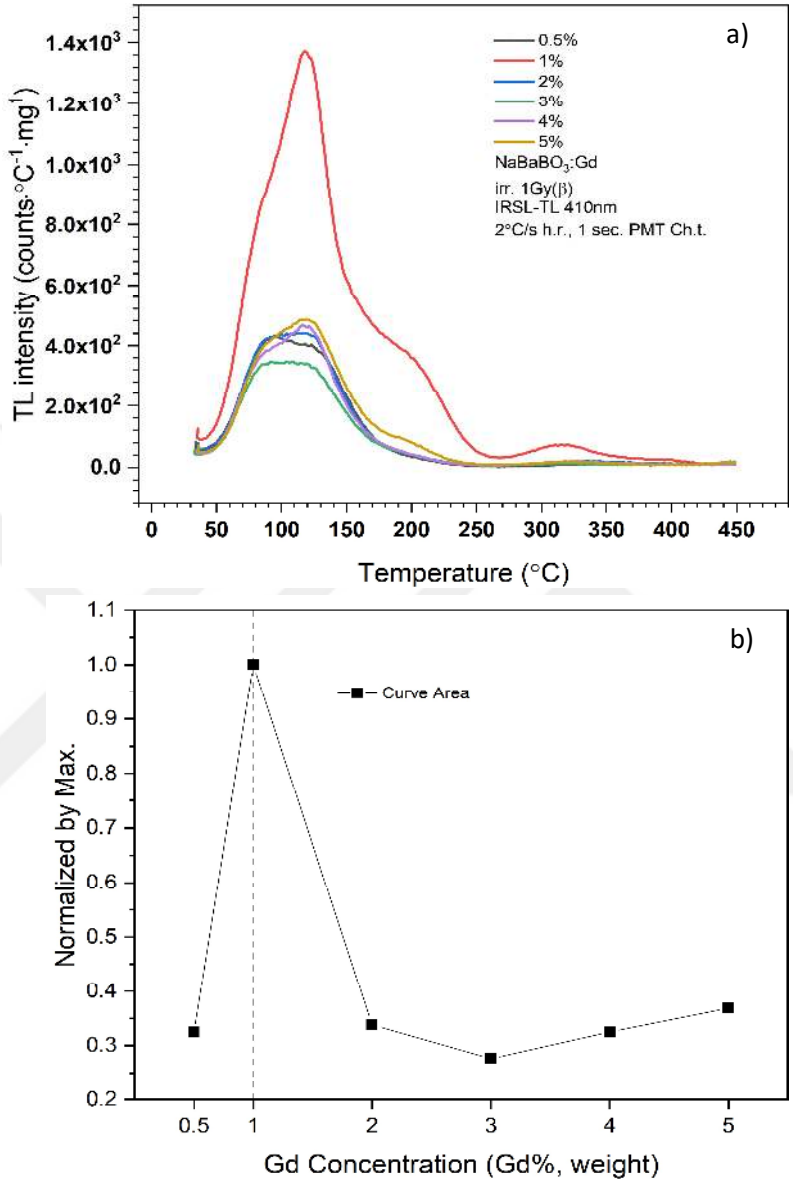

Figure 4.11. a) TL glow curves of $NaBaBO_3:Gd^{3+}$(x%, weight; x= 0.5, 1, 2, 3, 4, 5) recorded after β dose of 1Gy, heating rate of 2°C/s from room temperature up to 450°C, and with IRSL-TL 410nm filter combination. b) TL glow curve area per dopant concentration. All values normalized by maximum one.

After optimal TL filter combination, and gadolinium concentrations are determined, rest of the TL experiments will be TL preheat experiment for $NaBaBO_3:Gd^{3+}$(1%, weight) sample. Figure 4.12 shows the results of preheat test.

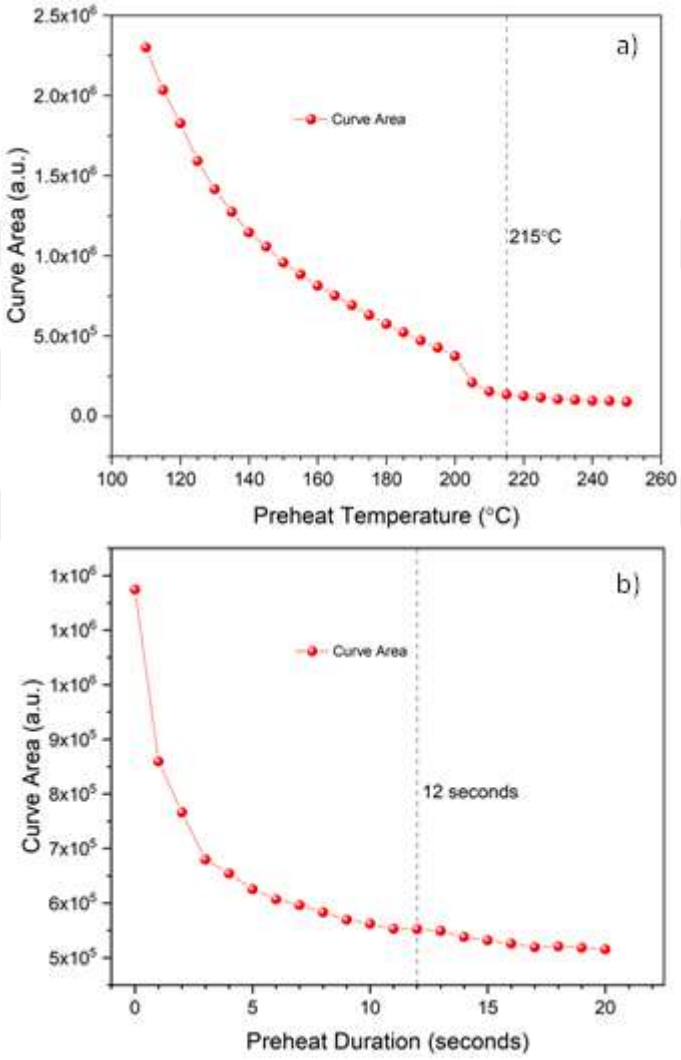

Figure 4. 12.Preheat trends of $NaBaBO_3:Gd^{3+}$(1%, weight): a) Preheat temperature trend b) Preheat duration trend at 215 °C.

Fig.4.12-a shows the details of preheat temperature test results. For the optimal preheat temperature, $NaBaBO_3:Gd^{3+}$(1%, weight) sample, irradiated with β dose of 1Gy, then preheated up to 110°C from room temperature with a heating rate of 2°C/s; and then heated from room temperature up to 450°C with the same heating rate while TL emission was recorded with "IRSL, TL 410 nm" filter combination. This process is repeated between 110°C-250°C with an interval of 5°C for each increase. Figure 4.12-b shows the details of preheat time trend. For time trend step 215°C was temperature value but this time at this temperature $NaBaBO_3:Gd^{3+}$(1%, weight) sample waited for varying preheat duration from 0 up to 20 seconds. From the experimental observations optimal preheat time was determined as 12 seconds. Thus, rest of the TL experiments of Gd doped $NaBaBO_3$ will be completed on $NaBaBO_3:Gd^{3+}$(1%, weight) sample by using IRSL-TL 410 nm filter combination, with a preheat condition of 215°C for 12 seconds (heating rate is 2°C/s).

4.1.4. Synthesis, XRD, TL Filter Test, and Preheat Test Results of Tb^{3+} Doped $NaBaBO_3$ Samples

Synthesis of terbium doped $NaBaBO_3$ phosphor had been completed by using the materials listed in Table 3.4 and calculating chemical materials regarding the chemical equation given with Eqn.4.1. All the input materials were weighed, mixed including terbium nitrate as much as necessary amount that calculated for a set of concentrations as: 0.5%, 1%, 2%, 3%, 4%, 5% with respect to weight. Then thermally treated as described for optimal condition to synthesize the undoped $NaBaBO_3$ material in ash furnace at 400°C for 1 h then at 900°C for 5 hours.

Each of the $NaBaBO_3:x\%Tb^{3+}$ (x=0.5, 1, 2, 3, 4, 5) samples' x-ray diffraction analysis spectrum compared with the reference pattern data of $NaBaBO_3$ host material (98-008-0110). From the analysis results it was observed that crystalline structure is matching. In Figure 4.13 reference XRD pattern data (plotted with bars), undoped, 0.5% Tb doped, 1%Tb doped, 2% TB doped, 3% Tb

doped, 4% Tb doped, and 5% Tb doped $NaBaBO_3$ respectively from down to up as line plots.

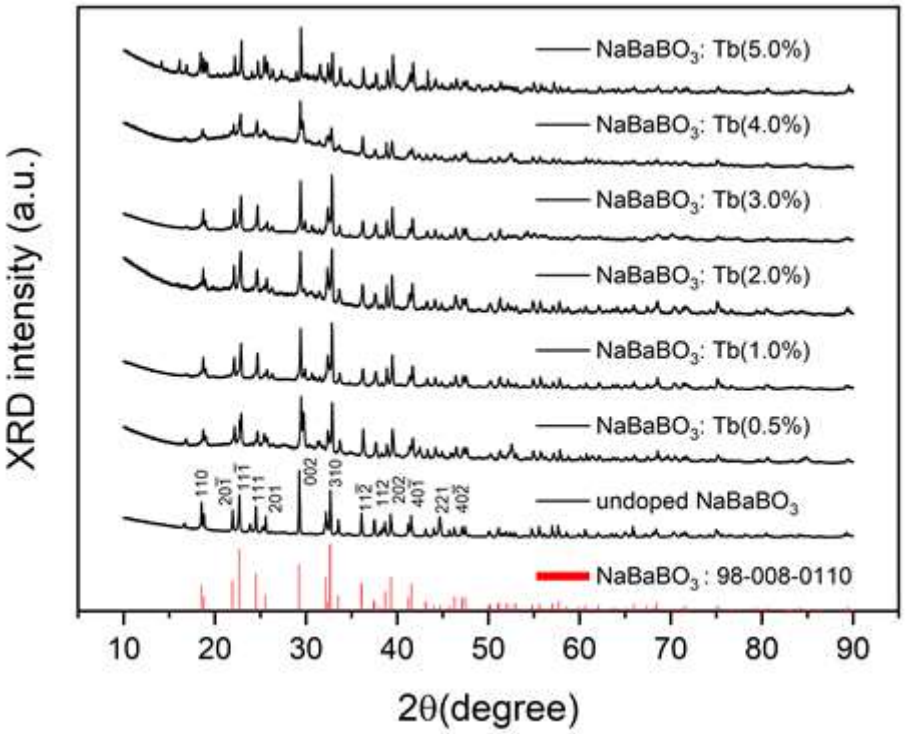

Figure 4.13. XRD pattern data of $NaBaBO_3$ as reference (98-008-0110), and all the produced samples as undoped, Terbium doped $NaBaBO_3$ with different concentrations as 0.5%, 1%, 2,%, 3%, 4%, 5% in total weight of Tb^{3+}+$NaBaBO_3$.

Tb^{3+} doped $NaBaBO_3$ samples were irradiated with β dose of 5Gy TL filter test to determine the optimal filter for reading TL emission sensitively. A pellet of ~30 mg weight, 8 mm in diameter, and ~1 mm in thickness were prepared. Each pellet sample analyzed with the sequence file given in Fig.4.3. In Figure 4.14 TL filter test result of $NaBaBO_3$: Tb^{3+} (2%, weight) after β irradiation of 5Gy, heated from room temperature up to 450°C with a constant heating rate of 2°C/s.

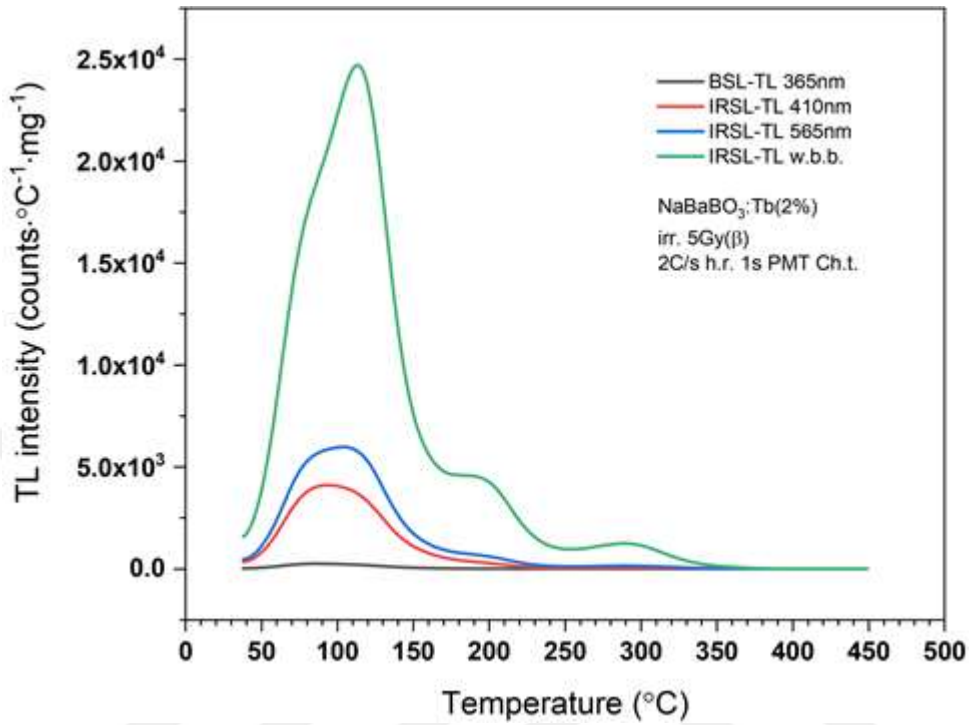

Figure 4.14. TL glow curves of $NaBaBO_3:Tb^{3+}$(2%, weight) recorded after β dose of 5Gy, heating rate of 2°C/s from room temperature up to 450°C, and with four different filter combinations.

It was observed from the TL filter test that, IRSL-TL wideband blue combination to be the most sensitive to TL emission spectrum of Tb^{3+} doped $NaBaBO_3$ samples among the other three combinations. With that result, glow curve area value per dopant concentration plotted as a trend to determine the optimal Tb^{3+} concentration.

In Figure 4.15-a glow curves of each Tb^{3+} doped $NaBaBO_3$ sample recorded after 5Gy of β irradiation dose and recoded with the optimal TL filter combination (IRSL, TL wideband blue). In Figure 4.15-b curve area per Tb^{3+} concentration plot is shown. Experimental results showed that

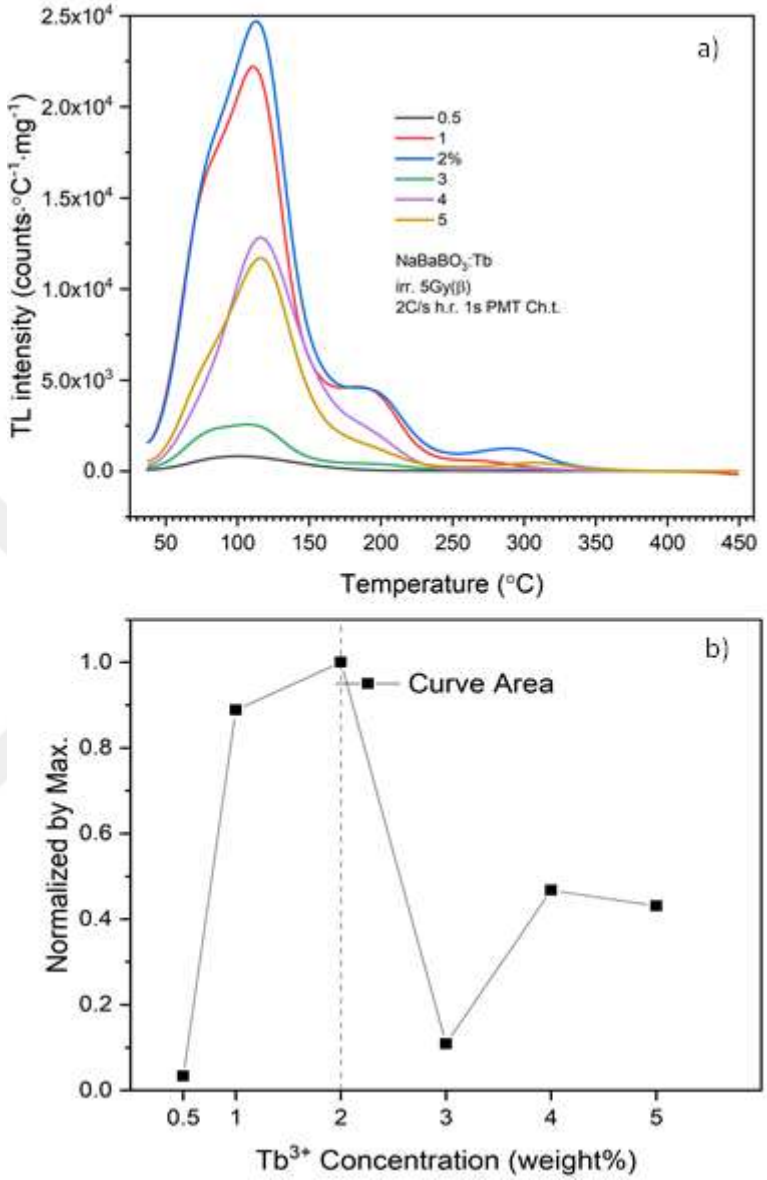

Figure 4.15. a) TL glow curves of $NaBaBO_3:Tb^{3+}$(x%, weight; x= 0.5, 1, 2, 3, 4, 5) recorded after β dose of 1Gy, heating rate of 2 °C/s from room temperature up to 450 °C, and with IRSL-TL wideband blue filter combination. b) TL glow curve area per dopant concentration. All values normalized by maximum one.

After determining optimal TL filter combination and optimal dopant concentration, next test was to determine the optimal preheat conditions in terms of preheat temperature first then the preheat duration at that temperature. In Figure 4.16 preheat test results are given as curve area per preheat temperature, and curve area per preheat duration at determined preheat temperature.

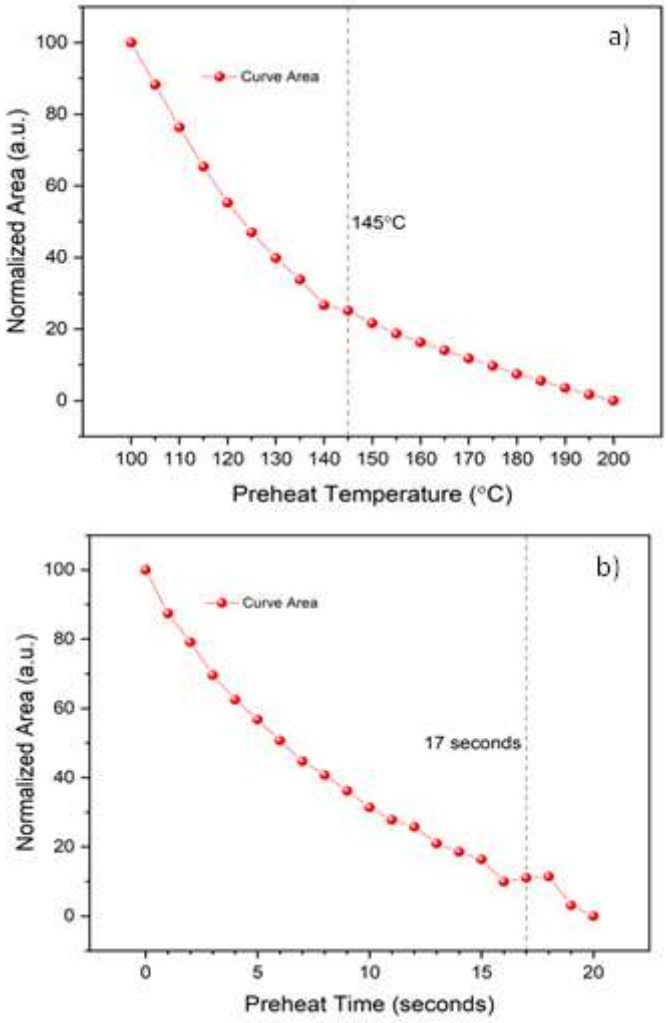

Figure 4.16. Preheat trends of $NaBaBO_3:Tb^{3+}$(2%, weight): a) Preheat temperature trend b) Preheat duration trend at 145°C.

For the preheat test experiment $NaBaBO_3:Tb^{3+}$(2%, weight) sample irradiated with 1Gy of β dose, then preheated up from room temperature up to 100C° with a heating rate of 2 °C/s and cooled back to room temperature. Following this preheating process, a TL reading was done from room temperature up to 450°C with a heating rate of 2 °C/s then cooled back to room temperature. This process had been completed for each preheat value between 100°C and 200°C with a 5°C increase for each preheat value. A plot of curve area recorded by using IRSL, TL wideband blue filter combination shows that optimal preheat temperature is 145°C for $NaBaBO_3:Tb^{3+}$(2%, weight). Next experimental step was to determine preheat duration. $NaBaBO_3:Tb^{3+}$(2%, weight) sample irradiated and then preheated up to 145°C with abovementioned heating rate, but this time duration of keeping the sample is varied for duration of time between 0-20 seconds with an interval of 1 second each time. It was determined from Fig.4.16-a and Fig.4.16-b that preheat at 145°C for 17 seconds is optimal preheat condition for $NaBaBO_3:Tb^{3+}$(2%, weight) sample while reading with abovementioned TL filter combination and heating rate.

4.1.5. Synthesis and XRD Results of Yb^{3+} Doped $NaBaBO_3$ Samples and Eu^{3+} Doped $NaBaBO_3$ Samples

Synthesis of x%Yb^{3+} (x= 0.5, 1, 2, 3, 4, 5) doped $NaBaBO_3$ and x%Eu^{3+} (x= 0.5, 1, 2, 3, 4, 5) completed with chemical equation given with Eqn.4.1.5 and chemical materials that were listed with Table 3.5, and Table 3.6 respectively. For thermal treatment 400°C 1 hour and then 900°C 5 hours applied, but none of the production was successful. This time thermal procedure was varied as 400°C 1 hour then 900°C 4 hours; 400°C 1 hour then 900°C 2 hours. Since none of the synthesis gave a successful production for synthesized $NaBaBO_3:Yb^{3+}$ and $NaBaBO_3:Eu^{3+}$ samples those two type materials do not have any TL results in this Ph.D. thesis.

4.2. Dose Response Experiment Results

4.2.1. Dose Response Experiment Results of Undoped $NaBaBO_3$ Sample

TL dose response experiment determines any phosphor material's sensitive dose range in terms of linearity. For this experiment, TL readings had been completed with IRSL, TL 565 nm TL filter combination, 2°C/s eating rate, 1 second PMT channel time with varying the irradiation dose of β in a range of 0.115 to 55Gy. It should be noted that in 2018 when TL experiments of undoped $NaBaBO_3$ had been being conducted, dose rate of radioactive source vas ~0.115 Gy/s. In Figure 4.17 TL glow curves of undoped sample recorded after different irradiation dose are given.

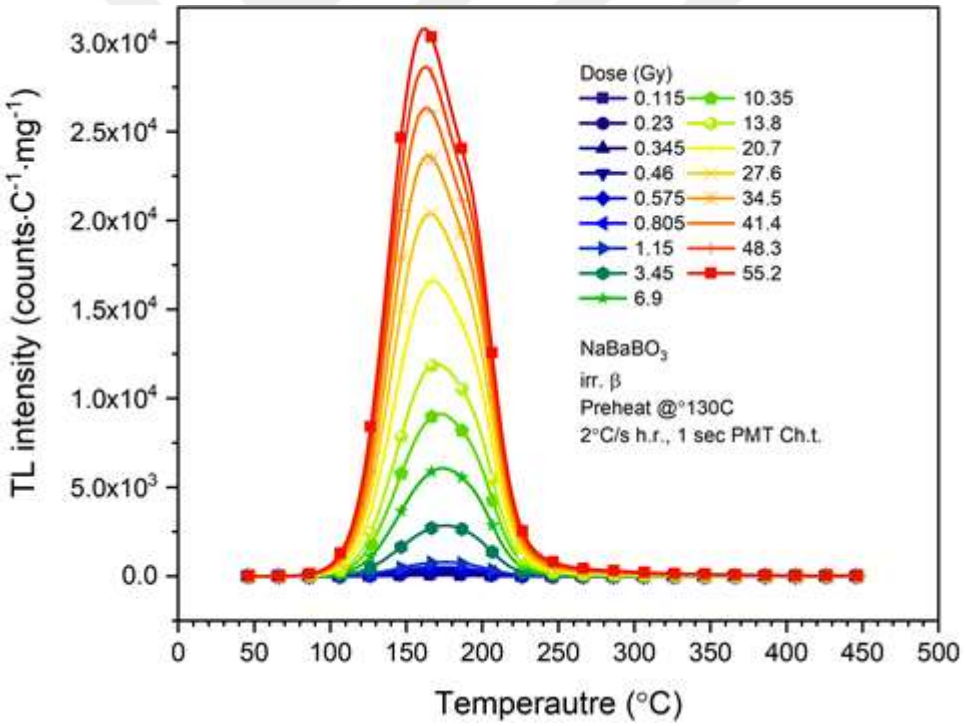

Figure 4.17. TL glow curves of $NaBaBO_3$ recorded after different β dose, with a heating rate of 2°C/s from room temperature up to 450°C, and with IRSL, TL 565nm TL filter combination.

TL glow curve are of curves given in Fig.4.17 versus applied irradiation dose can be seen from Figure 4.18 in log-log scale to determine the linear dose range.

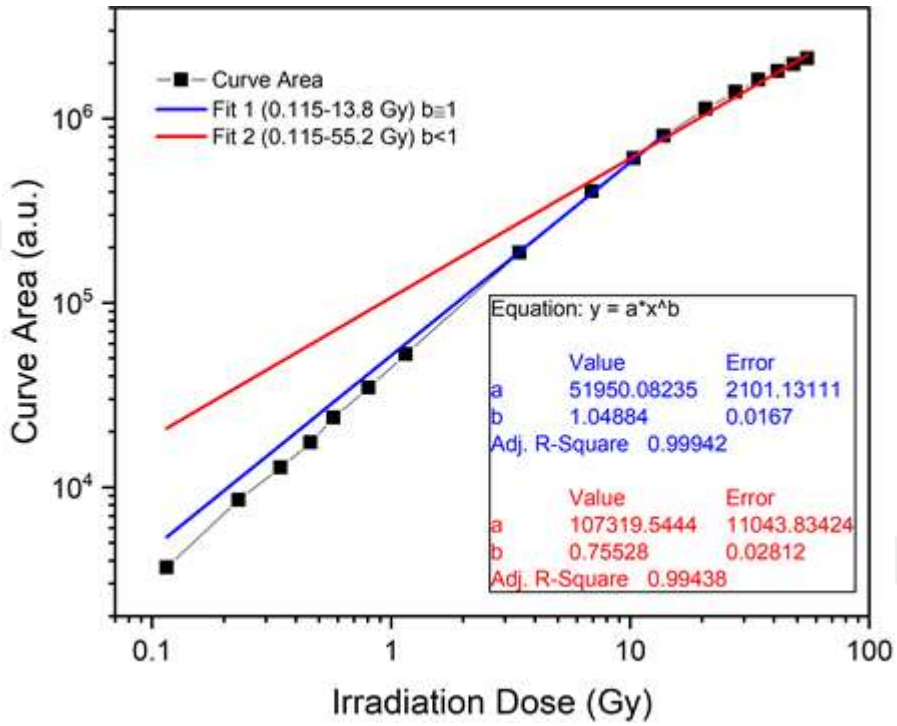

Figure 4.18. Linearity graph of undoped $NaBaBO_3$. X- axis is irradiation dose, y-axis is TL curve area both axes are in logarithmic scale.

Linearity characteristics can be determined by a graph similar to Fig.4.18 after fitting distribution with a function $y = ax^b$ where a and b are constants, x represents the dose, y represents TL intensity (or integral of curve). Dose range is linear if b is 1; lower than 1 means sub linear; greater than 1 means super linear (or supra linear) (Chen and McKeever, 1997; Pagonis et al., 2006). From curve area trend given in Fig.4.18, for β source, this materials linearity characteristics was observed that, from 0.115 Gy up to 13.8 Gy it is linear. After this upper dose limit of fit, trend goes to a sub-linear range (b<1).

4.2.2. Dose Response Experiment Results of Ce^{3+} Doped $NaBaBO_3$ Sample

For dose response experiment of Ce^{3+} doped samples, optimal filter IRSL-TL 565 nm combination, thermal stimulation from room temperature up to 450°C with a 2°C/s heating rate TL readings; and a condition of preheat at 160°C for 20 seconds with 2°C/s heating rate after each irradiation step was applied. TL glow curves recorded after β irradiation values of 0.1, 0.5, 1, 2, 3, 4, 5, 6, 7, 8, 9, 10Gy are given in Figure 4.19.

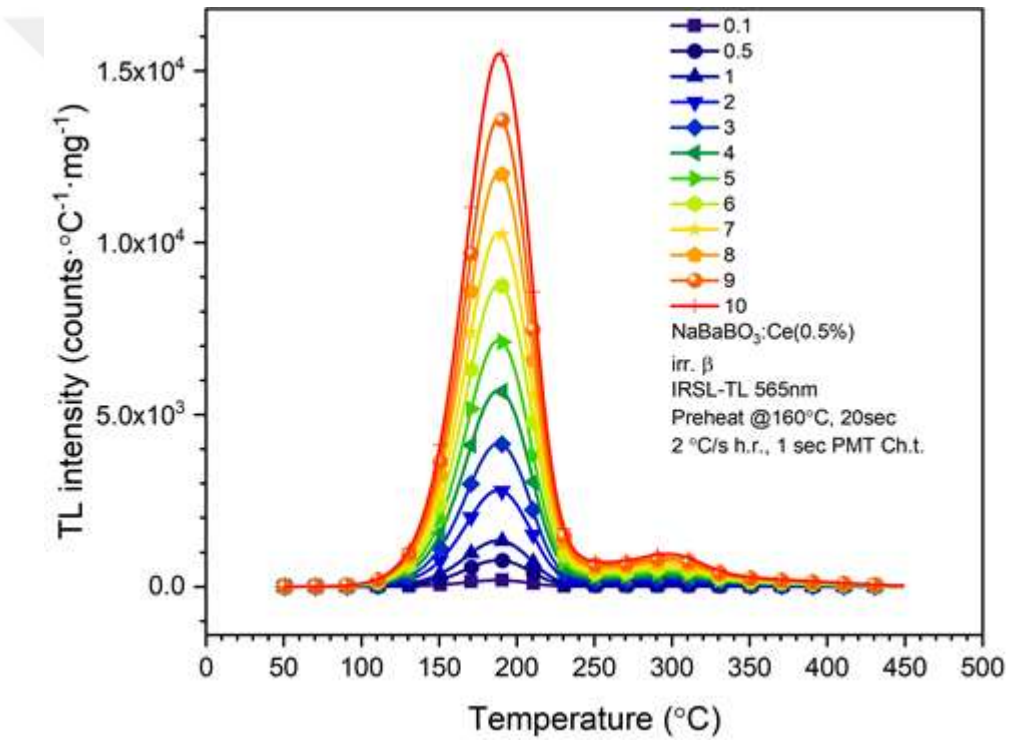

Figure 4.19. TL glow curves of $NaBaBO_3$:Ce(0.5%, weight) recorded with a heating rate of 2 °C/s from room temperature up to 450 °C by using IRSL, TL 565nm TL filter combination.

TL dose response characteristics of $NaBaBO_3:Ce^{3+}$(0.5%, weight) after β irradiation is given with Figure 4.20 as a plot of TL glow curve area versus irradiation dose in log-log scale.

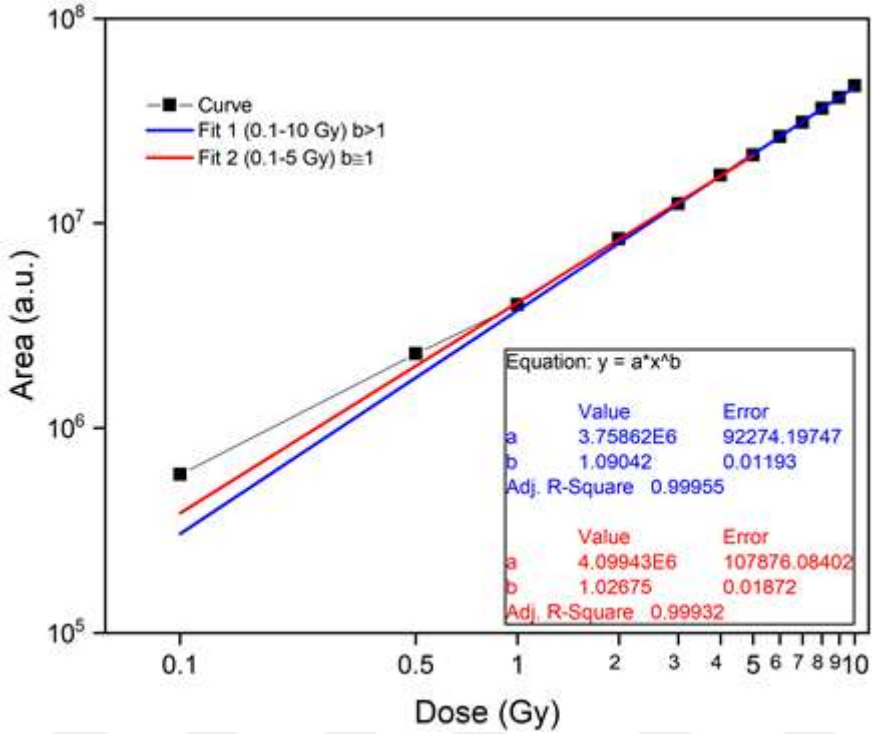

Figure 4.20. TL glow curve area of $NaBaBO_3:Ce^{3+}$(0.5%, weight) per irradiation dose.

Regions of interest for fit of function $y = ax^b$ are 0.1-10Gy and 0.1-5Gy that gives b value as b=1.09 and b=1.02 respectively.

4.2.3. Dose Response Experiment Results of Gd^{3+} Doped $NaBaBO_3$ Sample

Dose response experiment of $NaBaBO_3:Gd^{3+}$(1%, weight) was conducted by reading TL signals from room temperature up to 500°C with a heating rate of 2 °C/s and with IRSL-TL 410nm TL filter combination for a set of β irradiation dose as 0.5, 1, 2, 3, 4, 5, 6, 7, 8, 9, 10, 15, 20Gy. After each irradiation step and before TL signal reading a preheat step, which is at 215°C preheat temperature for a preheat duration of 12 seconds as the result of aforementioned preheat test of $NaBaBO_3:Gd^{3+}$(1%, weight) sample, was applied for each irradiate-preheat-TL

readout-background signal readout cycle. In Figure 4.21 recorded TL glow curves are given for all applied β doses.

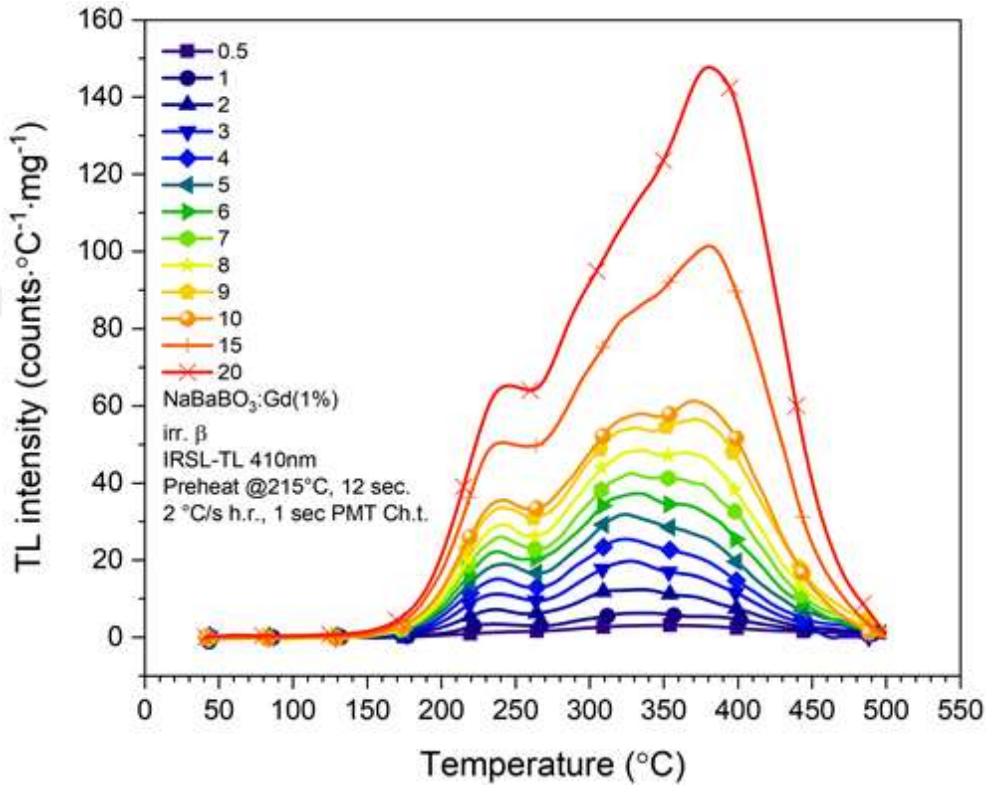

Figure 4.21. TL glow curves of $NaBaBO_3:Gd^{3+}$(1%, weight) recorded with a heating rate of 2 °C/s from room temperature up to 500 °C by using IRSL, TL 410nm TL filter combination.

A log-log scaled graph of TL glow curve area per irradiation dose is given in Figure 4.22.

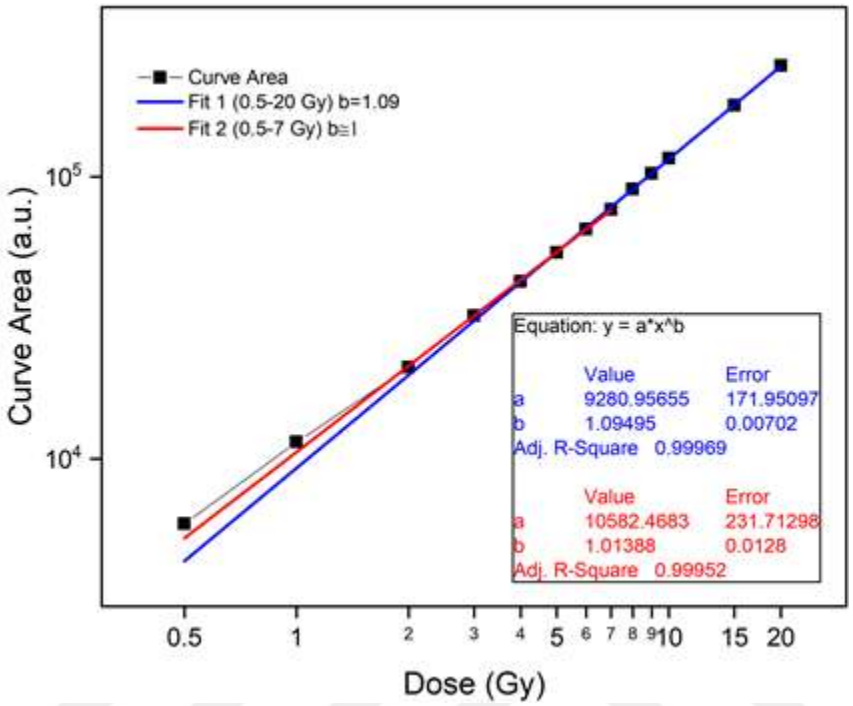

Figure 4.22. TL glow curve area of $NaBaBO_3:Gd^{3+}$(1%, weight) per irradiation dose.

It can be seen from Fig.4.22, two different regions of interest for fit function $y = ax^b$ give two different b values. For dose range 0.5-7Gy of β dose, trend can be accepted perfectly linear; for another range of β dose 0.5-20Gy can be accepted nearly linear for having a linearity index-b equals to 1.09.

4.2.4. Dose Response Experiment Results of Tb^{3+} Doped $NaBaBO_3$ Sample

TL dose response investigation was completed with a β dose set as 0.1, 0.5, 1, 2, 3, 4, 5, 6, 7, 8, 9, 10, 15, 20, 25, 30, 35, 40Gy. IRSL-TL wideband blue filter combination as optimal bandpass filter combination, thermal stimulation from room temperature up to 450°C with a heating rate of 2°C/s, a preheat at 145°C for 17 seconds after each irradiation step were applied to TL glow curve reading

sequence. Recorded glow curves $NaBaBO_3:Tb^{3+}$(1%, weight) for TL dose response experiment are shown in Figure 4.23.

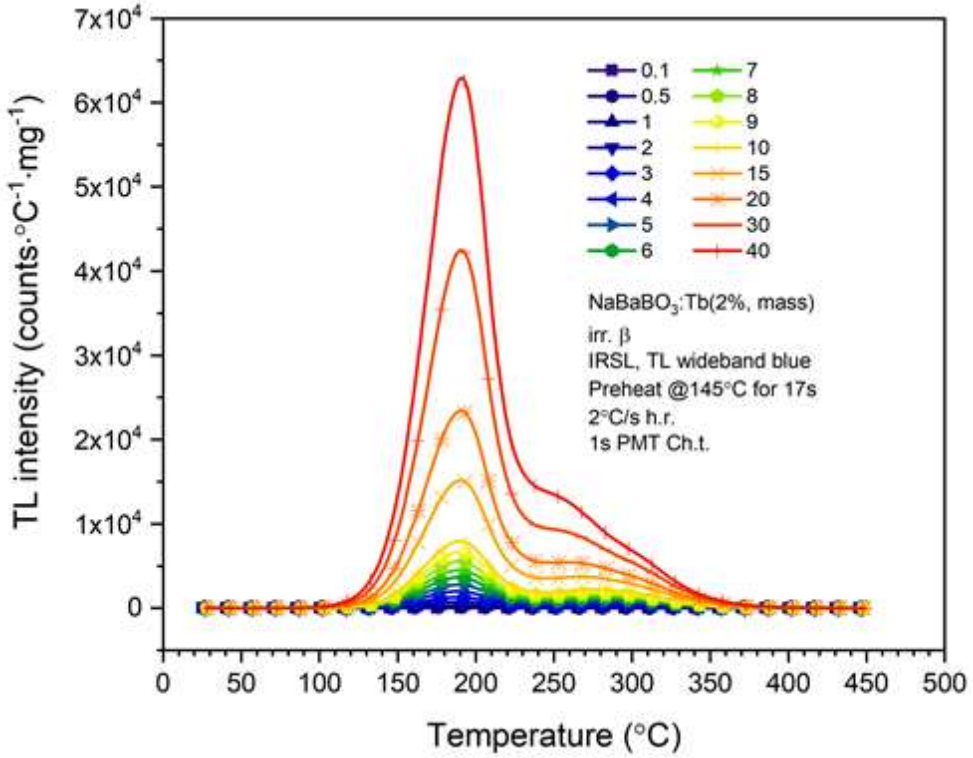

Figure 4.23. TL glow curves of $NaBaBO_3:Tb^{3+}$(2%, weight) recorded with a heating rate of 2 °C/s from room temperature up to 450 °C by using IRSL, TL wideband blue TL filter combination.

Dose response trend is graphed as TL glow curve area versus irradiation dose as axes log-log scaled in Figure 4.24. Trend is fitted with the function of $y = ax^b$ where y is TL glow curve area, x is irradiation dose to, a and b are constants. With this fit, value of linearity index b is determined as 1.36 for the dose range 0.1-40Gy and 1.46 for dose range 1-10 Gy β dose.

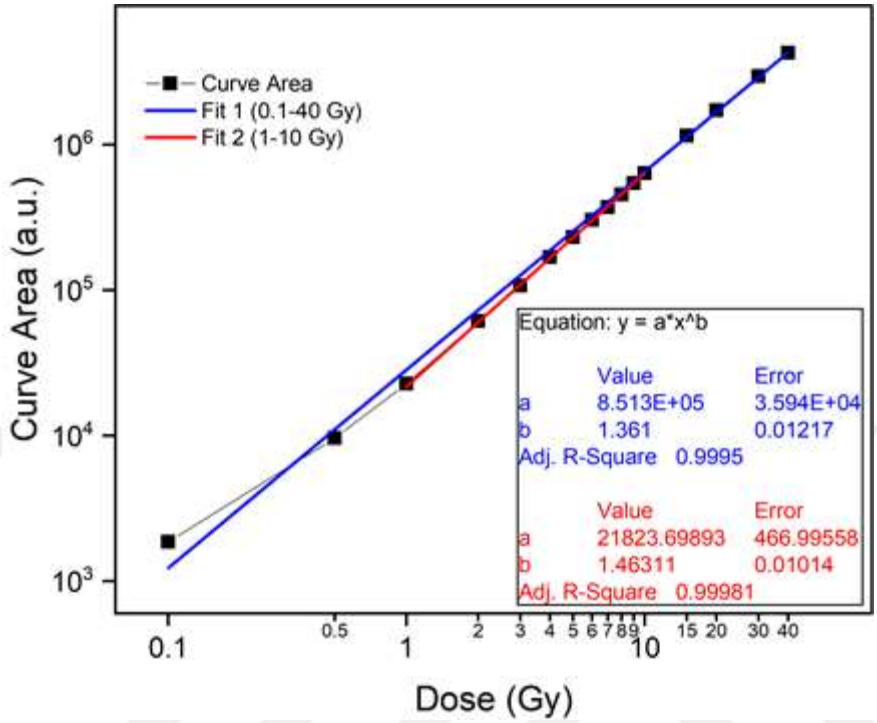

Figure 4.24. TL glow curve area of $NaBaBO_3:Tb^{3+}$(2%, weight) versus irradiation dose.

4.3. Various Heating Rates Experiment Results

4.3.1. VHR Experiment Results of Undoped $NaBaBO_3$ Sample

Pellet sample of undoped $NaBaBO_3$ with ~25mg weight was irradiated with 5Gy of β dose then preheated up to 130°C with a constant heating rate of 2°C/s. Then TL signal readout completed with various heating rates with a thermal stimulation from room temperature up to 450°C, then cooled back to room temperature. A background signal reading was also completed for corresponding heating rate. Heating rates that were used for this experimental procedure was 0.5, 1, 2, 3, 4, 5, 6, 7, 8, 9, 10, 13, 15, 17, 20 °C/s. All the TL glow curves recorded from this experiment are given in Figure 4.25. TL filter combination used for this experiment was the one that determined for undoped $NaBaBO_3$, or IRSL-TL 565nm in other words.

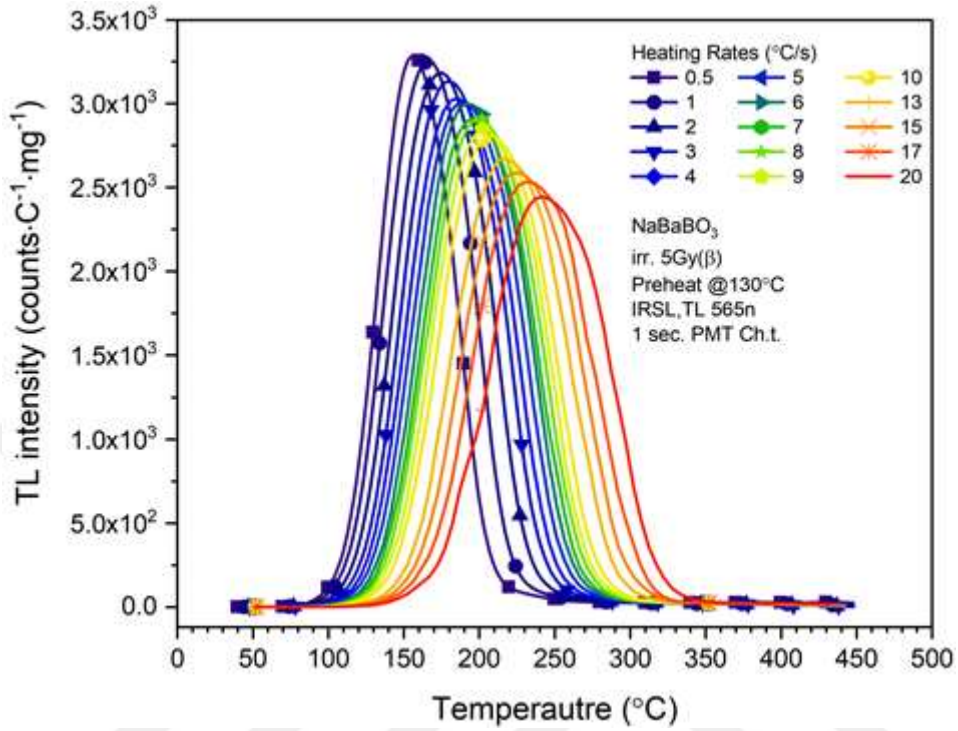

Figure 4.25. TL glow curves of undoped $NaBaBO_3$ recorded for VHR experiment.

From Fig.4.25 it can be seen as it was observed after VHR experiment that peak intensity-I_m decreased, full width at half maximum increased, peak temperature T_m decreased while heating rate increased. Curve area has a decreasing trend with the increase of heating rate which is opposite of expected behavior of being nearly constant. This is due to thermal quenching which was mentioned and referred in "Materials and Methods" chapter. Above mentioned trends of peak temperature, peak intensity, FWHM, and curve area per heating rate are given in Figure 4.26. Additionally, peak temperature trend is given also for temperature lag effect corrected.

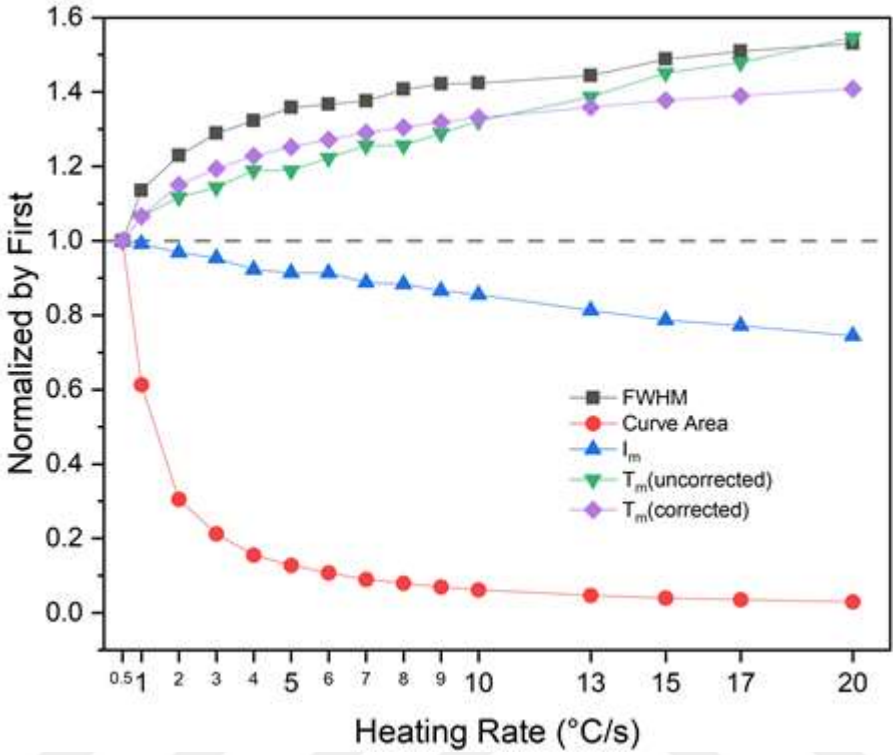

Figure 4.26. Trends of FWHM, Curve Area, I_m, T_m(corrected), and T_m(uncorrected) versus applied heating rates for VHR experiment of undoped $NaBaBO_3$.

Temperature lag correction was done by using Eqn.3.21 and Eqn.3.22 and shown in Fig.4.23. A plot of $ln(T_m^2/\beta)$ vs $1/k_B T_m$ was created for T_m before and after temperature lag. Each of trend is fitted with a linear equation to estimate the activation energy of peak location. Here this assumption was done as if this glow curve is the result of the photon emission from the trapped electrons of single energy level. From the slope of each fit corresponding activation energy is estimated, and for the intercept value vibration frequency of trapped electrons is calculated from $intercept = ln(E/sk_B)$ equation as mentioned in "Materials and Methods" chapter for Hoogenstraaten method and its equation-Eqn.3.19. Peak temperature values are tabulated in Table 4.1.

Table 4.1. Peak temperature values before and after temperature lag correction for peak temperature values of undoped $NaBaBO_3$.

	Peak Temperature (°C)	
H.R. (°C/s)	Uncorrected	Corrected
0.5	156.62	156.62
1	166.98	166.98
2	174.97	180.16
3	179.09	187.00
4	186.23	192.39
5	186.15	196.14
6	191.50	199.23
7	196.69	202.12
8	196.81	204.38
9	201.92	206.59
10	207.05	208.55
13	217.23	212.81
15	227.34	215.76
17	231.66	217.63
20	242.23	220.59

In Figure 4.27, mentioned temperature lag trend for peak temperature before and after temperature lag correction, linear fit of each trend and parameters of each fit are given. $ln(T_m^2/\beta)$ vs $1/k_B T_m$ distribution is fitted with line and r-square value got dramatically better after temperature lag correction; before the correction r-square value was 0.89736 and after correction it became 0.99813. As Hoogenstraaten method suggested, slope of linear fit is equal to activation energy of the trapped electrons at this trap level or trap depth in other words in units of electron volts. Vibration frequency of trapped electrons to such a trap can be estimated from the value that fit intercepts y-axis: As method suggests, frequency factor can be calculated from $intecept = ln(E/sk_B)$ in units of per unit time (or Hertz in other words).

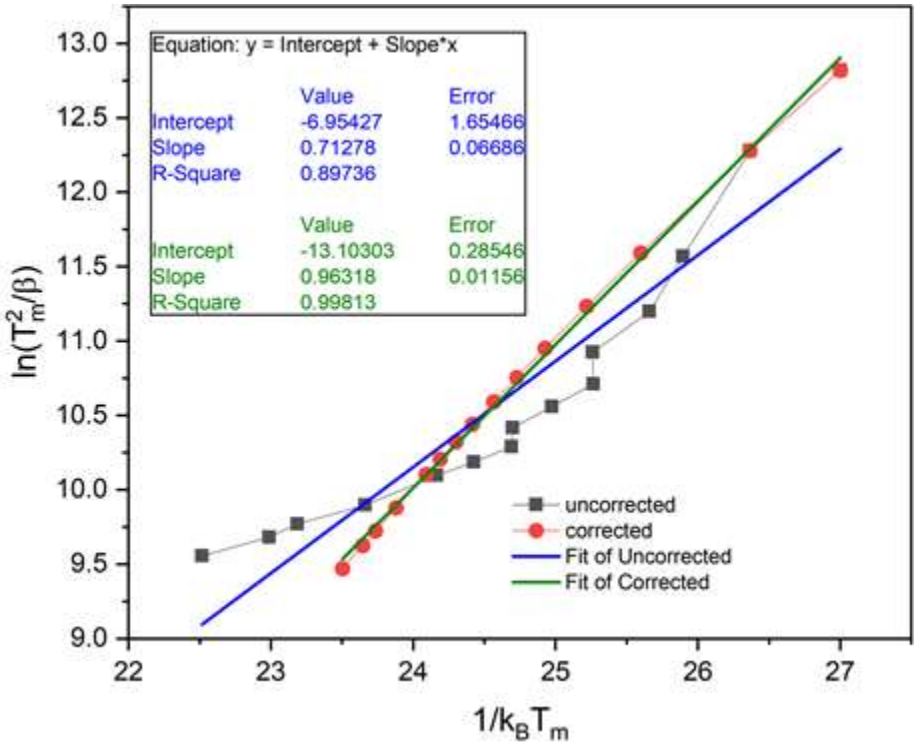

Figure 4.27. A graph of T_m(corrected), and T_m(uncorrected) per applied heating rates trend for undoped $NaBaBO_3$.

Estimated activation energies and escape frequencies as before and after correction with Hoogenstraaten method are given in Table 4.2.

Table 4.2. Estimated activation energy and frequency factor values with and without temperature lag correction.

	Activation Energy-E(*eV*)	Frequency Factor-s (sec^{-1})
uncorrected	0.71	8.67E6
corrected	0.96	5.48E9

Activation energy value is calculated also with Eqn.3.18 and Eqn.3.20 with uncorrected and corrected peak temperature values, and given in Table 4.3.

Table 4.3. Calculated activation energy with standard error of mean before and after temperature lag correction done by using Eqn.3.18 and 3.20.

	Activation Energy-E_a (eV)			
	Booth-Bohun-Porfianovitch		Gartia et. al	
H.R (°C/s)	Uncorrected	Corrected	Uncorrected	Corrected
0.75	0.85	0.85	0.91	0.91
1	1.13	0.88	1.18	0.93
2	1.32	1.02	1.25	0.94
3	1.21	1.03	1.12	0.94
4	1.34	1.04	1.24	0.95
5	1.11	0.91	1.15	0.96
6	1.04	0.92	1.07	0.95
7	1.10	0.92	1.12	0.96
8	1.02	0.93	1.04	0.96
9	0.96	0.93	0.98	0.96
10	0.88	0.94	0.89	0.95
13	0.80	0.95	0.82	0.95
15	0.78	0.95	0.80	0.95
17	0.79	1.02	0.74	0.95
Mean	1.02±0.05	0.95±0.02	1.02±0.04	0.95±0.004

Curve area has a decreasing trend as shown in Fig.4.26 due to thermal quenching. To calculate thermal quenching parameters, for this set of experimental results, curve area recorded with 0.5°C/s was assumed as if unquenched. For the calculation Eqn.3.24 is applied and a graph of $ln[(A/I_{QUE}) - 1]$ versus $1/kT_m$ is given in Figure 4.28. A is the curve are recorded with 0.5°C/s, I_{QUE} is the curve area value recorded with heating rate that is greater than 0.5°C/s. Quenching parameters W and C are estimated from linear fit of this distribution: Slope of this fit as equal to -W; intercept as equal to ln(C) and tabulated in Table 4.4.

Table 4.4. Thermal quenching parameters W and C for undoped $NaBaBO_3$.

Thermal Quenching Parameters	
W (eV)	C
0.87±0.1	1.85E10

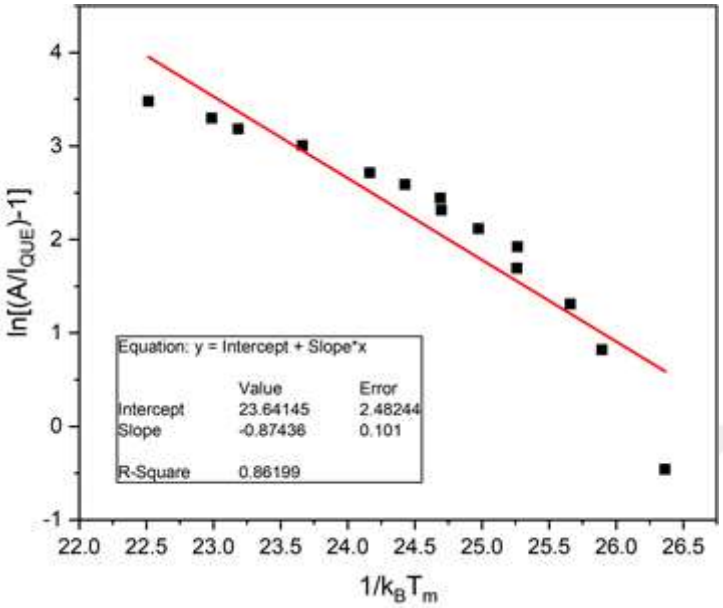

Figure 4.28. Thermal quenching graph of undoped $NaBaBO_3$ as $ln[(A/I_{QUE}) - 1]$ versus $1/kT_m$ fitted with linear equation. Slope is -W, exp(intercept) is C.

4.3.2. VHR Experiment Results of $NaBaBO_3:Ce^{3+}$(0.5%) Sample

In this experimental step, pellet formed sample of $NaBaBO_3:Ce^{3+}$(0.5%, weight) powder with ~30mg irradiated with 1 Gy of β dose, then heated with a 2°C/s heating rate up to optimal preheat temperature 160°C and kept at this temperature for 20 seconds and then cooled back to room temperature. After irradiation and preheat step completed, a thermal stimulation applied with 0.5°C from room temperature up to 500°C, then cooled back to room temperature. Afterwards, a TL background signal was recorded with the same heating rate and preheat condition. This cycle of irradiation-preheating-TL signal reding- TL background signal reading completed for a set of heating rates as 0.5, 0.75, 1, 2, 3, 4, 5, 6, 7, 8, 9, 10 °C/s. IRSL-TL 565 nm was used as TL bandpass filter combination since it was determined as the optimal one for reading the TL

emission signal of $NaBaBO_3:Ce^{3+}$(0.5%, weight). Recorded TL signals, of this VHR experiment, are given in Figure 4.29.

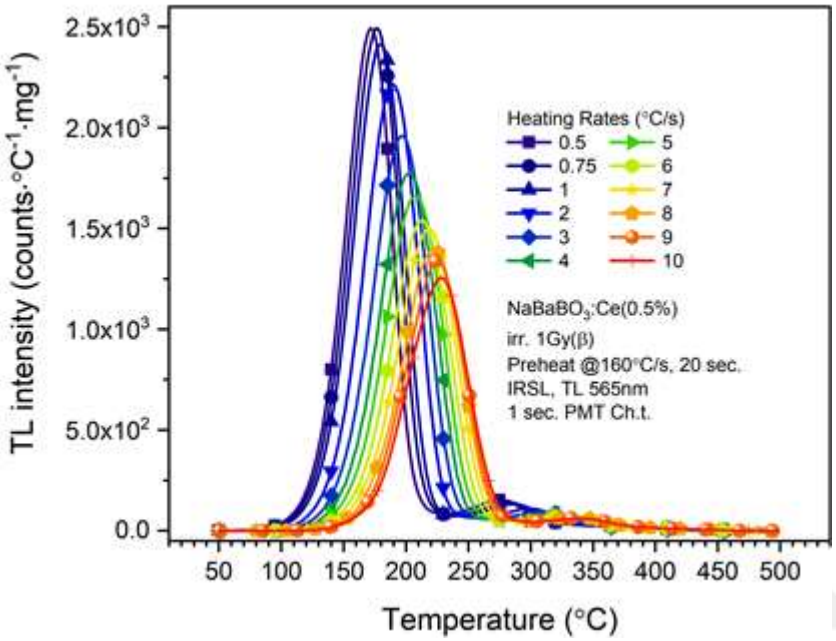

Figure 4.29. TL glow curves of $NaBaBO_3:Ce^{3+}$(0.5%, weight) recorded with various heating rates under same conditions except for heating rate.

It is obviously seen that peak intensity decreased as heating rate increased, which means that normal heating rate behavior was observed. Glow curve has pattern with two maxima and they are not isolated. For this reason, FWHM and individual peak area values weren't graphed to show their trend per heating rate; but instead, total glow curve are trend is shown in Figure 4.30-a. Temperature lag correction was done for both peak temperature values as they can be determined without problem; but FWHM could not be determined due to borders of peaks were mixed each other's regions. Peak intensity trend for these two maxima is also given in Figure 4.30-a and Figure 4.30-b respectively.

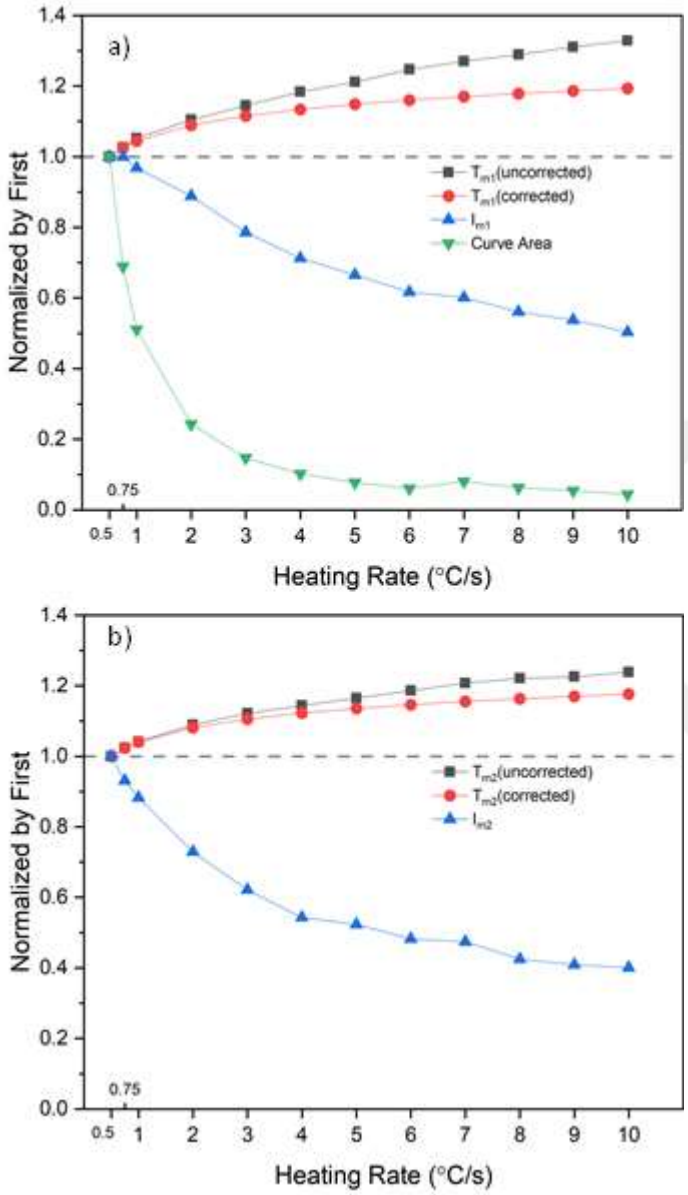

Figure 4.30. VHR trends of $NaBaBO_3:Ce^{3+}$(0.5%, weight) as normalized by their first value: a) Trend of curve area, peak intensity, peak temperature as uncorrected and corrected for maxima 1; b) Trend of peak intensity, peak temperature as uncorrected and corrected for maxima 2.

Peak temperature values are tabulated in Table 4.5 for both maxima 1 and maxima 2 as with and without temperature lag correction.

Table 4.5. Peak temperature values for maxima 1 and maxima 2 before and after temperature lag correction for peak temperature values of $NaBaBO_3:Ce^{3+}(0.5\%)$.

	Peak Temperature (°C)			
	Maxima 1		Maxima 2	
H.R.(°C/s)	Uncorrected	Corrected	Uncorrected	Corrected
0.5	171.46	171.45	275.25	275.24
0.75	175.95	175.94	281.82	281.81
1	180.46	179.12	286.61	286.48
2	189.36	186.80	299.95	297.72
3	196.33	191.28	308.78	304.30
4	202.94	194.47	314.89	308.96
5	207.68	196.94	320.73	312.58
6	213.80	198.96	326.45	315.54
7	217.81	200.66	332.46	318.04
8	221.02	202.14	336.03	320.20
9	224.73	203.45	337.34	322.11
10	227.82	204.61	340.91	323.82

Trend graph of $ln(T_m^2/\beta)$ vs $1/k_BT_m$ created by using peak temperature value given with and without temperature lag correction for maxima 1 and maxima 2 are given in Figure 4.31. Each trend distribution is fitted with a line function to estimate activation energy and frequency factor from slope and intercept values, respectively. Such estimations may give overestimated values due to overlapping peaks originating from close-by energy levels as mentioned and referred in "Material and Methods" chapter. In other words, glow curve may be superposition of more than one peak. It can be seen from the Table 4.5 that, peak temperature values got lower after correction was applied, except for first two heating rates. Method suggests that first two heating rates are assumed as effect of temperature lag is negligible as mentioned and referred in "Materials and Methods" chapter.

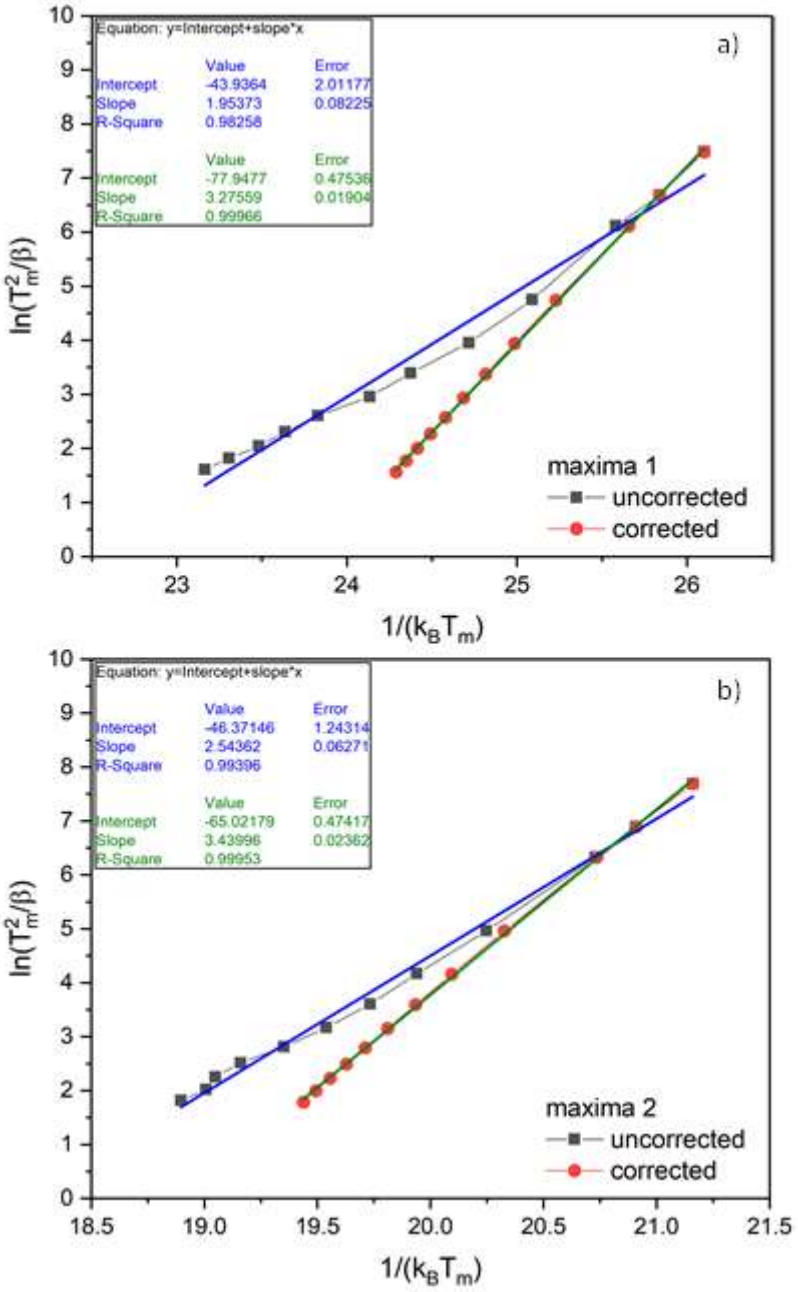

Figure 4.31. Plots of $ln(T_m^2/\beta)$ vs $1/k_B T_m$ of $NaBaBO_3:Ce^{3+}$(0.5%, weight) linear fits of trends and their fit values: a) for maxima 1 as corrected and uncorrected b) for maxima 2 as corrected and uncorrected.

$ln(T_m^2/\beta)$ vs $1/k_B T_m$ trends have better linear distributions as can be understood from the r-square values: For maxima 1 (or peak 1) 0.98258 and 0.99966 before and after temperature lag correction respectively; for maxima 2 (or peak 2) 0.99396 and 0.99953 before and after temperature lag correction respectively. As this method, Hoogenstraaten, suggested: Slope of fit line is activation energy and frequency factor frequency factor can be calculated from $intecept = ln(E/sk_B)$ in units of. Activation energy and escape frequencies for maxima 1 and maxima 2 tabulated in Table 4.6. Activation energy value was calculated by using Eqn.3.18 and Eqn.3.20 and tabulated for maxima 1 and maxima 2 in Table 4.7 and Table 4.8. respectively.

Table 4.6. Estimated activation energy and frequency factor values, with and without temperature lag correction, by using Hoogenstraaten method.

		Activation Energy-E(eV)	Frequency Factor-s (sec^{-1})
Maxima 1	uncorrected	1.95±0.08	2.73E23
	corrected	3.27±0.02	2.71E38
Maxima 2	uncorrected	2.54±0.06	4.06E24
	corrected	3.44±0.02	6.91E32

Table 4.7. Calculated activation energy of maxima 1 of $NaBaBO_3:Ce^{3+}$ (0.5%).

	Activation Energy-E_a (eV)			
	Booth-Bohun-Porfianovitch		Gartia et. al	
H.R.(°C/s)	Uncorrected	Corrected	Uncorrected	Corrected
0.75	1.48	1.48	1.55	2.29
1	1.26	1.49	1.28	2.53
2	1.43	1.65	1.26	2.45
3	1.36	1.67	1.12	1.54
4	1.27	1.68	1.01	1.26
5	1.09	1.55	0.96	1.10
6	1.01	1.56	0.88	1.02
7	0.99	1.56	0.86	0.94
8	0.98	1.57	0.84	0.89
9	0.95	1.57	0.81	0.87
10	0.94	1.57	0.79	0.83
Mean	1.18±0.6	1.58±0.02	1.06±0.08	1.49±0.21

Table 4.8. Calculated activation energy of maxima 2 of $NaBaBO_3:Ce^{3+}$ (0.5%).

	Activation Energy-E_a (eV)			
	Booth-Bohun-Porfianovitch		Gartia et al.	
H.R. (°C/s)	Uncorrected	Corrected	Uncorrected	Corrected
0.75	1.52	1.52	1.33	1.33
1	1.52	1.54	1.32	1.34
2	1.59	1.73	1.17	1.28
s3	1.55	1.76	1.08	1.24
4	1.54	1.77	1.03	1.20
5	1.32	1.61	1.02	1.23
6	1.28	1.62	0.97	1.21
7	1.22	1.62	0.95	1.24
8	1.21	1.63	0.91	1.20
9	1.24	1.64	0.93	1.20
10	1.22	1.64	0.92	1.21
Mean	1.40±0.0.05	1.64±0.03	1.07±0.05	1.25±0.02

From the results of calculation for activation energy using Hoogenstraaten, Booth-Bohun-Porfianovitch, and Gartia et al. it can be summarized that they are different than each other's. It might be due to first two methods are derived from first order kinetics and are developed for isolated peaks; although third method is valid for any kinetic order between 1-2.5, still it assumes that peak temperature belongs to an isolated peak. As shown in Figure 4.26 curve area is dramatically decreasing with the increase of heating rate. This behavior, effect of thermal quenching, was also seen for undoped sample. In order to calculate quenching parameters W and C, a distribution of $ln[(A/I_{QUE}) - 1]$ versus $1/kT_m$ was fitted with a line equation, Figure 4.32. Thermal quenching parameters W and C of maxima 1 and maxima 2 are tabulated in Table 4.9., and reference heating rate for pairs is 0.5°C/s.

Table 4.9. Thermal quenching parameters W and C for undoped $NaBaBO_3:Ce^{3+}$

	Thermal Quenching Parameters	
	W (eV)	C
maxima 1	1.31±0.14	4.42E14
maxima 2	1.75±0.16	5.93E15

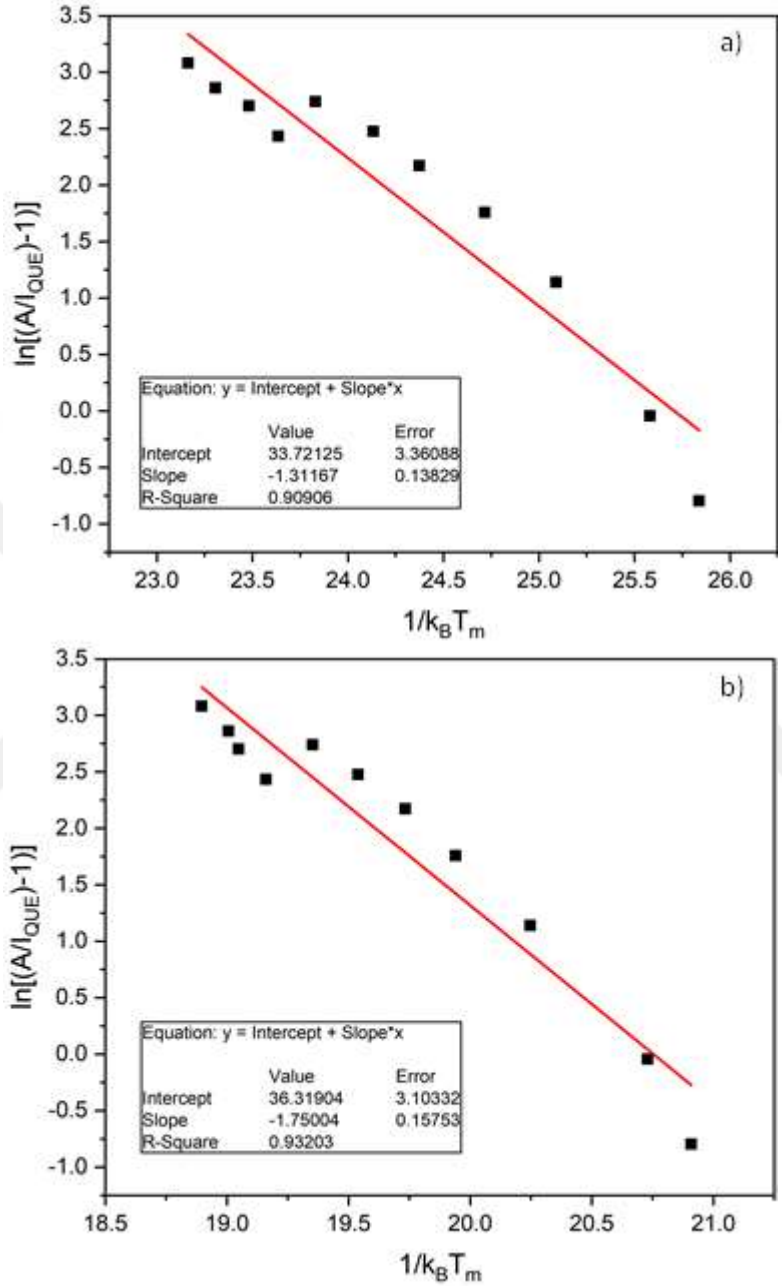

Figure 4.32. $ln[(A/I_{QUE}) - 1]$ versus $1/kT_m$ graphs and their fits to estimate thermal quenching parameters W and C : a) for maxima 1 b) for maxima 2 of $NaBaBO_3:Ce^{3+}$(0.5%, weight).

4.3.3. VHR Experiment Results of $NaBaBO_3:Gd^{3+}$(1%) Sample

Pellet formed $NaBaBO_3:Gd^{3+}$(1%, weight) sample, ~30mg, was irradiated with 5Gy of β dose and then preheated at 215°C for 12 seconds, then cooled back to room temperature. Temperature ramp-up was 2°C/s for preheat step. After sample the preheat step, a TL reading was completed with IRSL-TL 410nm filter combination and 0.5°C/s heating rate for main TL signal reading and cooled back to room temperature; after this, one more time a TL reading was completed with the same heating rate, same band pass filter combination. Heating rate of preheat was used constantly 2°C/s after the irradiation step. Whole experimental procedure was completed by varying the heating rate of TL reading as 0.5, 1, 2, 3, 4, 5, 6, 7, 8, 9, 10°C/s. TL glow curves, which were recorded by using above given heating rate values, are given in Figure 4.33. VHR trends of maxima 1 and 2 are shown with Figure 4.34.

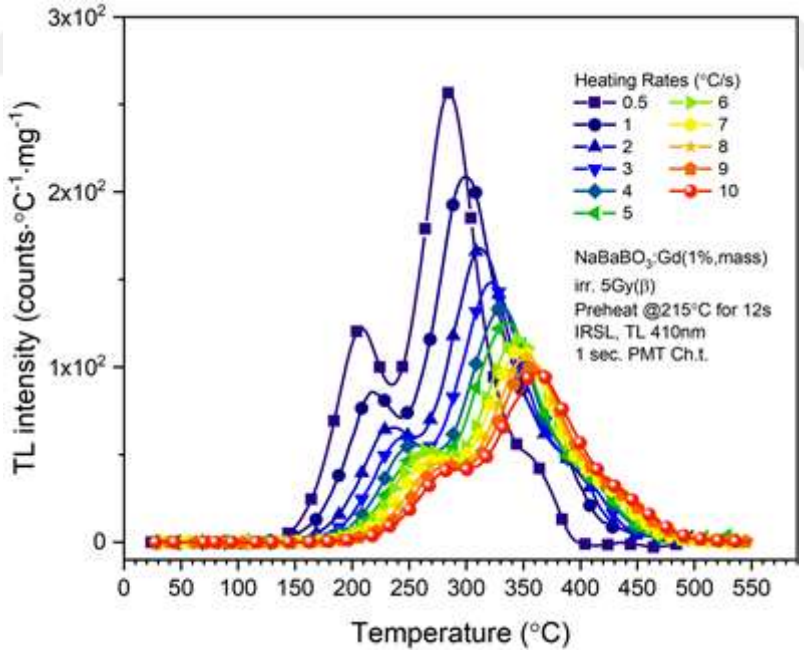

Figure 4.33. TL glow curves of $NaBaBO_3:Gd^{3+}$(1%, weight) recorded with various heating rates under same conditions except for heating rate.

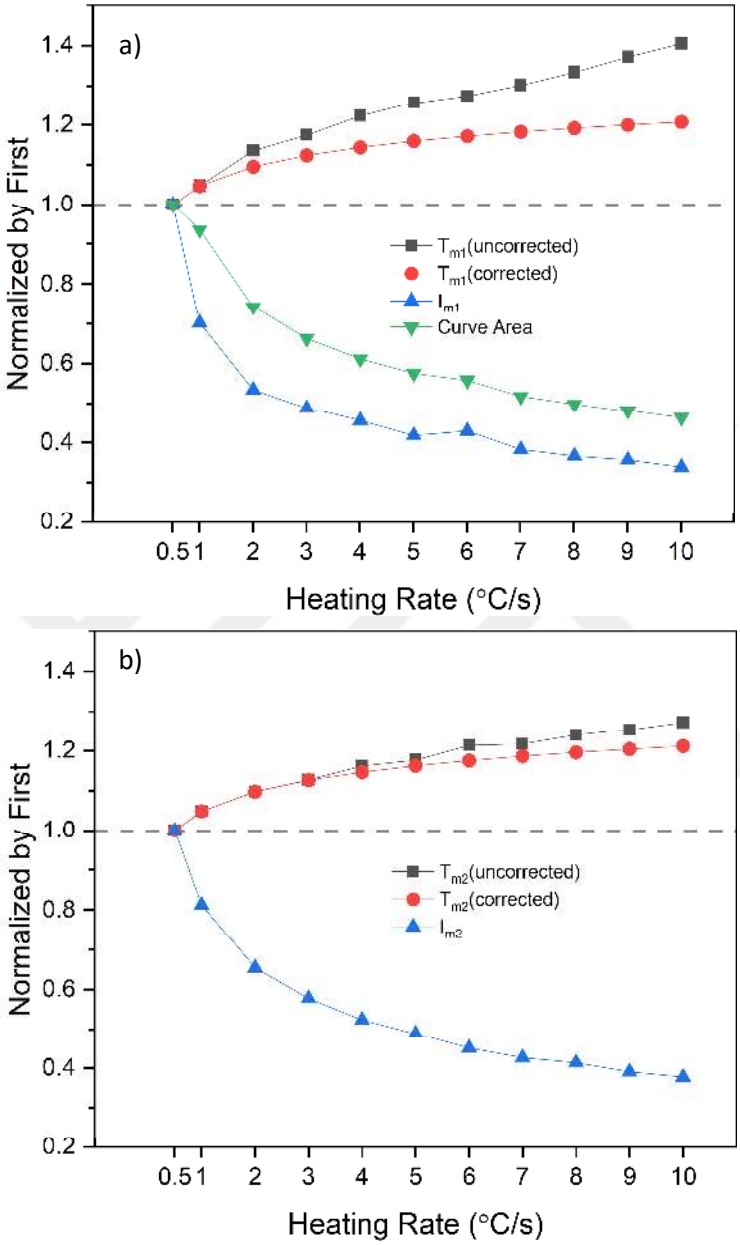

Figure 4.34. VHR trends of $NaBaBO_3:Gd^{3+}$(1%, weight) as normalized by their first value: a) Trend of curve area, peak intensity, peak temperature as uncorrected and corrected for maxima 1; b) Trend of peak intensity, peak temperature as uncorrected and corrected for maxima 2.

Heating rate behavior is normal; peak intensities decreased, peak temperatures sifted towards higher values as the heating rate increased, Fig.4.33 and Fig.4.34. For the FWHM it would be misleading (even if it could be done for this curve) since in this glow curve only two maxima (or peak) can be seen clearly; but they are not isolated, and this makes very hard to determine the FWHM. TL glow curve area trend of $NaBaBO_3:Gd^{3+}$ (1%, weight) is decreasing as similar to undoped $NaBaBO_3$, and $NaBaBO_3:Ce^{3+}$ (0.5%, weight) samples' curve are trends per heating rate.

Peak temperature values are tabulated in Table 4.10 for both maxima 1 and maxima 2 as with and without temperature lag correction.

Table 4.10. Peak temperature values for maxima 1 and maxima 2 before and after temperature lag correction for peak temperature values of $NaBaBO_3:Gd^{3+}$(1%).

	Peak Temperature (°C)			
	Maxima 1		Maxima 2	
H.R. (°C/s)	Uncorrected	Corrected	Uncorrected	Corrected
0.5	208.24	208.24	285.24	285.24
1	218.22	218.22	299.22	299.22
2	236.53	228.20	313.30	313.20
3	244.56	234.04	321.56	321.38
4	254.52	238.18	331.52	327.18
5	261.62	241.39	335.62	331.68
6	265.29	244.02	346.13	335.36
7	270.89	246.24	347.16	338.47
8	277.69	248.16	353.63	341.16
9	285.63	249.86	357.82	343.54
10	292.58	251.37	362.98	345.66

Activation energies of maxima one and maxima 2 were calculated by using Hoogenstraaten method, and $ln(T_m^2/\beta)$ vs $1/k_B T_m$ are shown in Figure 4.35. Those trends are shown before and after temperature lag correction on the peak temperatures of maxima 1 and maxima 2.

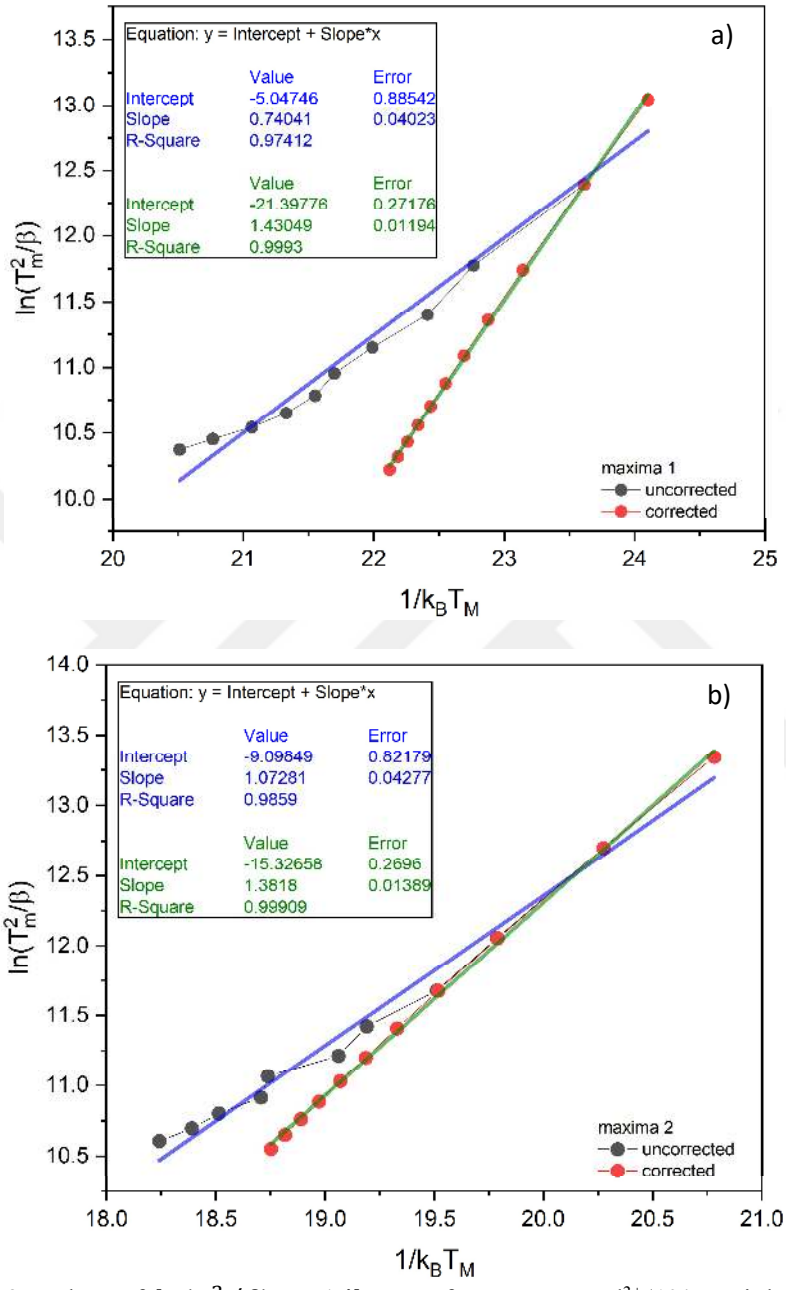

Figure 4.35. Plots of $ln(T_m^2/\beta)$ vs $1/k_B T_m$ of $NaBaBO_3:Gd^{3+}$(1%, weight), linear fits of trends and their fit values: a) for maxima 1 as corrected and uncorrected b) for maxima 2 as corrected and uncorrected.

From the Fig.3.35 it can be interpreted that, distributions got better linear likelihoods after temperature lag effect correction: r-square values of fits applied before and after correction changed from, respectively for maxima 1 and maxima 2, 0.97412 and 0.9859 to 0.9993 and 0.99909. Table of estimated activation energies and frequency factors of maxima 1 and maxima 2 are given with Table 4.11. Again, it should be noted that those estimations are derived for isolated peaks, in contrast here peaks are not isolated.

Table 4.11. Estimated activation energy and frequency factor values, with and without temperature lag correction, by using Hoogenstraaten method.

		Activation Energy-E(*eV*)	Frequency Factor-s (sec^{-1})
Maxima 1	uncorrected	0.74±0.04	1.34E6
	corrected	1.43±0.01	3.26E13
Maxima 2	uncorrected	1.07±0.04	1.11E8
	corrected	1.38±0.01	7.27E10

Activation energy values of both peaks were also calculated with “two different heating rates” by using Eqn.3.18 and Eqn.3.20 and tabulated as Table 4.12 and Table 4.13.

Table 4.12. Calculated activation energy of maxima 1 of $NaBaBO_3:Gd^{3+}$ (1%).

	Activation Energy-E_a (*eV*)			
	Booth-Bohun-Porfianovitch		Gartia et. al	
H.R.(°C/s)	Uncorrected	Corrected	Uncorrected	Corrected
1	1.33	1.33	0.69	0.69
2	0.95	1.36	0.57	0.79
3	0.97	1.38	0.64	0.88
4	0.90	1.39	0.61	0.92
5	0.87	1.40	0.59	0.92
6	0.89	1.40	0.64	0.98
7	0.86	1.41	0.61	0.95
8	0.82	1.42	0.58	0.96
9	0.78	1.42	0.56	0.97
10	0.74	1.42	0.53	0.97
Mean.	0.91±0.05	1.39±0.01	0.60±0.01	0.90±0.03

Table 4.13. Calculated activation energy of maxima 2 of $NaBaBO_3:Gd^{3+}$ (1%).

	Activation Energy-E_a (eV)			
	Booth-Bohun-Porfianovitch		Gartia et al.	
H.R.(°C/s)	Uncorrected	Corrected	Uncorrected	Corrected
1	1.27	1.27	0.96	0.96
2	1.30	1.30	0.97	0.97
3	1.31	1.32	0.98	0.98
4	1.21	1.33	0.90	0.99
5	1.24	1.34	0.92	0.99
6	1.11	1.35	0.83	0.99
7	1.17	1.36	0.86	0.99
8	1.12	1.36	0.83	1.00
9	1.11	1.37	0.82	0.99
10	1.08	1.38	0.80	1.00
Mean	1.19±0.03	1.34±0.01	0.89±0.02	0.99±0.004

Estimation results of activation energy by using Hooggenstraaten, BBP, and BBP like method suggested by Gartia et al. gave different values. Those results might be due to existence of multiple peaks but one peak which may be dominant over the other(s) under a peak temperature region. This will be better understood from the results of T_m-T_{stop} experiment.

Thermal quenching parameters W and C were estimated from fit values of the fits applied on the distributions created as $ln[(A/I_{QUE}) - 1]$ versus $1/kT_m$ graph by using peak temperature and TL glow curve area for both maxima. $ln[(A/I_{QUE}) - 1]$ versus $1/kT_m$ trends are shown in Figure 4.36; and estimated thermal quenching parameters of $NaBaBO_3:Gd^{3+}$(1%, weight) are given with Table 4.14.

Table 4.14. Thermal quenching parameters W and C for $NaBaBO_3:Gd^{3+}$ (1%).

	Thermal Quenching Parameters	
	W (eV)	C
maxima 1	0.82±0.11	3.19E7
maxima 2	1.18±0.18	3.49E9

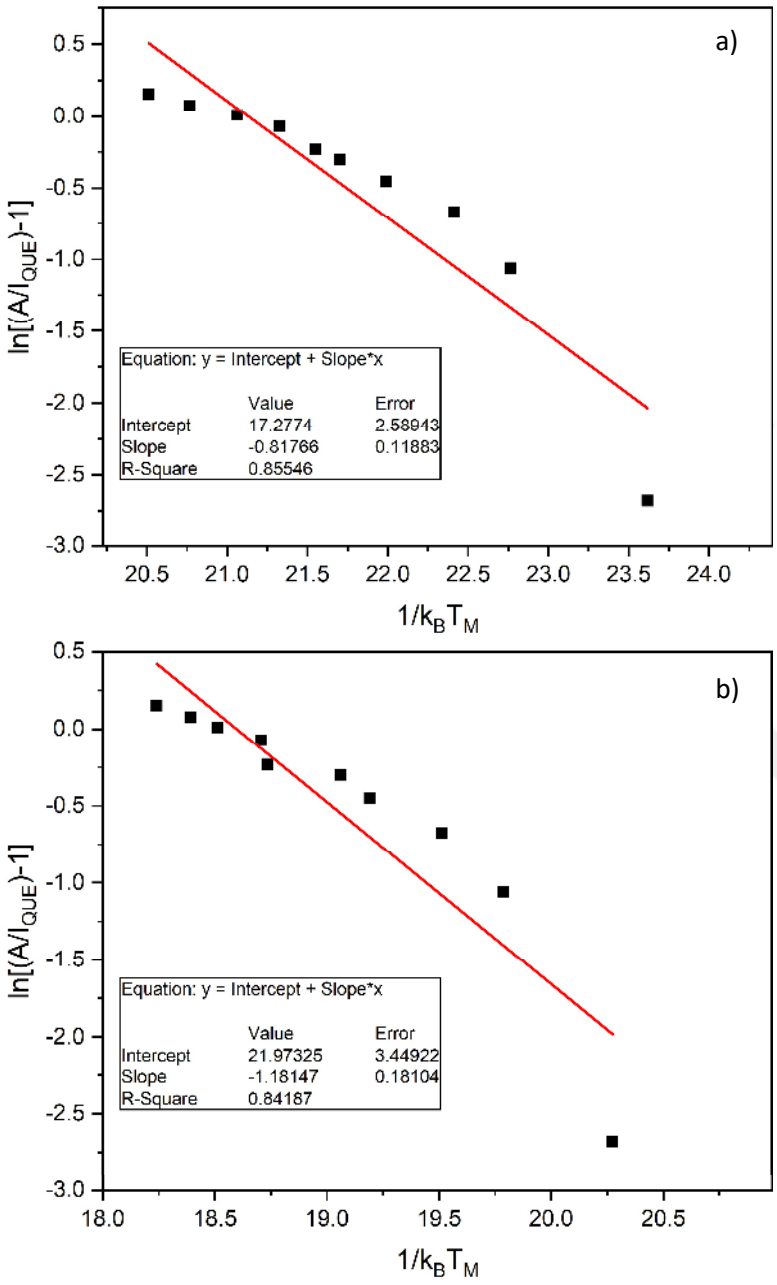

Figure 4.36. $ln[(A/I_{QUE}) - 1]$ versus $1/kT_m$ graphs and their fits to estimate thermal quenching parameters W and C: a) for maxima 1 b) for maxima 2 of $NaBaBO_3:Gd^{3+}$(1%, weight).

4.3.4. VHR Experiment Results of $NaBaBO_3:Tb^{3+}$(2%) Sample

A pellet with ~30mg weight was produced from $NaBaBO_3:Tb^{3+}$(2%, weight) sample. For the VHR experiment various heating rates were used for TL reading process. Before each TL reading, sample was irradiated with 2Gy of β dose, then preheat with a heating rate of 2°C/s from room temperature up to 145°C and kept at this temperature for 17 seconds, then cooled back to room temperature as determined with optimal preheat condition test. TL reading of sample was completed by using IRSL-TL wideband blue TL filter combination with different heating rates while irradiation dose, preheat conditions kept same. Heating rate for TL reading was varied as 0.5, 1, 2, 3, 4, 5, 6, 7, 8, 9, 10°C/s. TL glow curves recorded with mentioned heating rates are shown in Figure 4.37. VHR trends of observed maxima 1 and maxima 2 are shown in Figure 4.38.

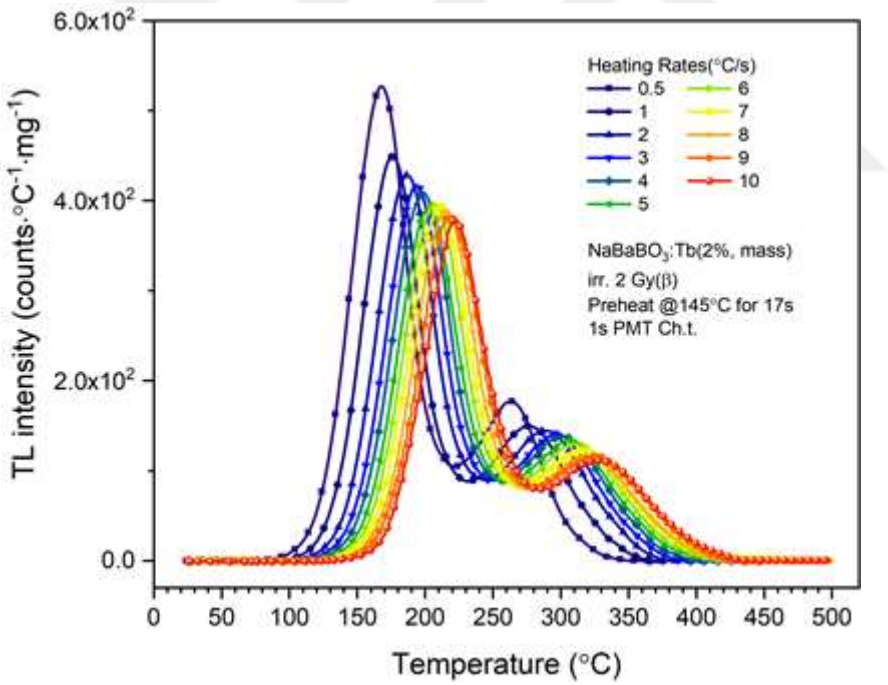

Figure 4.37. TL glow curves of $NaBaBO_3:Tb^{3+}$(2%, weight) recorded with various heating rates under same conditions except for heating rate.

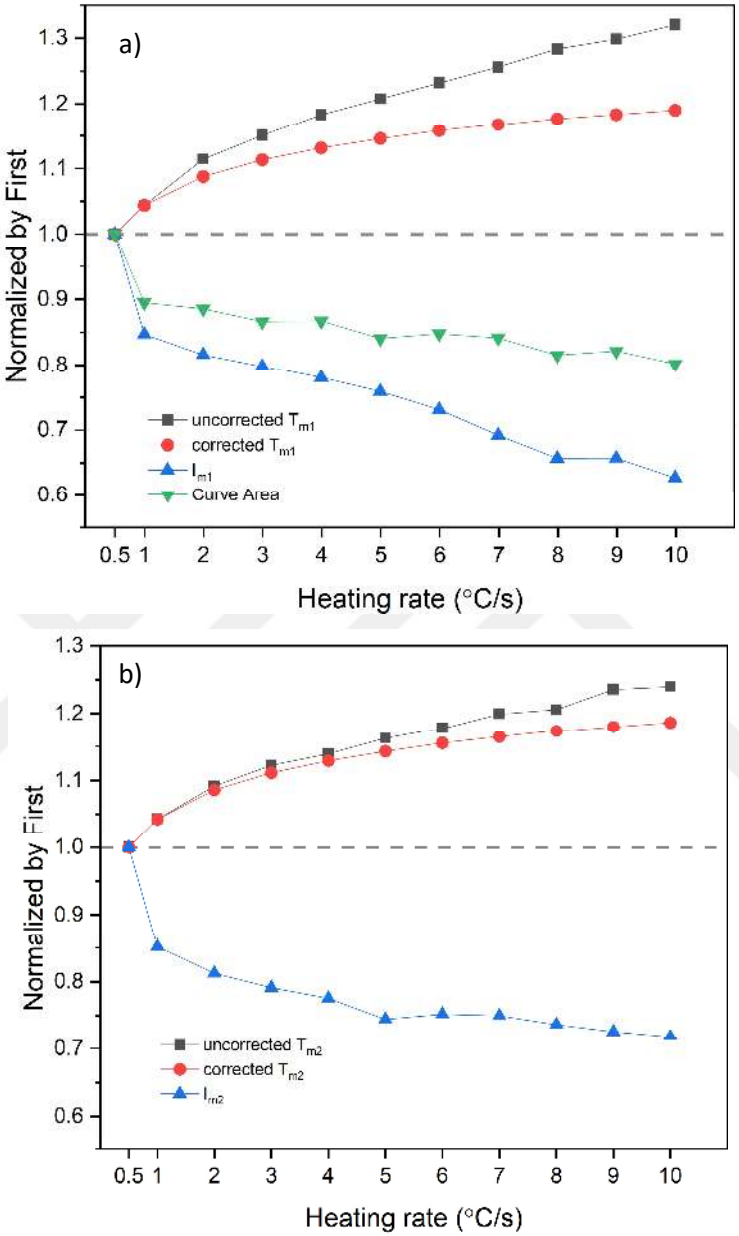

Figure 4.38. VHR trends of $NaBaBO_3:Tb^{3+}$(2%, weight) as normalized by their first value: a) Trend of curve area, peak intensity, peak temperature as uncorrected and corrected for maxima 1; b) Trend of peak intensity, peak temperature as uncorrected and corrected for maxima 2.

As the experimental results shown in Fig.4.37 and Fig.4.38, various heating rates characteristics of $NaBaBO_3:Tb^{3+}$(2%, weight) is normal: intensities of maxima 1 and maxima 2 have a decreasing trend; temperatures of maxima 1 and maxima 2 are increasing with the increase of TL reading's heating rate. Again, such a structure is consisting of more than one peak and they are not isolated, FWHM trends are absent for both maxima. This is similar to VHR results of undoped $NaBaBO_3$, $NaBaBO_3:Ce^{3+}$(0.5%, weight), $NaBaBO_3:Gd^{3+}$(1%, weight) samples.

A temperature lag correction was done by using procedure explained and referred in "Materials and Methods" chapter on peak temperature values of maxima 1 and maxima 2. Peak temperature values of maxima 1 and maxima 2 are listed in Table 4.15 as before and after the temperature lag correction.

Table 4.15. Peak temperature values for maxima 1 and maxima 2 of $NaBaBO_3:Tb^{3+}$ (2%) as before and after temperature lag correction.

	Peak Temperature (°C)			
	Maxima 1		Maxima 2	
H.R. (°C/s)	Uncorrected	Corrected	Uncorrected	Corrected
0.5	167.98	167.98	263.98	263.98
1	175.35	175.35	275.35	275.35
2	187.20	182.72	288.20	286.72
3	193.27	187.03	296.27	293.37
4	198.79	190.09	300.79	298.09
5	202.85	192.46	306.85	301.75
6	206.93	194.58	310.93	305.01
7	211.03	196.19	316.61	307.50
8	215.62	197.72	318.37	309.87
9	218.11	198.83	326.19	311.57
10	221.81	199.94	327.28	313.28

Using Hoogenstraaten method, activation energies of maxima one and maxima 2 were estimated by $ln(T_m^2/\beta)$ vs $1/k_B T_m$ trends, shown in Figure 4.39. Those trends are shown before and after temperature lag correction on the peak temperatures of maxima 1 and maxima 2.

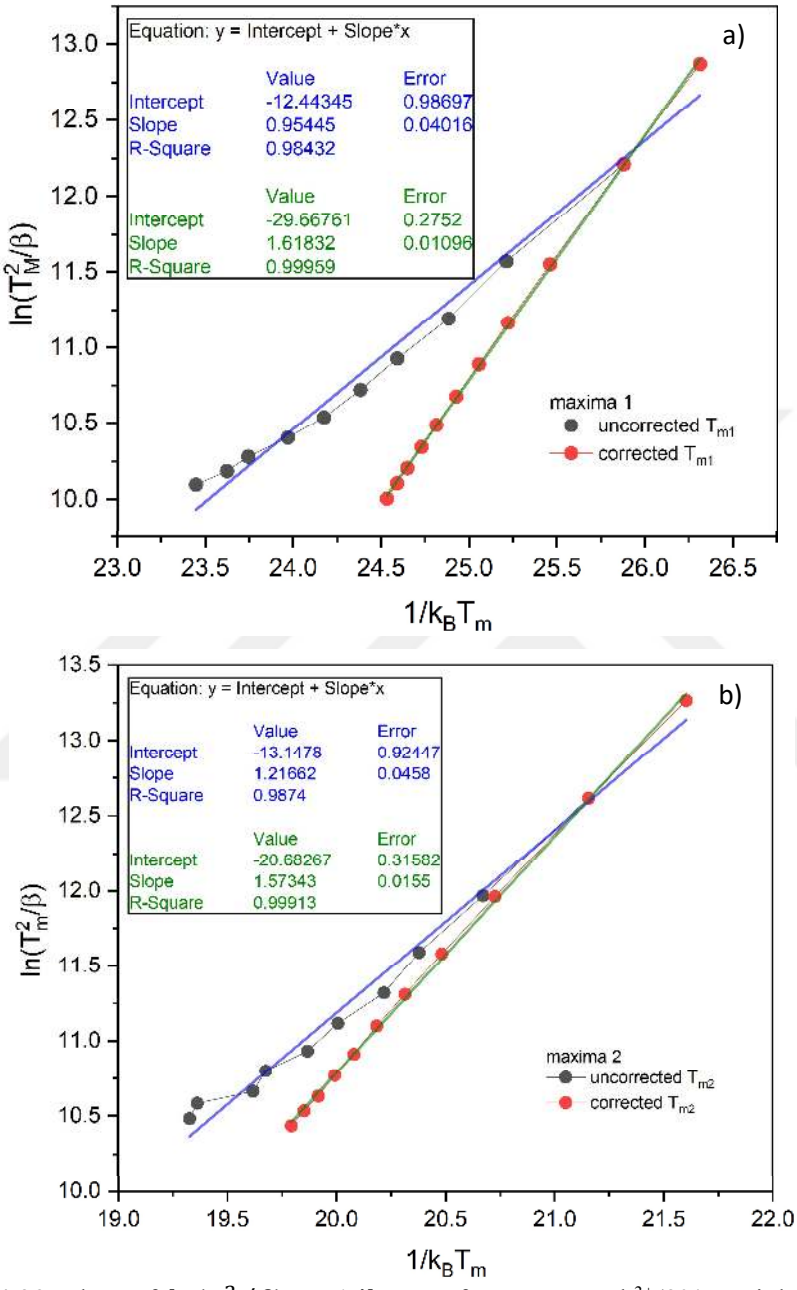

Figure 4.39. Plots of $ln(T_m^2/\beta)$ vs $1/k_B T_m$ of $NaBaBO_3:Tb^{3+}$(2%, weight), linear fits of trends and their fit values.: a) for maxima 1 as corrected and uncorrected b) for maxima 2 as corrected and uncorrected.

As seen from Fig.4.39 which shows the trends of $ln(T_m^2/\beta)$ vs $1/k_B T_m$ by using the peak temperature values of maxima 1 and maxima 2 as with/without temperature lag corrected values given in Table 4.15. As a result of line-like behavior of distributions got better. r-square values of the fits became closer to 1: from 0.98432 to 0.99959 for maxima 1; and from 0.9874 to 0.99913 for maxima 2. Obtained activation energies for this method is tabulated in Table 4.16.

Table 4.16. Estimated activation energy and frequency factor values, with and without temperature lag correction, by using Hoogenstraaten method.

		Activation Energy-E(eV)	Frequency Factor-s (sec^{-1})
Maxima 1	uncorrected	0.95±0.04	2.81E9
	corrected	1.61±0.01	1.44E17
Maxima 2	uncorrected	1.21±0.05	7.24E9
	corrected	1.57±0.02	1.75E13

Activation energy values of both peaks were also calculated with "two different heating rates" by using Eqn.3.18 and Eqn.3.20 and paring each heating rate value with 0.5 °C/s' peak temperature and intensity values, results are tabulated as Table 4.17 and Table 4.18.

Table 4.17. Calculated activation energy of maxima 1 of $NaBaBO_3:Tb^{3+}$ (2%).

	Activation Energy-E_a (eV)			
	Booth-Bohun-Porfianovitch		Gartia et. al	
H.R.(°C/s)	Uncorrected	Corrected	Uncorrected	Corrected
1	1.53	1.53	1.23	1.23
2	1.18	1.55	1.07	1.39
3	1.31	1.69	1.09	1.43
4	1.27	1.71	1.06	1.45
5	1.26	1.72	1.04	1.45
6	1.08	1.58	1.03	1.47
7	1.05	1.59	1.01	1.49
8	1.00	1.59	0.96	1.48
9	1.00	1.60	0.96	1.50
10	0.97	1.61	0.93	1.50
Mean.	1.16±0.06	1.62±0.02	1.04±0.03	1.44±0.03

Table 4.18. Calculated activation energy of maxima 2 of $NaBaBO_3:Tb^{3+}$ (2%).

	Activation Energy-E_a (eV)			
	Booth-Bohun-Porfianovitch		Gartia et al.	
H.R.(°C/s)	Uncorrected	Corrected	Uncorrected	Corrected
1	1.45	1.45	1.18	1.18
2	1.39	1.49	1.27	1.35
s3	1.52	1.66	1.28	1.40
4	1.57	1.67	1.32	1.42
5	1.51	1.69	1.27	1.43
6	1.33	1.52	1.25	1.42
7	1.27	1.53	1.18	1.40
8	1.30	1.53	1.18	1.38
9	1.19	1.55	1.10	1.40
10	1.22	1.55	1.11	1.39
Mean	1.38±0.04	1.57±0.03	1.21±0.02	1.38±0.02

Estimation results of activation energy by using Hoogenstraaten, BBP, and BBP-like method suggested by Gartia et al. gave different values. Those difference might be due to existence of multiple overlapping peaks under a peak temperature region or the kinetic order difference or both. This will be better understood from the results of T_m-T_{stop} experiment results.

Thermal quenching parameters W and C were estimated from fit values of the fits applied on the distributions created as $ln[(A/I_{QUE}) - 1]$ versus $1/kT_m$ graph by using peak temperature and TL glow curve area for both maxima. $ln[(A/I_{QUE}) - 1]$ versus $1/kT_m$ trends are shown in Figure 4.40; and estimated thermal quenching parameters of $NaBaBO_3:Tb^{3+}$(2%, weight) are given with Table 4.19.

Table 4.19. Thermal quenching parameters W and C for $NaBaBO_3:Tb^{3+}$.

	Thermal Quenching Parameters	
	W (eV)	C
maxima 1	0.31±0.03	3.11E2
maxima 2	0.40±0.04	5.07E2

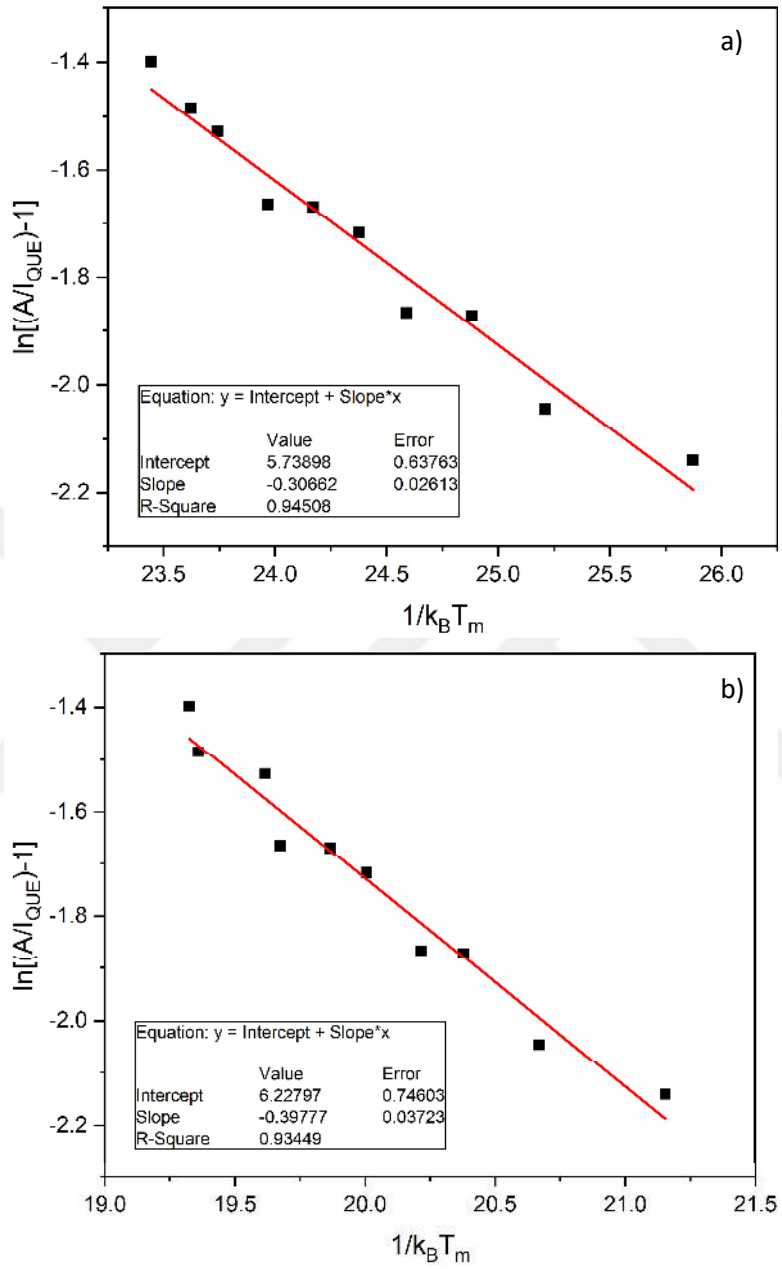

Figure 4.40. $ln[(A/I_{QUE}) - 1]$ versus $1/kT_m$ graphs and their fits to estimate thermal quenching parameters W and C: a) for maxima 1 b) for maxima 2 of $NaBaBO_3:Tb^{3+}$(2%, weight).

4.4. Reusability Experiment Results

4.4.1. Reusability Experiment Results of Undoped $NaBaBO_3$ Sample

In this experimental step, studied samples' TL emission signals are recorded under constant condition up to ten times; and then, curve area of the recorded signals was normalized by the mean value of a ten-readout set to show the trend how it deviates after many usages of the sample. In other words, this kind of measurement shows a dosimetry candidate material's measurement-wisely stability and reliability. Other than that, statistics of each ten-readout set were shown on the graphs to show how a sample deviate statistically.

In Figure 4.41 TL glow curves of undoped $NaBaBO_3$ recorded from a ten-readout cycle are shown.

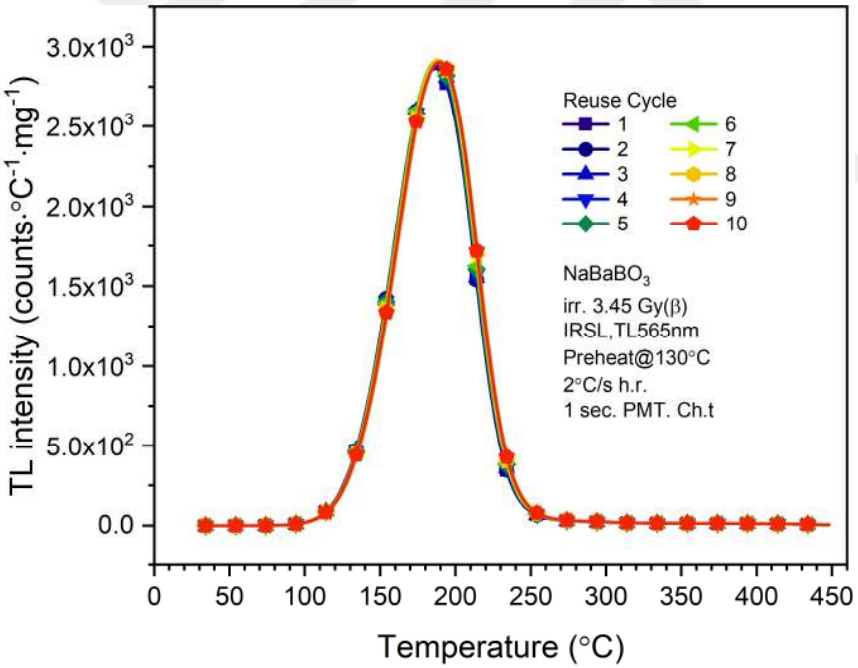

Figure 4.41. TL glow curves of udoped $NaBaBO_3$ recorded for reusability test for ten reuse cycles.

Details about the TL glow curves given in Fig.4.36: Undoped $NaBaBO_3$ pellet with ~25mg weight was irradiated with 3.45Gy β dose; then, preheated with a heating of 2°C/s from room temperature up to 130°C. As soon as temperature reached at 130°C, sample cooled back to room temperature without waiting at this temperature. IRSL-TL 565nm filter combination, a heating rate of 2C°/s from room temperature up to 450°C, condition was used for the TL main and background signals' readout.

In Figure 4.42, trend of curve area is given for this reusability experiment. Curve area trend was divided by mean value of distribution, and a ±5% limits are given. Additionally, a statistic box given as to see how does curve area deviates with respect to the mean value of the curve area distribution. Deviation of a measurement after a ten-reuse cycle is barely 1% w.r.t. mean value of the curve are distribution.

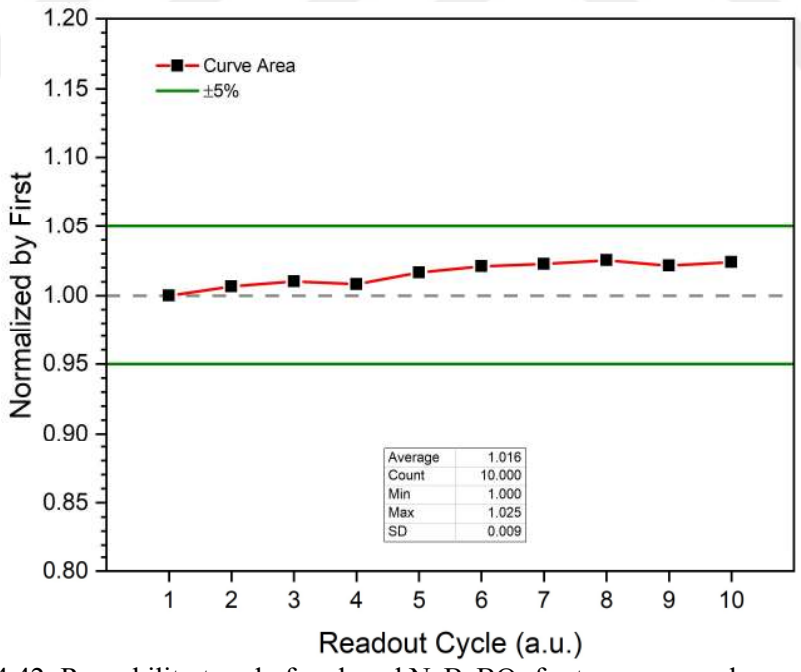

Figure 4.42. Reusability trend of undoped $NaBaBO_3$ for ten reuse cycles.

4.4.2. Reusability Experiment Results of $NaBaBO_3:Ce^{3+}$(0.5%) Sample

Reusability experiment for $NaBaBO_3:Ce^{3+}$ (0.5%, weight) was completed over a ten-reuse readout cycle. For this experimental step, an empty TL readout of pellet sample with ~30mg was done. Then, sample was irradiated with 1Gy of β dose. After that, optimal preheat condition 160°C for 20 seconds, and optimal TL readout filter combination IRSL-TL 565nm were used for each TL readout cycle both with a with a 2°C/s heating rate.

In Figure 4.43, recorded TL glow curves of $NaBaBO_3:Ce^{3+}$ (0.5%, weight) from this experiment are shown. In Figure 4.44, curve area trend with the statistics box is given that standard deviation of ten-reuse is ~2% which is sufficient since it is less than 5%.

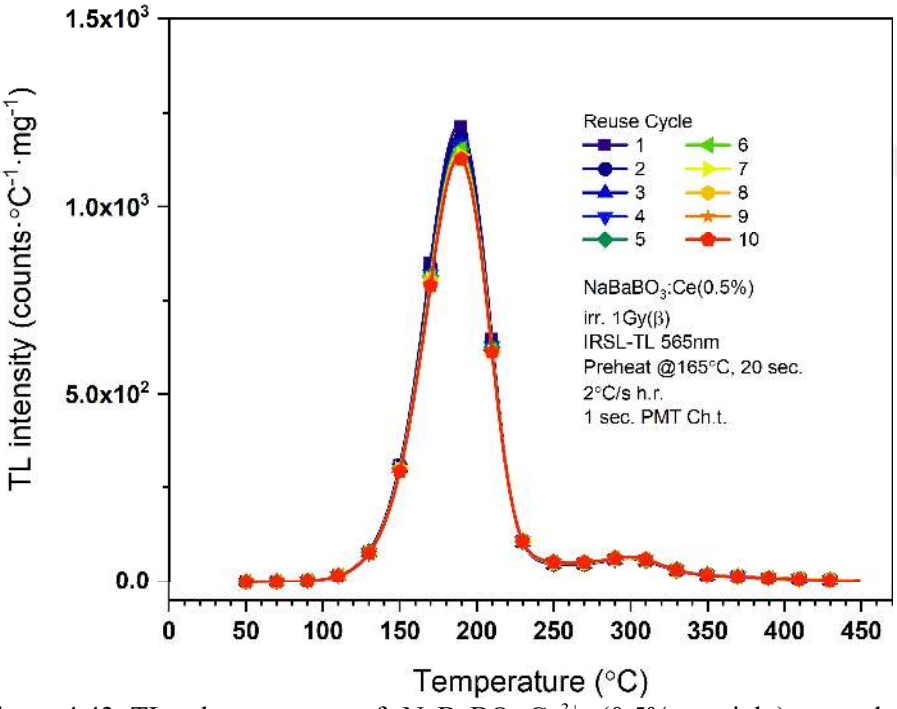

Figure 4.43. TL glow curves of $NaBaBO_3:Ce^{3+}$ (0.5%, weight) recorded for reusability test for a ten-reuse cycle.

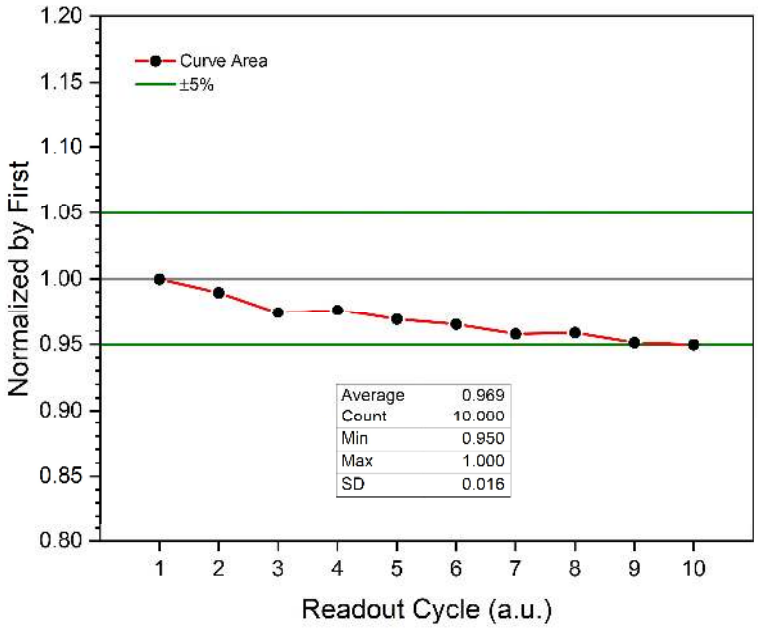

Figure 4.44. Reuse trend of $NaBaBO_3:Ce^{3+}$(0.5%, weight) for ten reuse cycles.

4.4.3. Reusability Experiment Results of $NaBaBO_3:Gd^{3+}$(1%) Sample

Reusability experiment of $NaBaBO_3:Gd^{3+}$(1%, weight) was completed with a ten-reuse cycle of irradiate-preheat-TL main signal reading-TL background signal reading: before starting the irradiation step. Firstly, a complete thermal cleaning on the pellet sample was done to make sure all the traps are emptied before filling them with the stimulated electrons of the irradiation step. In other words, a thermal stimulation from room temperature up to 500°C with a 2°C/s was completed. Then, sample with ~30mg irradiated with 5Gy of β dose. After that, the determined preheat condition applied on the sample, and then a TL reading from room temperature up to 500°C with a 2°C/s by using IRSL-TL 410nm filter combination was completed. Same thermal stimulation and temperature range was used for the reading of TL background signal. In Figure 4.45-a TL glow curves of reusability experiment of $NaBaBO_3:Gd^{3+}$(1%, weight) are given for this ten-reuse TL readout cycle.

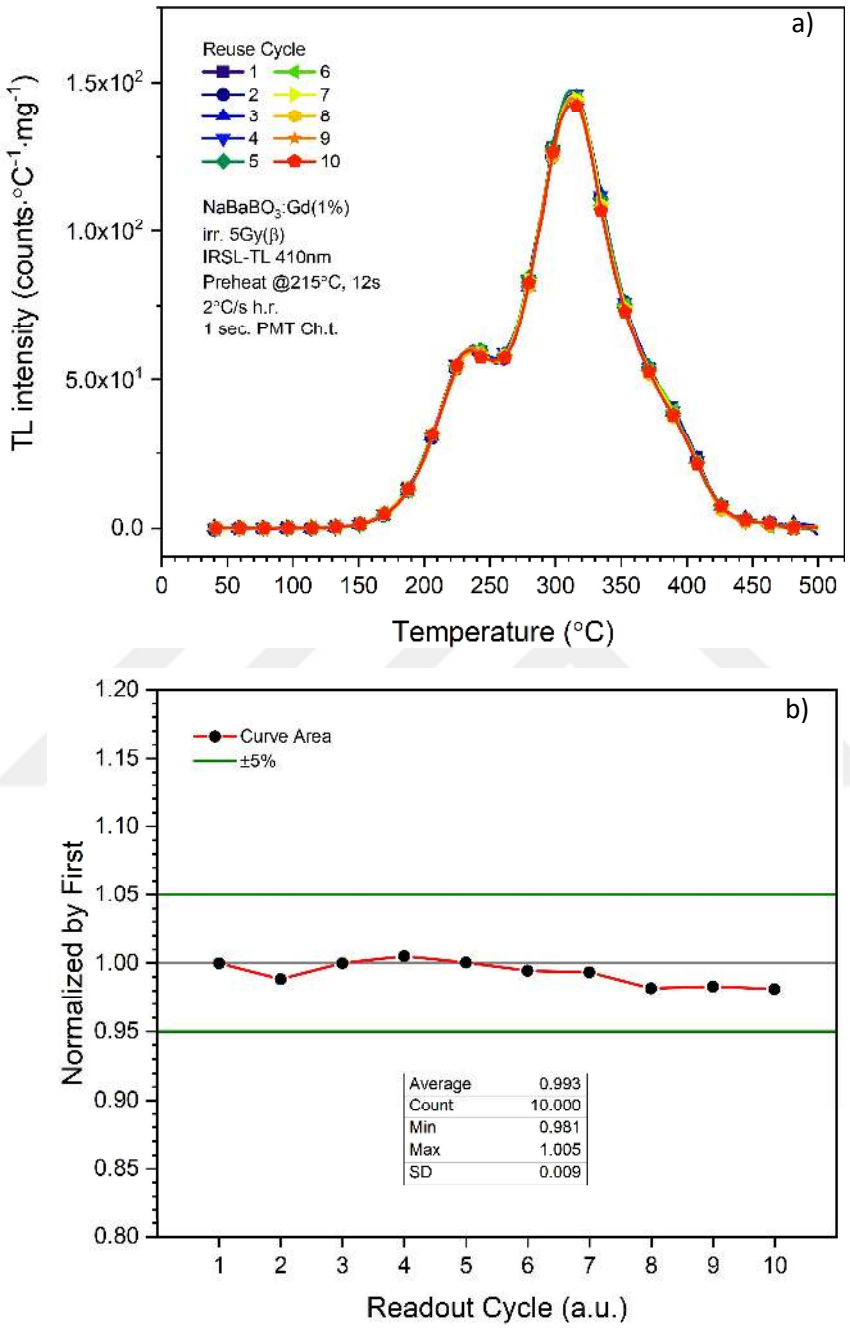

Figure 4.45. Reusability experiment reuslt of $NaBaBO_3:Gd^{3+}$(1%, weight): a) TL glow curves of ten reuse cycles b) Curve area trends of ten reuse cycles.

In Figure 4.45-b, glow curve area trend of ten-reuse cycle is given and as shown, standard deviation of these ten consecutive readouts is ~1%. When considered the 5% standard deviation as limit, it can be interpreted that, this material's TL reusability is very good at least for ten reuse cycles.

4.4.4. Reusability Experiment Results of $NaBaBO_3:Tb^{3+}$(2%) Sample

Pellet sample of $NaBaBO_3:Tb^{3+}$(2%, weight) with ~30mg weight was firstly thermally stimulated to empty electron traps if there any trapped electron exists. Then, sample was irradiated with a 5Gy β dose. After this, sample stimulated up to 145°C with a heating rate of 2°C/s and held there for 17 seconds and cooled back to room temperature with the cooling system of the TL/OSL reader system. IRSL-TL wideband blue filter combination was used for TL signal readings. This experiment was completed with ten reuse cycles, and curves are given in Figure 4.46.

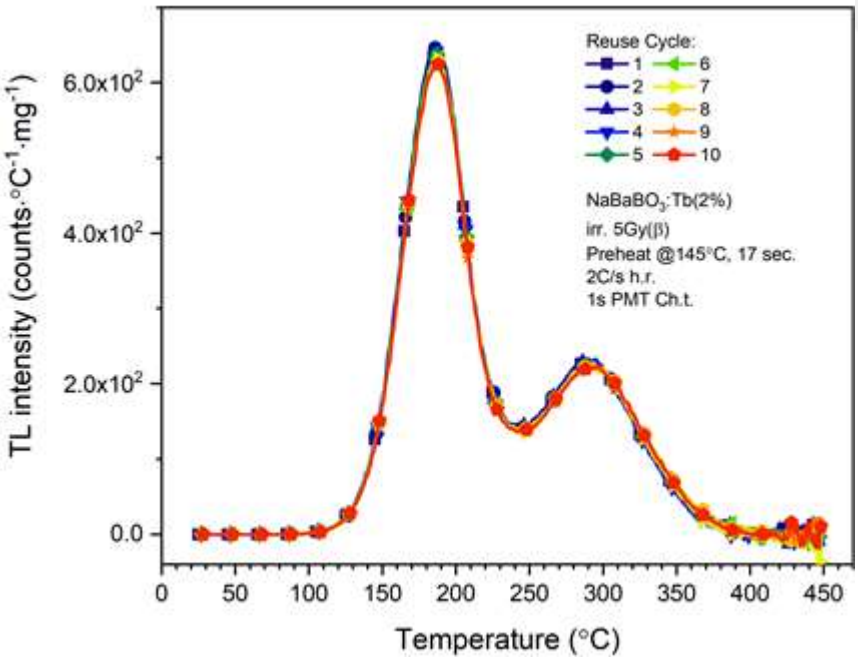

Figure 4.46. Reuse curves of $NaBaBO_3:Tb^{3+}$(2%, weight) for ten reuse cycles.

In figure 4.47 curve area trend is given for ten reuse curves which are given in Fig.4.41 for $NaBaBO_3:Tb^{3+}$(2%, weight). After ten reuse cycles, it was determined that, standard deviation of the sensitivity is 1.6% which is less than 5% limit. In other words, this material has a good reusability property for TL dosimetry.

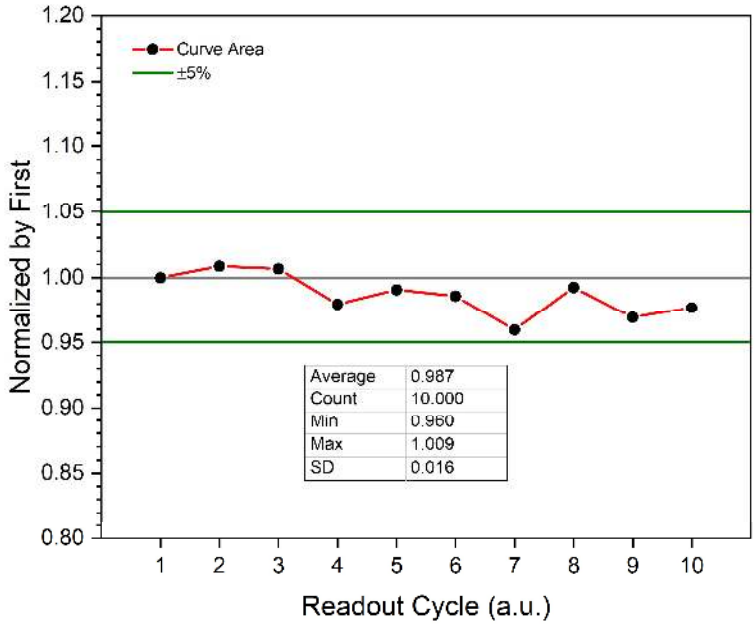

Figure 4.47. Reuse trend of $NaBaBO_3:Tb^{3+}$(2%, weight) for ten reuse cycles.

4.5. Results of T_m-T_{stop} Experiments and CGCD Analyses

4.5.1. Results of T_m-T_{stop} Experiments and CGCD Analysis for Undoped $NaBaBO_3$ Samples

In the T_m-T_{stop} experiment, a pellet sample of undoped $NaBaBO_3$ with ~30mg was irradiated with 3Gy of β dose, then preheated from room temperature up to 50°C with 2°C/s heating rate, then cooled back to room temperature. After preheat, TL reading was completed to record both main TL and background TL signals. This process was completed by changing only the preheat value up to 265°C. In the end, for each TL curve, an initial rise technique was applied and

Arrhenius plot was created, in Figure 4.40 an example plot is given. This plot is created by calculating the $ln(intensity)$ versus $1/k_BT$ where T is the thermal stimulation value.

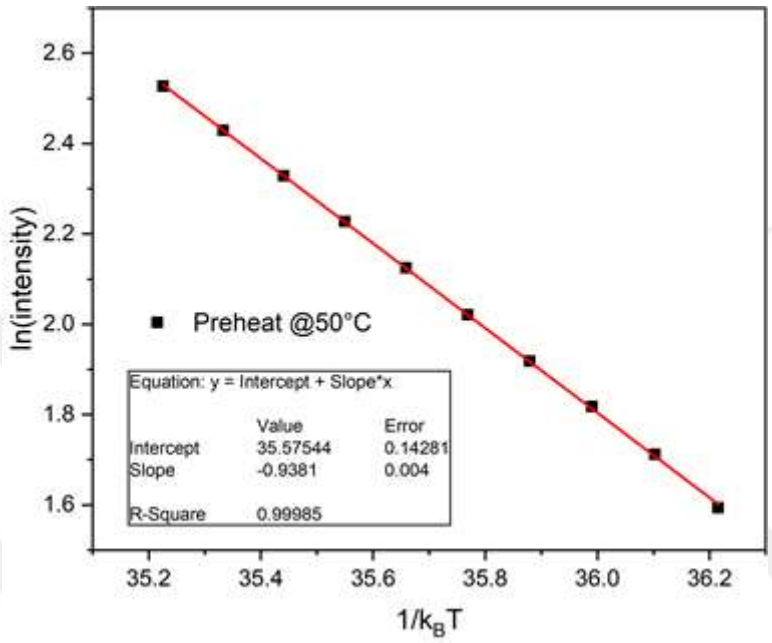

Figure 4.48. Arrhenius plot created for initial rise analysis technique for T_m-T_{stop} analysis of undoped $NaBaBO_3$. T_{stop} is the preheat temperature value.

In Fig.4.48 fit and fit values are given that, absolute value of the slope of fit is equal to the activation energy value and error of slope is equal to error on the estimated energy value. Intercept value (y-axis intercept) gives the natural logarithm of estimated vibration frequency value of the electrons assumed to be trapped at this energy level.

In Figure 4.49-a, a plot of such estimated activation values is plotted against the preheat temperature value (T_{stop} in other words) for T_m-T_{stop} analysis of undoped $NaBaBO_3$. In 4.49-b, computerized glow curve deconvolution results created by using the temperature and activation energy values as initial fitting parameters for trial-and-error protocol.

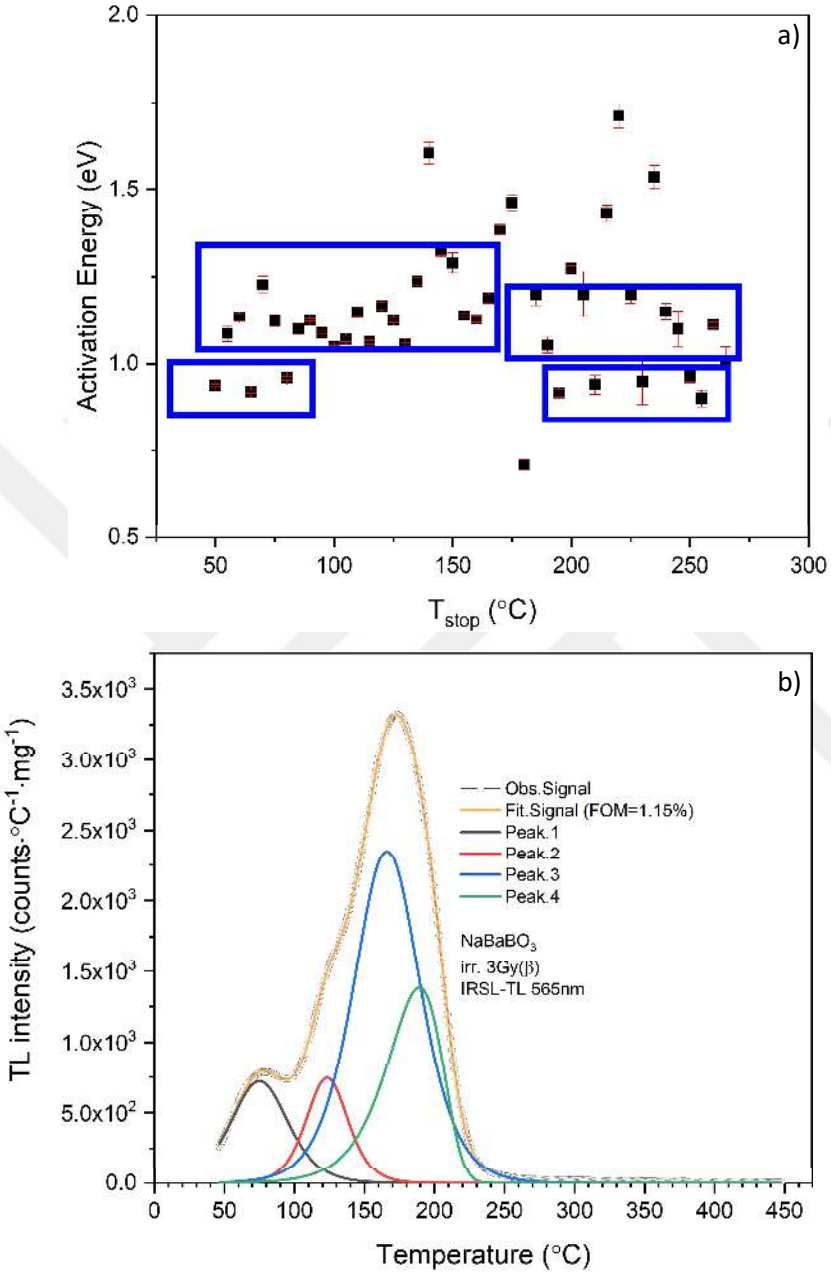

Figure 4.49. T_m-T_{stop} experiment and CGCD analyssi results for undoped $NaBaBO_3$: a) Activation energy versus T_{stop} b) CGCD curves with a FOM of 1.15%

Activation energy-*E*, s kinetic order-*b*, frequency factor-*s*, peak temperature-T_m values of each individual peak are given in Table 4.20.

Table 4.20. CGCD analysis's resulting parameters for undoped $NaBaBO_3$.

Peak List	E (eV)	s (sec^{-1})	b	T_m (°C)
Peak 1	0.76	1.26E+10	2.00	75.24
Peak 2	1.34	2.02E+16	2.00	123.54
Peak 3	1.05	1.18E+11	2.00	166.37
Peak 4	0.98	5.19E+09	1.06	189.48

From Fig.4.49 it can be interpreted that CGCD analysis made by referring the possible peak temperature and activation energy range as initial value for fitting gave a compatible result. In this analysis, general order equation given with Eqn.3.26 was used. As mention in the VHR analysis, TL glow curve has at least four different energy levels and those of mostly overlapping with each other.

4.5.2. Results of T_m-T_{stop} Experiment and CGCD Analysis for $NaBaBO_3:Ce^{3+}$ (0.5%) Samples

In the T_m-T_{stop} experiment step of $NaBaBO_3:Ce^{3+}$(0.5%, weight) preheat temperature value was varied between 50°C and 350°C with an increase of 5°C each time. Repeated initial rise results and estimated activation energy values are plotted in Figure 4.50-a. For the glow curve deconvolution again the same general order formula given in Eqn.3.26 was used; but this time six peaks model was chosen in the parametrization step of fit. Again, for fitting, initial parameters for peak temperature and activation energy are estimated with the results plotted in Fig.4.50-a. Obtained fit curves are given Figure 4.50-b as graph.

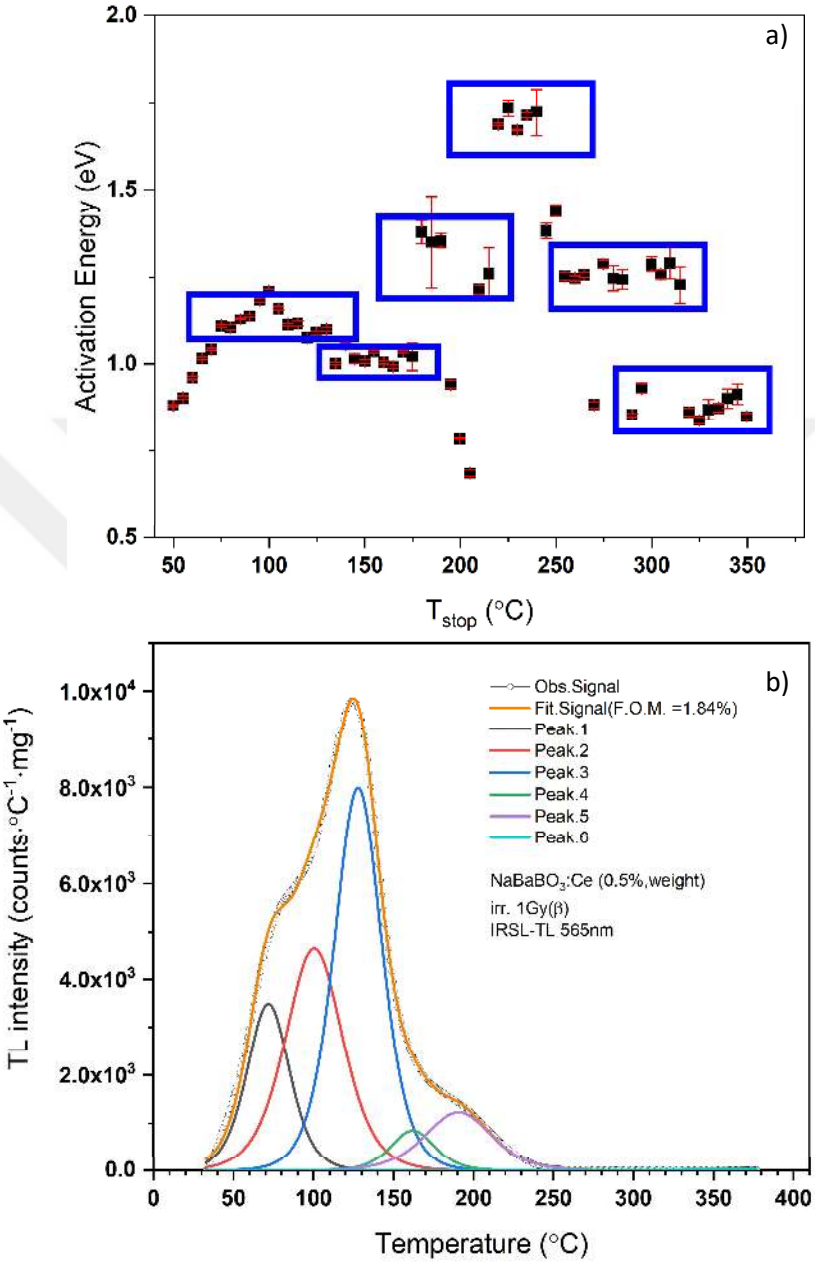

Figure 4.50. T_m-T_{stop} experiment and CGCD analyssi results for $NaBaBO_3:Ce^{3+}$ (0.5%) : a) Activation energy versus T_{stop} 1 b) CGCD curves with a FOM of 1.84%

In Table 4.21 as the values of activation energy-*E*, kinetic order-*b*, frequency factor-*s*, peak temperature-T_m values of each individual peak.

Table 4.21. Resulting parameters of CGCD analysis of $NaBaBO_3:Ce^{3+}$(0.5%).

Peak List	E (eV)	s (sec^{-1})	b	T_m (°C)
Peak 1	1.02	2.30E+14	1.40	66.92
Peak 2	0.99	1.47E+13	1.90	83.22
Peak 3	0.78	1.07E+09	1.01	120.62
Peak 4	1.13	1.16E+13	1.80	137.39
Peak 5	0.72	6.10E+06	1.30	183.58
Peak 6	1.31	8.88E+09	2.00	326.23

From the Fig.4.50, it can be seen that number of peaks, peak temperature, activation energy values are compatible with each other's.

4.5.3. Results of T_m-T_{stop} Experiment, and CGCD Analysis for $NaBaBO_3:Gd^{3+}$ (1%) Samples

Preheat value was varied from 50°C up to 400°C with 5°C increase each time, for T_m-T_{stop} experiment of $NaBaBO_3:Gd^{3+}$(1%, weight). A plot of activation energy value against the preheat value is given in Fig.4.51-a. A glow curve deconvolution was done using the peak temperature and activation energy values as initial fit parameters for general order equation given with Eqn.3.26. CGCD results are tabulated in Table 4.22.

Table 4.22. Resulting parameters of CGCD analysis of $NaBaBO_3:Gd^{3+}$(1%).

Peak List	E (eV)	s (sec^{-1})	b	T_m (°C)
Peak 1	0.92	9.42E+11	2.00	89.32
Peak 2	1.13	4.70E+13	1.74	120.61
Peak 3	1.05	1.62E+11	2.00	163.04
Peak 4	1.22	1.21E+12	1.82	199.69
Peak 5	1.35	4.02E+10	1.35	310.75
Peak 6	1.18	1.60E+08	1.61	359.88

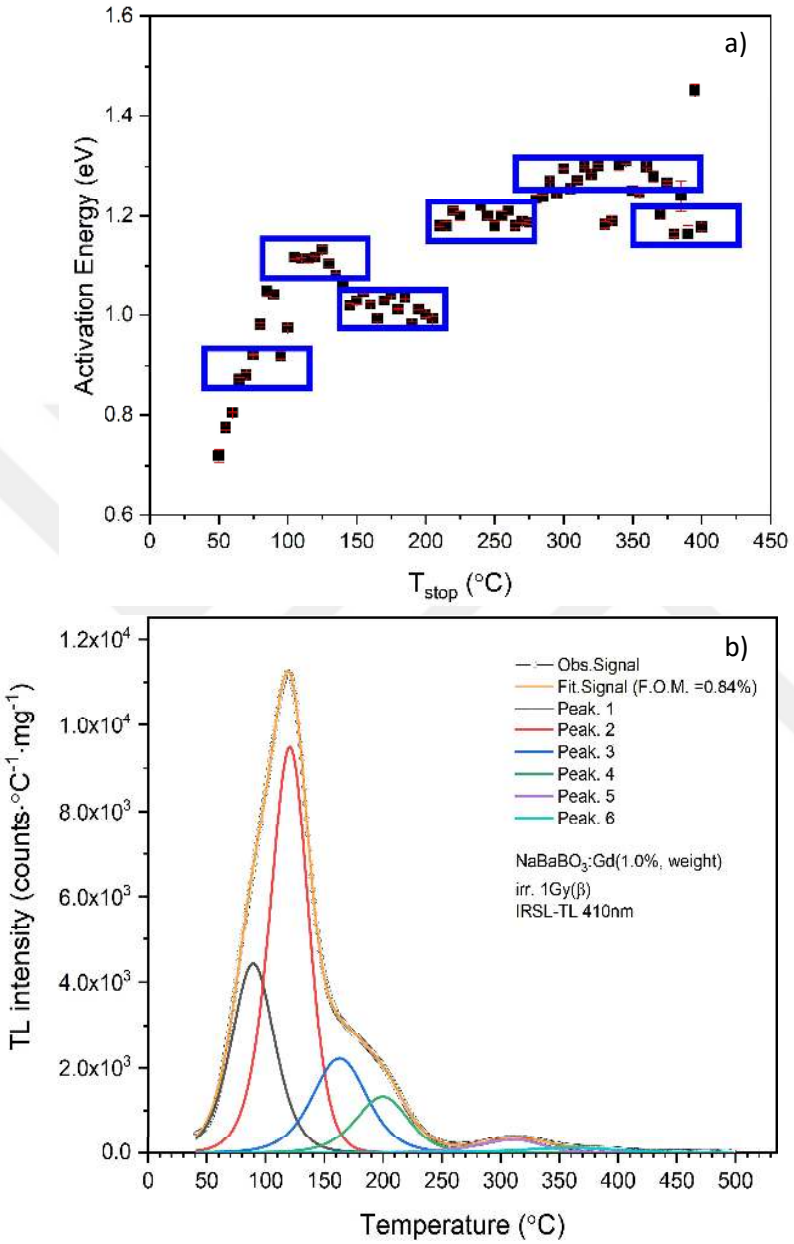

Figure 4.51. T_m-T_{stop} experiment and CGCD analyssi results for $NaBaBO_3:Gd^{3+}$ (1%) : a) Activation energy versus T_{stop} 1 b) CGCD curves with a FOM of 0.84%

As it can be seen from Fig.4.51-a and Fig.4.51-b, resulting glow curves' activation energies, peak temperatures are compatible with each other's. Fit has a good result as having a FOM value of 0.84%.

4.5.4. Results of T_m-T_{stop} Experiment, and CGCD Analysis for $NaBaBO_3:Tb^{3+}$ (2%) Samples

For the T_m-T_{stop} experiment step of $NaBaBO_3:Tb^{3+}$(2%, weight), preheat value varied from 100°C to 350°C with a 5°C increase each readout cycle as described for undoped one. A plot of activation energy values, which were estimated through initial rise method, against the preheat temperature is given with Figure 4.52-a. A glow curve deconvolution done by using general order equation given as Eqn.3.26 with the initial temperature and activation energy values estimated from Fig.4.44-a. CGCD parameters are given in Table 4.23.

Table 4.23. Resulting parameters of CGCD analysis of $NaBaBO_3:Tb^{3+}$(2%).

Peak List	E (eV)	s (sec^{-1})	b	T_m (°C)
Peak 1	1.2	1.38E+16	1.50	86.46
Peak 2	1.2	4.79E+14	1.50	118.70
Peak 3	1.2	4.36E+13	1.50	145.36
Peak 4	1.3	3.02E+13	1.50	183.96
Peak 5	1.4	1.27E+13	1.50	230.53
Peak 6	1.6	2.17E+13	1.50	291.42
Peak 7	1.3	3.59E+09	1.17	341.56

TL glow curve and resulting seven estimated glow peaks are given in Figure 4.52-b. CGCD analysis results are compatible with the T_m-T_{stop} experiment's results estimated with analysis done by repeated initial rise technique. Fit has FOM value as 1.75% which is smaller than 2.5 and good fit.

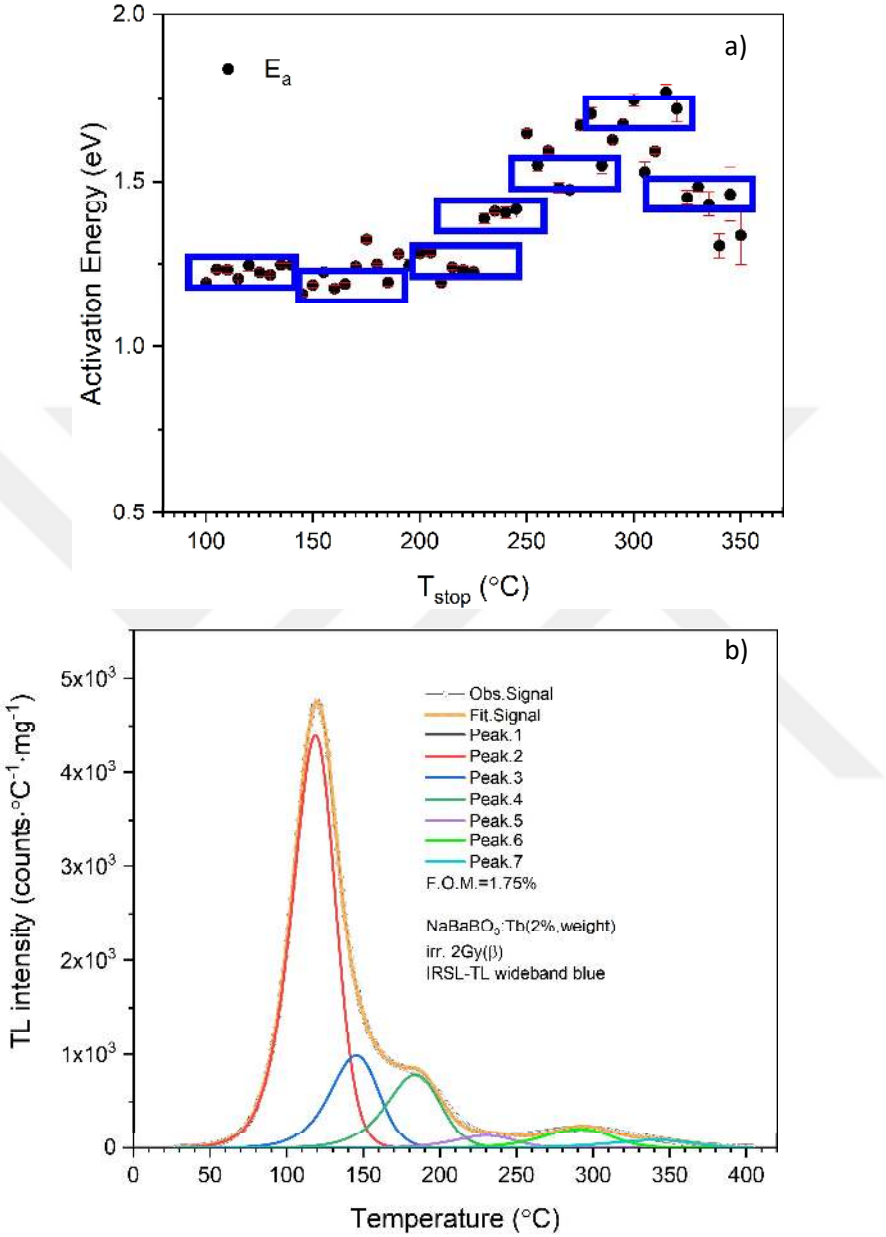

Figure 4.52. T_m-T_{stop} experiment and CGCD analyssi results for $NaBaBO_3:Tb^{3+}$ (2%) : a) Activation energy versus T_{stop} 1 b) CGCD curves with a FOM of 1.75%

5. CONCLUSION AND FUTURE STUDIES

In this thesis study $NaBaBO_3$ phosphor was synthesized via combustion synthesis method. Synthesis routine was optimized in terms of synthesis temperature and synthesis duration. It was determined that thermally treating the reactants at 400°C for 1 hour in ash furnace and then increasing the temperature up to 900°C and keeping for 5 hours and cooling back to room temperature slowly withing the furnace is the optimal synthesis condition for combustion synthesis of $NaBaBO_3$ crystal. Additionally, Ce^{3+}-doped, Gd^{3+}-doped, Tb^{3+}-doped $NaBaBO_3$ phosphor samples also synthesized for this study: $NaBaBO_3$:Ce^{3+} for 0.25, 0.5, 1, 2, 3, 4, 5, 6, 7, 8% Ce^{3+} concentrations in weight; $NaBaBO_3$:Gd^{3+} for 0.5, 1, 2, 3, 4, 5% Gd^{3+} concentrations in weight; $NaBaBO_3$:Tb^{3+} for 0.5, 1, 2, 3, 4, 5% Tb^{3+} concentrations in weight.

Crystal structure of each synthesized sample was confirmed via XRD analysis by comparing their x-ray diffractogram results with the reference XRD pattern data of $NaBaBO_3$ host crystal structure (98-008-0110). TL dosimetry characterization of samples were conducted by using Freiberg Instrument's LexygSmart TL/OSL reader system, and irradiating them with β particles from this system's internal $^{90}Sr/^{90}Y$ source which has irradiation rate ~0.11 Gy/s.

Optimal TL filter combination for undoped $NaBaBO_3$ sample's TL emission was determined as IRSL-TL 565nm named combination in which it has TL bandpass filters Schott-BG 39-Glass (3mm, 360-580 nm) and AHF-Brightline HC 575/25 interference (5mm, 550- 600nm). For the TL dosimetry study of this sample, a preheat value of 130°C was applied but T_m-T_{stop} analysis was conducted for whole range which un-preheated TL glow curve covers. Dose sensitivity was investigated for the dose range of 0.115 up to 55 Gy of β irradiation dose; and determined that, up to 14 Gy of β irradiation dose it has b=1.048 and can be accepted as linear. Minimum detectible dose for undoped $NaBaBO_3$ was determined as 6.15×10^{-4} Gy. For the heating rate behavior, it was observed that this

phosphor exhibits no anormal behavior; but thermal quenching effect was observed. Thermal quenching parameters were calculated by using whole glow curve area and observed maxima temperature value. Parameters of thermal quenching were estimated as 0.87±0.1 eV and 1.85×10^{10} respectively for W and C. Standard deviation of measurement sensitivity was investigated withing a ten consecutive irradiating-reading under same experimental conditions. It was observed that reusability has a standard deviation as 0.9% which is good for a TL dosimeter candidate when the 5% deviation limit is considered. Trap parameters were investigated both experimentally and theoretically by repeated initial rise analysis method on results of T_m-T_{stop} experiment and CGCD analysis. The analyses resulted that undoped $NaBaBO_3$ phosphor's TL glow curve consists of four peaks. Peak temperatures of those peaks are respectively 75, 123, 166, 190 °C. Corresponding trap depths are respectively 0.76, 1.34, 1.05, 0.98 eV. Frequency factors are 1.26×10^{10}, 2.02×10^{16}, 1.18×10^{11}, 5.19×10^{9} s^{-1}. Estimated kinetic order for those peaks are respectively 2, 2, 2, 1.6. Synthesis procedure and TL properties of undoped $NaBaBO_3$ sample was published in 2018 (Oglakci et al., 2019).

Ce^{3+}-doped $NaBaBO_3$ samples were synthesized with the synthesis procedure of undoped version. Ce^{3+} dopant was mixed in the synthesis step for the concentrations 0.25, 0,5, 1, 2, 3, 4, 5, 6, 7, 8% in weight. Crystal structures of resulting samples were confirmed via XRD analysis. Optimal TL filter combination was determined as IRSL-TL 565nm which is the combination of Schott-BG 39-Glass (3mm) and AHF-Brightline HC 575/25 interference (5mm) TL band-pass filters. Optimal Ce^{3+} was determined as 0.5%. It was determined that heating $NaBaBO_3$:Ce^{3+}(0.5%) phosphor with a heating rate of 2 °C/s up to 160 °C and keeping it at this temperature for 20 seconds was the optimal preheating condition for this material. Dose linearity parameter b was determined as 1.09 and 1.02 respectively for dose ranges 0.1-10 Gy and 0.1-5 Gy of β irradiation. Minimum detectible dose for Ce^{3+}-doped $NaBaBO_3$ was determined as 2.18×10^{-5} Gy. In the heating rate experiment, no anomaly was observed in terms of peak

intensity and peak temperature behavior under various heating rates. But peak area had a decreasing trend due to the existence of thermal quenching. Thermal quenching parameters were calculated by using whole glow curve area and peak temperatures per heating rate. Thermal quenching parameters W and C were calculated as 1.31±0.14 eV and 4.42×10^{14}; 1.75±0.16 eV and 5.93×10^{15} respectively for first and second peaks. Dose measurement sensitivity of this sample was tested by ten times reading the TL signal under same conditions. Thus, a standard deviation of 1.7% was observed for TL signal measurement sensitivity which is less than the 5% limit and good. T_m-T_{stop} experiment was conducted for whole TL glow curve by 5 °C increase in the preheating temperature. Repeated initial rise technique was employed for the analysis of the experimental data of T_m-T_{stop} experiment. CGCD analysis was also used for determining the number of electron traps. Probability range of peak temperature and trap depth for each peak were taken from the T_m-T_{stop} experiment results. It was estimated both through experimental CGCD results that TL glow curve of $NaBaBO_3:Ce^{3+}$(0.5%) phosphor contains at least six peaks with peak temperatures at 67, 83, 120, 137, 183, 326 °C. Corresponding trap depths were1.02, 0.99, 0.78, 1.13, 0.72, 1.31 eV; frequency factors were 2.3×10^{14}, 1.47×10^{13}, 1.07×10^{9}, 1.16×10^{13}, 6.1×10^{6}, 8.88×10^{9} s^{-1}; kinetic orders were 1.4, 1.9, 1.01, 1.8, 1.3, 2 respectively estimated for each peak. TL characteristics and synthesis of $NaBaBO_3:Ce^{3+}$ phosphor was published in 2020 (Oglakci et al., 2020).

$NaBaBO_3:Gd^{3+}$ phosphor samples were synthesized for Gd^{3+} concentrations as 0.5, 1, 2, 3, 4, 5% in weight. Synthesis conditions of undoped sample was used for those syntheses and Gd^{3+}-nitrate was mixed as required amount for each synthesis. Optimal TL filter combination was determined as IRSL-TL 410nm which is combination of Schott-BG 39-Glass (3mm), AHF-Brightline HC 414/46 interference (3.5mm), and Schott-NG 4-Glass(1.2mm) TL bandpass filters. 1% concentration of Gd^{3+} ion was determined to be the optimal amount for $NaBaBO_3:Gd^{3+}$ (1%) phosphor's TL signal quality in terms of peak intensity and

glow curve area of TL spectrum. It was experimentally observed that heating $NaBaBO_3:Gd^{3+}$ (1%) phosphor with a heating rate of 2 °C/s up to 215 °C and keeping it at this temperature for 12 seconds was the optimal preheating condition for this TL phosphor. Dose measurement linearity parameter b was calculated as 1.09 and 1.01 respectively for the dose ranges 0.5-20 Gy and 0.5-7 Gy of β. Minimum detectible dose for Gd^{3+}-doped $NaBaBO_3$ was determined as 1.32×10^{-3} Gy. Heating rate has no anormal behavior of TL intensity or dominant peak temperature; but TL glow curve area of $NaBaBO_3:Gd^{3+}$(1%) phosphor has a decreasing trend as observed in undoped $NaBaBO_3$ and $NaBaBO_3:Ce^{3+}$(0.5%) phosphor samples in their corresponding VHR experiments too. Thermal quenching parameters W and C were calculated for both peaks of $NaBaBO_3:Gd^{3+}$(1%) phosphor's TL glow curve as 0.82±0.11 eV and 3.19×10^{7}; 1.18±0.18 eV and 3.49×10^{9} by using TL glow curve area and peak temperature values. TL measurement was tested by ten times reading TL signal of the material under same conditions and a 0.9% deviation in the observed signals were determined. A T_m-T_{stop} experiment was conducted for whole TL glow curve of $NaBaBO_3:Gd^{3+}$ (1%) phosphor with a 5 °C increase in the preheating temperature. Repeated initial rise technique was employed for the analysis of the experimental data of this experiment. From the CGCD analysis it was estimated that TL glow curve of $NaBaBO_3:Gd^{3+}$ (1%) phosphor consists of six peaks with peak temperatures as 89, 120, 163, 200, 310, 359 °C. Corresponding Trap depths were estimated as 0.92, 1.13, 1.05, 1.22, 1.35, 1.18 eV; frequency factors were estimated as 9.42×10^{11}, 4.7×10^{13}, 1.62×10^{11}, 1.21×10^{12}, 4.02×10^{10}, 1.6×10^{8} s^{-1}; kinetic orders were estimated as 2, 1.74, 2, 1.82, 1.35, 1.62 respectively for each peak. Synthesis and TL characteristics of beta irradiated $NaBaBO_3:Gd^{3+}$ (1%) phosphor was published in 2021 (Oglakci et al., 2021).

$NaBaBO_3:Tb^{3+}$ phosphor samples were synthesized for Tb^{3+} concentrations in weight as 0.5, 1, 2, 3, 4, 5%, by applying the optimal synthesis condition of undoped $NaBaBO_3$ phosphor. Tb^{3+} concentrations were calculated in weight and

mixed in for each synthesis as Tb^{3+}-nitrates. Optimal TL filter combination was determined as IRSL-TL wideband blue which is the combination of TL bandpass filters Schott-KG 3-Glass(2mm), Schott-BG 25-Glass(3mm), and Schott-BG 39-Glass(3mm). Optimal concentration of Tb^{3+} dopant was determined as 2%. It was experimentally observed that heating $NaBaBO_3:Tb^{3+}$ (2%) phosphor with a heating rate of 2 °C/s up to 145 °C and keeping it at this temperature for 17 seconds was the optimal preheating condition for this TL phosphor. Dose response behavior of the sample was tested in 0.1-40 Gy of β dose range. Linearity characteristics parameter b and minimum detectible dose were calculated as 1.36 which is super linear and 1.62×10^{-3} Gy. VHR behavior was normal in terms of TL intensity and dominant peak temperatures of TL glow curve trend against the increasing heating rate; but $NaBaBO_3:Tb^{3+}$ (2%) also affected by thermal quenching as happened to undoped $NaBaBO_3$, $NaBaBO_3:Ce^{3+}$ (0.5%), $NaBaBO_3:Gd^{3+}$ (1%) phosphor samples. Thermal quenching parameters W and C were calculated for both peaks of $NaBaBO_3:Tb^{3+}$(2%) phosphor's TL glow curve as 31±0.13 eV and 3.11×10^{2}; 0.49±0.04 eV and 5.07×10^{2}. Standard deviation of dose measurement sensitivity was tested by ten times reading the TL signal of the material under same experimental conditions. Hence the deviation was determined as 1.6% which is less than the 5% acceptance level. It was determined from repeated initial rise technique analysis on the experimental results of T_m-T_{stop} experiment and from CGCD that, TL glow curve of $NaBaBO_3:Tb^{3+}$(2%) consists of 7 peaks. Peak temperatures of those peaks were estimated to be at 86, 118, 145, 184, 230, 291, 341 °C respectively for each peak. Trap depths were estimated as 1.2, 1.2, 1.2, 1.3, 1.4, 1.6, 1.3 eV; frequency factors were estimated as 1.38×10^{16}, 4.79×10^{14}, 4.36×10^{13}, 3.02×10^{13}, 1.27×10^{13}, 2.17×10^{13}, 3.59×10^{9} s^{-1}; kinetic orders were estimated as 1.5, 1.5, 1.5, 1.5, 1.5, 1.5, 1.17. A scientific article study is completed for the synthesis and TL characteristics of β irradiated $NaBaBO_3:Tb^{3+}$ phosphor, and results are processed to be published.

BIBLIOGRAPHY

Akselrod, M. S., Agersnap Larsen, N., Whitley, V. and McKeever, S. W. S. 1998 Thermal quenching of F-center luminescence in Al_2O_3:C, Journal of Applied Physics 84, 3364-3373.

Annalakshmi, O, Jose, M.T., Madhusoodanan, U., Venkatraman, B., Amarendra, G. 2013. Synthesis and thermoluminescence characterization of MgB4O7:Gd,Li, Radiation Measurements, Volume 59, Pages 15-22, ISSN 1350-4487.

Balarin, M., 1975. Direct evaluation of activation energy from half-width of glow peaks and a special nomogram. phys. stat. sol. (a), 31: K111-K114.

Balian, H.G., Eddy, N.W., 1977. Figure-of-merit (FOM), an improved criterion over the normalized chi-squared test for assessing goodness-of-fit of gamma-ray spectral peaks, Nuclear Instruments and Methods, Volume 145, Issue 2, Pages 389-395, ISSN 0029-554X.

Begum, M., Mizanur Rahman, A.K.M., Mahbuba Begum, Abdul-Rashid, H.A., Yusoff, Z., Bradley, D.A., 2018. Harnessing the thermoluminescence of Ge-doped silica flat-fibres for medical dosimetry, Sensors and Actuators A: Physical, Volume 270, Pages 170-176, ISSN 0924-4247.

Bos, A.J.J., Dielhof, J.B., 1991. The Analysis of Thermoluminescent Glow Peaks in CaF_2:Tm (TLD-300), Radiation Protection Dosimetry, Volume 37, Issue 4, 1 August 1991, Pages 231–239.

Bohun, A., 1954. Thermoemission und photoemission von Natriumchlorid. Czech. J. Phys. 4, Pages 91-93.

Booth, A.H., 1954. Calculation of electron trap depths from thermoluminescence maxima, Canadian Journal of Chemistry, Volume 32, Number 2, Pages 214-215.

Chen, R, 1969. On the Calculation of Activation Energies and Frequency Factors from Glow Curves, Journal of Applied Physics, 40, Pages 570-585.

Chen, R., 1969. Glow Curves with General Order Kinetics, Journal of The Electrochemical Society, 116, 1254.

Chen, R., Kirsh, Y., 1981. Analysis of Thermally Stimulated Processes. Pergamon Press, New York.

Chen and McKeever, 1997. Theory of thermoluminescence and related phenomena, World Scientific, Singapore, River Edge, N.J.

Chen, R. in: Horowitz, Y.S. (Ed.),1984. Thermoluminescence and Thermo-luminescent Dosimetry, Vol. 1, CRC Press, Boca Raton, FL.

Curie, D., 1963. Luminescence in Crystals, Wiley, New York.

Daniels, F., Boyd, C.A., Saunders, D.F, 1953. Thermoluminescence as a Research Tool, Science, 117, 343.

Dogan, T., Yüksel, M., Akça, S., Portakal, Z.G., Balci-Yegen, S., Kucuk, N. Topaksu, M., 2017. Normal and anomalous heating rate effects on thermoluminescence of Ce-doped ZnB_2O_4, Applied Radiation and Isotopes, Volume 128, Pages 256-262, ISSN 0969-8043.

Du Fay, C.F., 1738. The Notes of the observations about luminescence. Hist. De Acad. Roy. De Sci. De Paris, 3, 96pp.

Fasasi, A.Y., Balogun, F.A., Fasasi, M.K., Ogunleye, P.O., Mokobia, C.E., Inyang, E.P., 2007. Sens. Actuators A Phys., 135, 598–604.

Gartia, R.K., Ingotombi, S., Singh, T.S.G., Mazmudar, P.S., 1991. On the determination of the activation energy of a thermoluminescence peak by the two-heating-rates method, Journal of Physics D: Applied Physics, Volume 24, Number 1, 65.

Garlick, G.F.J., Gibson, A.F., 1948. The Electron Trap Mechanism of Luminescence in Sulphide and Silicate Phosphors. Proceedings of the Physical Society, 60, 574.

Gomez-Ros JM, Kitis G, 2002. Computerised glow curve deconvolution using general and mixed order kinetics. Radiation Protection Dosimetry, 101(1-4): 47-52.

Grossweiner, L.I., 1953. A Note on the Analysis of First-Order Glow Curves, Journal of Applied Physics 24, 1306-1307.

Halperin, A., Braner. A.,1960). Evaluation of thermal activation energies from glow curves, Physical Review Letters, 117, 408-415.

Hemam, R., Robindro Singh, L., Dorendrajit Singh, S., Sharan, R.N., 2018. Preparation of CaB_4O_7 nanoparticles doped with different concentrations of Tb^{3+}: Photoluminescence and thermoluminescence/optically stimulated luminescence study, Journal of Luminescence,Volume 197, 2018, Pages 399-405, ISSN 0022-2313.

Jiang, L.H., Zhang, Y.L., Li, C.Y., Hao, J.Q., Su,Q., 2007. Thermoluminescence properties of Ce^{3+} doped $LiSr_4(BO_3)_3$ phosphor, Mater.Lett., 61, 5107–5109.

Jiang, L.H., Zhang, Y.L., Li, C.Y., Hao, J.Q., Su, Q., 2010. Thermoluminescence studies of $LiSrBO_3:RE^{3+}$ (RE=Dy, Tb, Tm and Ce), Applied Radiation and Isotopes, Volume 68, Issue 1, 2010, Pages 196-200, ISSN 0969-8043.

Kitis, G., Tuyn, J., 1999. A simple method to correct for the temperature lag in TL glow-curve measurements, Journal of Physics D: Applied Physics. 31. 2065.

Kitis, G., Gomez-Ros, J.M., Tuyn, J.W.N., 1998. Thermoluminescence glow curve deconvolution functions for first, second and general orders of kinetics, Journal of Physics D: Applied Physics, **31**, 2636-2641.

Kitis, G., Polymeris G.S., Sfampa I.K., Prokic M., Meric N., Pagonis V., 2016. Prompt isothermal decay of thermoluminescence in MgB_4O_7:Dy, Na and LiB_4O_7:Cu, In dosimeters. Radiation Measurements, 84: 15-25.

Kitis, G., Vlachos, N.D., 2013. General semi-analytical expressions for TL, OSL and other luminescence stimulation modes derived from the OTOR model using the Lambert W-function, Radiation Measurements, 48: 47-54.

Lushchik, C.B., 1956. The Investigation of Trapping Centers in Crystals by the Method of Thermal Bleaching, Soviet Physics—JETP, 3, 390-399.

Leonardo V.S. França, Oswaldo Baffa, 2020. Boosted UV emission on the optically and thermally stimulated luminescence of CaB_6O_{10}:Gd,Ag phosphors excited by X-rays, Applied Materials Today, Volume 21,100829, ISSN 2352-9407

May, C.E., Partridge, J. A., 1964. Thermoluminescent Kinetics of Alpha-Irradiated Alkali Halides, The Journal of Chemical Physics 40, 1401-1409.

McKeever, S.W.S., 1980. On the analysis of complex thermoluminescence. Glow-curves: Resolution into individual peaks. phys. stat. sol. (a), 62: 331-340.

McKeever, S.W.S., 1985. Thermoluminescence of Solids. Cambridege University Press, England, 450pp.

McKeever, S.W.S., Moscovitch, M and Towndsend, P.D., 1995. Thermo-luminescence dosimetry materials: Properties and Uses. Nuclear Technology Publishing, England, 204pp.

Miljanic, S., Ranogajec-Komor, M., Knežević, Ž., Vekić, B., 2002. Main Dosimetric Characteristics of Some Tissue-equivalent TL Detectors, Radiation Protection Dosimetry, Volume 100, Issue 1-4, Pages 437–442.

Misra, S.K., Eddy, N.W. 1979. IFOM, a formula for universal assessment of goodness-of-fit of gamma ray spectra, Nuclear Instruments and Methods, Volume 166, Issue 3, Pages 537-540, ISSN 0029-554X.

Nagpure, P.A., Omanwar, S.K., 2012. Synthesis and luminescence characteristics of terbium (III) activated $NaSrBO_3$, Journal of Rare Earths, Volume 30, Issue 9, Pages 856-859, ISSN 1002-0721.

Nicholas, K.H., Woods, J., 1964. The evaluation of electron trapping parameters from conductivity glow curves in cadmium sulphide, Br. J. Appl. Phys., 15, 783

Oglakci, M., Akça, S., Halefoglu, Y.Z., Dogan, T., Ayvacikli, M., Karabulut, Y., Topaksu, M., Can, N., 2019. Characterization and thermoluminescence behavior of beta irradiated $NaBaBO_3$ phosphor synthesized by combustion method, Ceramics International, Volume 45, Issue 6, Pages 7011-7017, ISSN 0272-8842.

Oglakci, M., Topaksu, M., Can, N., 2020. Thermoluminescence glow curves of beta irradiated $NaBaBO_3$: Ce^{3+} phosphor synthesized by combustion method, Sensors and Actuators A: Physical, Volume 315, 112299, ISSN 0924-4247.

Oglakci, M., Topaksu, M., Souadi, G., Can, N., 2021. Thermoluminescence study and trapping parameters of beta irradiated $NaBaBO_3$:Gd^{3+} phosphor, Journal of Luminescence, Volume 238, 118245, ISSN 0022-2313.

Pagonis V., Kitis, G., Furetta, C., 2006. Numerical and Practical Exercies in Thermoluminescence, Springer, New York.

Peng, J., Dong, Z.B., Han, F.Q., 2016. tgcd: An R package for analyzing thermo-luminescence glow curves. SoftwareX, 5: 112-120.

Parfianovich, I.A., 1954. On the determination of the energy depth of capture levels in crystal phosphors, J. Exp. Theor. Phys., SSSR 26, 696-703.

Randall, J.T. and Wilkins, M.H.F., 1945. Phosphorescence and Electron Traps. Proceedings of the Royal Society, A184, 366.

Richter, D., Pintaske, R., Dornich, K., Krbetschek, M., 2012. A novel beta source design for uniform irradiation in dosimetric applications. Ancient TL 30(2): 57–63.

Richter, D., Richter, A., Dornich, K., 2013. lexsyg -a new system for luminescence research, Geochronometria, 40, 220–228.

Richter, D., Richter, A., Dornich, K., 2015. Lexsyg smart - A luminescence detection system for dosimetry, material research and dating application, Geochronometrıa, 42, 202–209.

Rozaila, Z.S., Alyahyawi, A., Kahander, M.U., Amin, Y.M., Bradley, D.A., Maah, M.J., 2016. Ge and B doped collapsed photonic crystal optical fibre, a potential TLDmaterial for low dose measurements, Radiat. Phys. Chem., 126, 9–13.

Sadek, A.M., Eissa, H.M., Basha, A.M., Carinou, E., Askounis, P., Kitis, G., 2015. The deconvolution of thermoluminescence glow-curves using general expressions derived from the one trap-one recombination (OTOR) level model,Applied Radiation and Isotopes, Volume 95,Pages 214-221, ISSN 0969-8043Sunta, 2015

Sanyal, B., Natarajan, V, Chawla, S.P., Sharma, A., 2010. TL and EPR studies of CaSO4:Dy phosphor to investigate its efficiency in measurement of foodirradiation dose at sub-ambient temperature, Radiat. Meas., 45.

Singh, L.L., Gartia, R.K., 2013. Theoretical derivation of a simplified form of the OTOR/GOT differential equation, Radiation Measurements, 59: 160-164.

Singh, L.L., Gartia R.K., 2014. Glow-curve deconvolution of thermoluminescence curves in the simplified OTOR equation using the Hybrid Genetic Algorithm. Nuclear Instruments and Methods in Physics Research B, 319: 39-43.

Singh, L.L., Gartia R.K., 2015. Derivation of a simplified OSL OTOR equation using Wright Omega function and its application. Nuclear Instruments and Methods in Physics Research B, 346: 45-52.

Sunta, C.M., 2015. Unraveling Thermoluminescence, vol. 202 of Springer Series in Materials Science, Springer, India.

Tu, J.-M. and Keszler, D.A., 1995. $BaNaBO_3$. Acta Cryst. C, 51: 1962-1964.

Yazici, A.N., Doğan, M., Kafadar, V.E., Toktamiş, H., 2006. Thermoluminescence of Ce-doped BaB_4O_7. Nuclear Instruments and Methods in Physics Research Section B: Beam Interactions with Materials and Atoms, Volume 246, Issue 2, Pages 402-408, ISSN 0168-583X.

CURRICULUM VITAE

Mehmet Oğlakçı was born on 31st of March 1984 in Osmaniye. He studied Physics at Çukurova Unviversity in Adana. He received his B.Sc. degree in 2011 and in the same year, he started his master's education in high energy physics at Çukurova University, in Adana. He completed his master thesis studies at CERN, in Geneva, Switzerland in the period of June-November 2013. His master thesis subject was about the effect of the radiation damage on the calorimeter jets' measurements. He completed his master thesis with the title as "Determination of The Calibration Factors of HPDs and SiPMs using Calorimeter Jets", and in August 2014 he got his M.Sc. degree. In September 2014 he started his Ph.D. education at Çukurova University. In 2015-2017, he participated in the CMS experiment for six-month periods as a physicist at CERN in Geneva, Switzerland. For the Ph.D. thesis he had studied standard model particle jets. However, in addition to his thesis studies in nuclear physics, he continued his studies in particle physics by contributing to the design of the Far water Cherenkov detector, which is a neutrino detector within the scope of the ESSnuSB project. He is working on thermoluminescence dosimetry, nuclear physics, and particle physics.